Hierarchical Structure Function Models of Biopolymer Networks

Thesis submitted to the Institute of Fundamental Sciences, Massey University,

New Zealand in partial fulfilment of the requirements for the degree of

Doctor of Philosophy in Physics

Palmerston North, October 2011

Erich Schuster

Supervisor: Assoc. Prof. Martin A.K. Williams

Co-Supervisor: Dr. Leif Lundin

Abstract

This project aimed to bridge the structure-function divide in polysaccharide networks so that the rheological properties of multi-chain assemblies might be predicted from the fine structures of the constituent polymers and their mode of assembly. The polysaccharide pectin is an important constituent of the plant cell wall and when cured into a gel the mechanical properties of its networks have recently come into the focus of research via extensive microrheological studies, in which interesting connections between the gel's mechanical response, gelation conditions and the pectin fine structure were discovered. This tunability makes it therefore a promising model system for further experiments and computer-aided investigations, and accordingly it is the focus of this thesis.

Firstly, a small angle X-ray scattering study of different microrheologically well-characterized ionotropic pectin gels was undertaken to gain insights into the structures of the assembled elementary network strands. The SAXS results paired with molecular modelling confirm that gels which are semiflexible from a microrheological point-of-view contain large bundles of aggregated dimers compared to the more flexible networks, where predominantly single chain sections and dimers are found to contribute. These later gels can be formed among other ways using a biomimetic methodology exploiting plant enzymes.

Secondly, after learning that networks could be experimentally manifest where single chains form the majority of links between nodes, in contrast to the better known hierarchical structures of polysaccharide gels, a computational approach was pursued to investigate the behaviour of biopolymer networks comprised of single polysaccharide chains using the experimentally measured force extension relation for pectin. This exhibits interesting force-induced conformational transitions that have been investigated in their own right. A 2-dimensional model was initially chosen for practical purposes. The study supports the hypothesis that conformational transitions could have biological significance as stress-switches in signalling processes, but that they are unlikely to affect the bulk rheological properties of tissue.

Finally, the model was further expanded into 3-dimensions to test quantitatively its predictions of the shear moduli of such systems. To this end a comparison with rheological prestress experiments on enzymatically induced pectin gels was undertaken. The model was found to successfully describe the observed nonlinear rheology for completely percolated, strong gels, based only on the polymer concentration and an experimentally accessible single chain force-extension relationship; for the first time providing a true bottom-up example to the properties of soft materials.

Acknowledgements

Thanks first to Bill Williams for being such an enthusiastic and supportive supervisor and to my co-supervisor Leif Lundin for invaluable guidance, regardless of being located in Melbourne. Thanks for introducing me to this interdisciplinary field, giving me the possibility to attend conferences and the great flexibility when it came down to balance the lab and tide times. Discussions - not just about pectin - with Padmesh Anjukandi, Yacine Hemar and Romaric Vincent have been fun and stimulating. I also want to acknowledge the helpful collaborators at CSIRO, especially Stephen Homer for the help with the prestress experiment, as well as Sofia Øiseth, Andrew Leis, Sandra Crameri and Alex Hyatt for providing the TEM images, the SAXS/WAXS beamline team at the Australian Synchrotron, in particular Nigel Kirby, and Kate Nairn for support during the running of the SAXS experiments. Many thanks to Aurelie Cucheval for help with the sample preparations and the microrheological analysis, and also for all the (long) coffee breaks. Cheers to all the members of the biopolymer group, especially Stephen Keen, Lisa Kent, Brad Mansel and Davide Mercadante. It was great to have 'obnoxious' discussions in the office and the odd beer after hours. I am grateful for all my friends: thanks to the NZ-crew, it made life overseas very enjoyable, and cheers as well to the guys in Austria for the continuous 'online-support'. Zu guter Letzt möchte ich meinen Eltern und Geschwistern meinen herzlichen Dank aussprechen - eure Unterstützung war auch am anderen Ende der Welt grandios. En Anne, dank je wel voor de inspiratie en alle moois dingen die we samen doen.

This research is supported by the Commonwealth Scientific and Industrial Research Organisation (CSIRO), Australia.

Contents

List of Figures

List of Tables

List of Publications

[P1] E. Schuster, L. Lundin and M.A.K. Williams, *Insights into the potential functionality of single-chain force-induced conformational transitions in polymer networks: Implications for polysaccharide signaling in the plant cell wall,* Physical Review E **82**, 051927 (2010).

[P2] E. Schuster, A. Cucheval, L. Lundin and M.A.K. Williams, *Using SAXS to reveal the degree of bundling in the polysaccharide junction-zones of micro-rheologically-distinct pectin gels,* Biomacromolecules **12**, 2583 (2011).

[P3] E. Schuster, L. Lundin and M.A.K. Williams, *Biomimetic Polysaccharide Gels Allow Quantitative Bottom-Up Prediction of Network Mechanics,* submitted.

List of Abbreviations

AE	Affine entropic regime
AFM	Atomic force microscopy
AM	Affine mechanical regime
AN	Affine network model
CE	Capillary electrophoresis
CEWLC	Clickable extensible wormlike chain
CG	Conjugate gradient
DFT	Density-functional theory
DM	Degree of methylesterification
DN	Discrete Network Model
DP	Degree of polymerisation
DWS	Diffusing wave spectroscopy
EANC	Elastically-active network chain
EWLC	Extensible wormlike chain
FE	Force-extension
GWLC	Glassy wormlike chain
HG	Homogalacturonan
HWLC	Helical wormlike chain
MR	Microrheology
MSD	Mean-square displacement
NA	Non-affine regime
OZ	Ornstein-Zernike equation
PGA	Polygalacturonic acid
PME	Pectinmethylesterase

pPME	plant PME
SANS	Small angle neutron scattering
SAXS	Small angle X-ray scattering
SEC	Subelastic chain model
TEM	Transmission electron microscopy
WLC	Wormlike chain

Chapter 1

Literature review & background

1.1 Introduction

"What do we mean by soft matter? Americans prefer to call it 'complex fluids,' and this does indeed bring in two of the major features..." the founding father of soft matter research, Pierre-Gilles de Gennes, started his nobel lecture [1] with this hint at the complexities waiting in this field of condensed matter science. The questions addressed in the studies of soft matter are not answerable by models of crystalline solids or of simple liquids - the answer lies somewhere in between. A main characteristic of such materials is that thermal fluctuations even at room temperature can play a significant role in determining the response of the material. Everyday examples of soft matter include soaps, paints, gels, plastics, liquid crystals and most of our own bodies and the food we eat.

The constituents of biological soft materials are classified in the simplest case as polysaccharides, polypeptides or polynucleotides depending on their monomeric subunits and form macromolecules such as e.g. DNA, RNA, proteins, starch or cellulose. Their structures and their response to force on the single-molecule level are now almost routinely accessible with tools such as atomic force microscopes (AFM) and optical tweezers. Further advances in microscopy and scattering techniques allow the determination of the structure of network strands and their assembly in biopolymer networks, so that the ultimate goal of any material scientist can be tackled: a *bottom up approach* [2]; an approach where a material with desired properties can be designed by a directed formation of the single-molecule constituents into macroscopic assemblies. But the whole is often greater than the sum of its parts and the knowledge of just single molecule properties not enough. Rheological parameters of all kinds of different biomaterials are available [3], but to close the gap and design

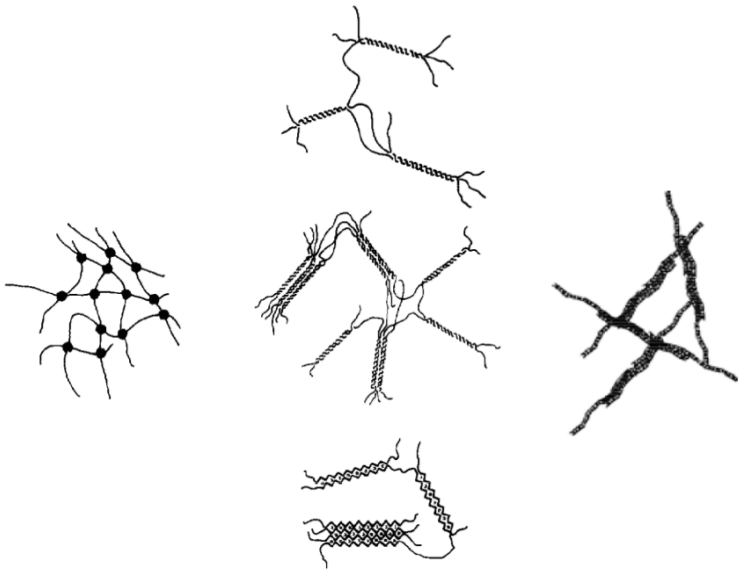

Figure 1: Molecular mechanisms of the network formation in biopolymers [4]. (left) point cross-linking, (middle) different modes of chain association, (right) rodlike structures.

materials, information about the constituents' assembly and interaction is equally important. That is where modelling systems becomes essential and theoretically treating networks with different degrees of sophistication can build up understanding for the phenomena observed in experiments. Figure 1 sketches a few different models of network formation.

The outline of the thesis is as follows: the content of this Chapter intends to give a review over the literature background and to highlight the motivation for the performed studies. Specific literature to understand the elaborations in the other Chapters is provided along the way, as each of the Chapters can be viewed and read independently.

1.2 Theoretical approaches

Since the pioneering work on the theory of polymer physics in the middle of the twentieth century by Flory - e.g. [5] - the foundations for the theories of rubber elasticity and polymer dynamics [6, 7] were laid. An essential part of this theoretical framework lies in the description of the macroscopic mechanical properties

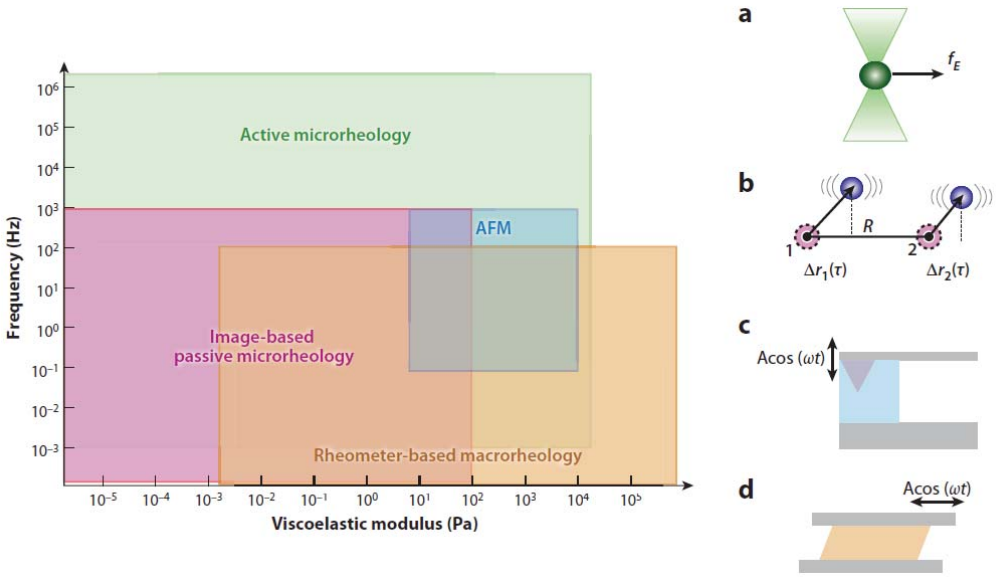

Figure 2: Overview of the rheological techniques to probe soft materials [9] and their range of operation. (a) Active microrheology using optical tweezers to force probe particles [10]. (b) Passive two-point microrheology using image-based particle tracking [11]. (c) Dynamic material deformation using atomic force microscopy [12]. (d) Oscillatory macrorheology [13].

of soft matter systems by assuming simplifying microscopic set-ups, as described in the different models below. Rheology - the study of the deformation and flow of materials in response to an applied force - deals with the measurement of these properties. A schematic of prominent experimental methods for rheological measurements is displayed in Figure 2 and a profound elaboration of the methods and techniques used can be found in [8, 9].

1.2.1 Rubber elasticity

A polymer gel is a three-dimensional network of polymer chains joined together by connections due to covalent chemical bonds (chemical gels) or physical interactions (hydrogen bonds or electrostatic forces in physical gels). Such polymeric materials typically exhibit a liquid state before the gelation; and indeed their atomic structure at the nanometre scale can be almost indistinguishable from the liquid state after the gelation. Such gels maintain a fixed shape and behave as elastic or viscoelastic solids. Rubber is an important example of these polymer networks.

The elastic modulus of rubber is 10^5 times smaller than that of steel, but rubber can be stretched by several hundred percent strain without breaking. Furthermore its elastic constant increases with temperature and is approximately proportional to the absolute temperature. This can be explained due to the thermal motion of the polymer chains: if the end of a chain is pulled, the number of allowable configurations (the entropy) is reduced - generating a tension that acts to return the chain back to a state with higher entropy (more allowable configurations). This mechanism of an entropic spring is comparable with the pressure caused in an ideal gas as a reaction on a confining container. Classical rubber elasticity reaches its limits when used to investigate generically more complex semiflexible biopolymer systems, where the bending stiffness of the chains cannot be neglected any more, but it can describe the visco-elastic properties of flexible polymer gels reasonably well.

The Helmholtz energy F of such a gel is defined as internal energy U minus the product of temperature T and entropy S

$$F = U - TS \tag{1.1}$$

Differentiating F with respect to the system length L, which equals the force f applied to deform this system, and by taking into account the *Maxwell relations* one gets

$$f = \left(\frac{\partial F}{\partial L}\right)_{T,V} = \left(\frac{\partial U}{\partial L}\right)_{T,V} - T\left(\frac{\partial S}{\partial L}\right)_{T,V} = f_E + f_S \tag{1.2}$$

with the enthalpic term f_E, the change of internal energy with sample length, and the entropic term f_S, the change of entropy with sample length times the temperature. If one knows the temperature dependence of the force, the Flory construction is a simple method to separate enthalpic from entropic contributions [14]. In crystalline structured systems, metals for example, f_E dominates as the internal energy as the deviation from the equilibrium lattice conformation increases. Ideal polymer networks instead have only entropic contributions to elasticity, and the energetic part $f_E = 0$ vanishes. Therefore one observes in rubber the opposite behaviour of metals - the network strands lose conformational entropy when stretched, making $\partial S/\partial L < 0$ and thereby the restoring force increases with increasing temperature.

The simplest approaches to theoretically capture the mechanics of polymer networks are summarized by **Unentangled network models**. The *Affine network model* - first proposed by Kuhn [15, 16] - assumes affine deformation, i.e. the rel-

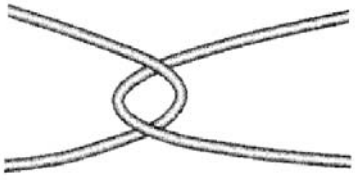

Figure 3: A schematic drawing of two entangled chains.

ative deformation of each network strand is the same as the relative macroscopic deformation, and reflects the entropic elasticity of polymer chains. It predicts for uniaxial deformation the following shear modulus

$$G = \nu kT \tag{1.3}$$

with the number of strands per volume ν and the Boltzmann constant k. The network modulus increases as expected with temperature (like the pressure of an ideal gas). The *Phantom network model* implements the idea of fluctuating cross-links, assuming that strands are ideal chains with ends joined at cross-links, and strands on the surface of the network are attached to a non-fluctuating elastic boundary. The fluctuations soften the network and lower the energy. Replacing the fluctuating strands by a smaller number of elastically effective ideal chains leads to

$$G = \nu_1 kT \tag{1.4}$$

where ν_1 ($\nu_1 < \nu$) is the difference of elastically effective strands and effective cross-links per volume. This means that the shear modulus is always smaller than in the Affine network model.

The *finite extensibility* of single chains can explain some experimental deviations from the previous classical predictions of the stress-deformation dependence, i.e. the hardening at higher deformations (strain stiffening). This is due to the non-Gaussian statistics of the strongly deformed chains; as the finite chain extensibility causes deviations in this regime from Hooke's law, which governs the force-extension at small to intermediate extensions.

However, many real networks have larger moduli than both of these models. Therefore not only constraints of strands by permanent cross-links have to be considered but

also topological chain interactions (Figure 3), that can be time-scale dependent and which can be treated by models of **entangled rubber elasticity**. The *Edwards tube model* treats entanglement by the introduction of a network strand confining tube. A quadratic constraining potential acts on every monomer, as each monomer is driven out of the minimum (primitive path) by thermal fluctuations (with an energy in the order of kT): these thermal fluctuations define the tube diameter. In unentangled models the fluctuations of monomers are in the order of the strand size, however the entanglement restricts the fluctuations to a tube of smaller diameter. De Gennes called this confined motion "reptation" [17]. A single polymer chain of DNA, stretched with optical tweezers, showed tube-like motion during its relaxation [18], as predicted by the tube model. However, strain softening and stiffening cannot be explained within this model due to the deformation independence of the confining potential. A further generalization are the *Constrained fluctuations models*, where in dense systems the topological restrictions of the chains' fluctuations are implemented via a mean-field approach [19, 20]. The non-affine tube model of Rubinstein and Panyukov [21] also takes non-affine local deformations into account. This deformation dependence of the confining tube explains the non-classical stress-strain relation of rubber at intermediate strains - strain softening - as the deformed strands reduce the constraining potential. The *Mooney-Rivlin model* is an alternative phenomenological approach, compared to the previous molecular models, to describe the elastic behaviour of networks. Thereby the energy is expanded as a power series in the three strain invariants - combinations of the squared shear-stress eigenvalues - and leads to the Mooney-Rivlin equation [22]. The experimental data of the uniaxial extension of networks are modelled well.

1.2.2 Cascade theory

One reason why rubber elasticity does not fully explain biopolymer networks is due to the fact that these networks are grown in ways that can mean they are not homogeneously distributed. The statistical theory for branching processes: Cascade theory [23, 24], is an approach to evaluate the properties of rubber elasticity via an estimation of the wastage of chains during the network building process of gelation. Such inhomogeneity can be incorporated by estimating the number of elastically-active network chains (EANCs) [25, 26] and cross-links involved in the network; where an EANC is a segment of the network which is deformed as the network is deformed and which contributes to the overall increase in energy accompanying the deformation.

As has been reported by Clark [27], the shear modulus of a fully-cured biopolymer gel can be written using the expression

$$G = [N\overline{f}\alpha(1-\overline{\nu})^2(1-\beta)/2]aRT \tag{1.5}$$

This method factorises the modulus into two terms, one describing the number of EANCs (the quantity in square brackets); and the second factor aRT is a measure of the average contribution per mole of EANCs to the energy increase per unit strain (expected to be close to the value of classical rubber elasticity $a = 1$, although some cases of high concentrations show $a > 1$) and hence to the modulus. The number of EANCs depends on the two key elements of cascade theory, the extinction probability ν and the scaling quantity β, both variables of the functionality $\overline{f}$ (number of sites along each molecule potentially available for cross-linking), and the fraction of these sites, α, which have reacted when a fully-cured gel has formed.

Clark [28] modelled literature results for the variation of the elastic modulus of kappa-carrageenan gels using cascade theory successfully, but the behaviour found for this polysaccharide - gelling via junction zone formation is assumed - it is not expected to be universal as $\overline{f}$ is unrelated to molecular weight in general, e.g. for globular proteins. Biopolymer gelation of thermoreversible gels [29] has also been treated, as has the kinetics of gelation [4]. A drawback was reported for systems inhering colloidal aggregation [30], as the cascade model seriously underestimates the sensitivity of gel moduli to concentration changes in such microphase-separated biopolymer systems.

1.2.3 Dynamics of flexible polymers

The random motion of pollen grains in water, or more generally of colloidal particles in solvent, is called Brownian motion. This extensively studied dynamic phenomenon [31] arises from the thermal motion of the solvent molecules, as the colloidal particle gets randomly hit from different directions. The mean-square displacement (MSD) of such a particle during time t is proportional to time t and the diffusion coefficient D,

$$\langle [r(t) - r(0)]^2 \rangle \approx Dt \tag{1.6}$$

yielding, that the characteristic distance travelled by the particle grows as $\sqrt{t}$. Such a non-differentiable trajectory was hard to swallow around 1900. Einstein was the first to treat it successfully in 1905 [32] by focusing on the thermodynamics of the suspended particles and argued that the number density of the particles $n(r,t)$ in

such a system can be regarded in a state of dynamic equilibrium between a diffusion current and a drift current, thus leading to the Stokes-Einstein relation

$$D = \frac{kT}{\zeta} = \frac{kT}{6\pi\eta r} \tag{1.7}$$

which links D to the friction coefficient ζ of the fluid. For particles in dilute solutions Stokes found that ζ can be expressed in terms of the viscosity η of the fluid and the particle size, yielding the expression above for the case of spherical particles of radius r. Einstein further applied a probabilistic model to describe the fluctuations of the Brownian particles - this approach can nowadays be seen as part of the fluctuation-dissipation theorem - and recovered the diffusion equation

$$\frac{\partial n(r,t)}{\partial t} = D\nabla^2 n(r,t) \tag{1.8}$$

a deterministic equation for the particle density $n(r,t)$. This explains how the random walk of single particles can generate smooth behaviour on the macroscopic scale. However, the Stokes-Einstein equation is valid just for purely viscous systems; polymeric systems are visco-elastic materials whose dynamics required new models to be understood.

The *Rouse model* [33] was the first molecular model to successfully describe the dynamics of polymers. The chain in solution is represented by beads which are connected by springs (Figure 4), therefore it is also referred to as "bead-spring model". The beads only interact with each other through the connecting springs. Each bead is characterized by its own independent friction ζ; the solvent is assumed to be freely draining through the chain as it moves. The model assumes diffusive motion for the whole bead-spring chain, with a total friction coefficient as the sum over the single ζ; and using the Stokes-Einstein relation (Eq. 1.7) a characteristic time, the Rouse time τ_R, during which the polymer diffuses a distance of the order of its size R, can be estimated via Eq. 1.6

$$\tau_R \approx \frac{\zeta}{kT} N R^2 \tag{1.9}$$

On time scales shorter than τ_R the chain exhibits visco-elastic modes, however a simple diffusive motion dominates on longer time-scales.
Ideal flexible polymers are fractal objects, whose size is related to the number of monomers (of length b) in the chain via a power law [6]

$$R \approx bN^{1/2} \tag{1.10}$$

The Rouse time for such a chain can be expressed in terms of the monomer relaxation time τ_0,

$$\tau_0 \approx \frac{\zeta b^2}{kT} \tag{1.11}$$

the time scale for the motion of individual beads; and leads via Eq. 1.10 to a quadratic dependence of the Rouse time on the number of monomers in a chain

$$\tau_R \approx \tau_0 N^2 \tag{1.12}$$

The times presented so far represent the longest relaxation time of unentangled polymers of length R. To understand the viscoelastic response of polymeric liquids in more detail, the full spectrum of relaxation times must be considered. As polymers are self-similar objects, smaller sections of a polymer chain with g monomers relax just like a polymer chain that has g monomers. Considering the different relaxation modes of the bead-spring chain results therefore in N corresponding relaxation times

$$\tau_p \approx \tau_0 \left(\frac{N}{p}\right)^2 \tag{1.13}$$

Mode N has the shortest relaxation time, representing the relaxation time τ_0 of a chain consisting of just one monomer (bead), and mode 1 respectively represents the complete chain with the longest relaxation time τ_R. Further, the stress relaxation modulus $G(t)$[1] at time τ_p is proportional to the thermal energy and the number density of sections with with N/p monomers (treated within the framework of the affine network model, see Eq. 1.3)

$$G(\tau_p) \approx \frac{kT}{b^3}\frac{\phi p}{N} \overset{Eq.1.13}{=} \frac{kT}{b^3}\phi\Big(\frac{\tau_p}{\tau_0}\Big)^{-1/2} \tag{1.14}$$

with b being the average spacing between the beads and the volume fraction ϕ of the polymer. For times $\tau_0 < t < \tau_R$ this results in a prediction for the stress relaxation modulus following a power-law

$$G(t) \propto t^{-1/2} \tag{1.15}$$

and similarly using the Boltzmann superposition principle to relate the shear storage G' and loss moduli G'' to $G(t)$ for an oscillatory shear stress, this results in

[1] Imposing a step strain of magnitude γ onto a viscoelastic solid, $G(t)$ is defined as the ratio of the stress remaining after a time t and the magnitude of this step strain.

predictions for the moduli following the same power-law

$$G'(\omega) \cong G''(\omega) \propto \omega^{1/2} \tag{1.16}$$

and agrees well with experiments on a number of flexible polymers and biopolymers [34, 35].

Systems with an MSD which increases with time with an exponent < 1 are called sub-diffusive, as on short time scales the visco-elastic response dominates and the movement of the chains is constrained; and the normal diffusive behaviour, with an exponent equalling 1 (the frequency domain is related to the time evolution of the MSD via a Laplace transformation [36]; the diagram in Figure 5 shows possible methods of data inversion to provide the moduli G', G'') gets delayed to times longer than the Rouse time. The dynamics of the coupled beads cause therefore a slower relaxation of the single polymer at high frequencies. The model resembles best the behaviour of unentangled chains in a polymer melt, as the hydrodynamic interactions are screened by the presence of other chains and reaches its limits when used to predict the diffusion constant, as a predicted scaling of $D \sim 1/N$ deviates from experimental observations. The idealized assumption of the freely draining solvent does not hold any more once polymers in dilute solution are considered, therefore more hydrodynamic details need to be incorporated.

That is where the *Zimm model* provides an extension by implementing the inter-bead hydrodynamic interactions [37]. Similar considerations of the characteristic time during which the polymer diffuses a distance of the order of its size R, as above for the Rouse model, lead to the Zimm time τ_Z

$$\tau_Z \approx \frac{\eta}{kT} R^3 \overset{Eq.1.10}{\approx} \frac{\eta b^3}{kT} N^{3/2} \approx \tau_0 N^{3/2} \tag{1.17}$$

where the inclusion of the hydrodynamic interactions in a solvent with viscosity η, is taken into account via Stokes law $\zeta \approx \eta R$ for the whole polymer chain of fractal size R. This leads with similar arguments as above to the following stress relaxation

$$G(t) \approx \frac{kT}{b^3} \phi \Big(\frac{t}{\tau_0} \Big)^{-2/3} \tag{1.18}$$

for times $\tau_0 < t < \tau_Z$. The diffusion coefficient in the Zimm model scales $D \sim 1/N^{1/2}$ as in good experimental agreement. In semidilute solutions, the hydrodynamic interactions affect the dynamics up to the scale of the correlation length. E.g. unentangled chains in semidilute solution, chain sections within a correlation volume relax by Zimm motion and the sections of chain larger than the correlation

length relax by Rouse motion. This is the simplest example for a system, in which a hierarchy of relaxation processes occur [6].

The stress relaxation dynamics of dense entangled systems can be understood in terms of an initial Rouse single chain relaxation process, followed by a plateau modulus in which the chain reptates out of its original confining tube [6]. The three dimensional diffusion coefficient is predicted by the simple reptation model to scale as $D \sim 1/N^2$.

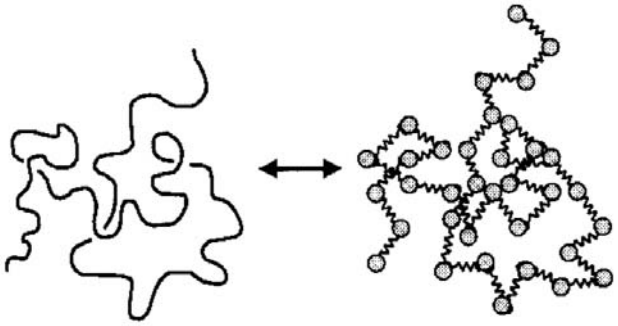

Figure 4: Sketch of the Rouse model [6]; a chain of N monomers is mapped onto a bead-spring chain.

1.2.4 Semiflexible polymer physics

When investigating cytoskeletal networks and biological gels one reaches the limits of classical polymer physics and models which incorporate a more rigid single chain response on small length scales to capture the observed phenomena are needed. This motivates the application of semiflexible polymer theories [6, 39]; characterized by the following properties:

Considering a semiflexible filament, e.g. F-Actin [40], it can be shown by geometric considerations that the angular correlation of points along the filament backbone decays exponentially. This is characterized by the parameter l_P, the distance over which the angular correlation decreases to $1/e$ of its initial value [39]. l_P is from now on referred to as the *persistence length*, see Table 1.1 for examples of some biopolymers and their persistence length. A natural energy scale for a rod subject to Brownian motion is kT. This is the typical kinetic energy of a molecule due to thermal fluctuations. The *wormlike chain (WLC) or Kratky-Porod model* [41] describes the single filament response of semiflexible polymers by examining an ide-

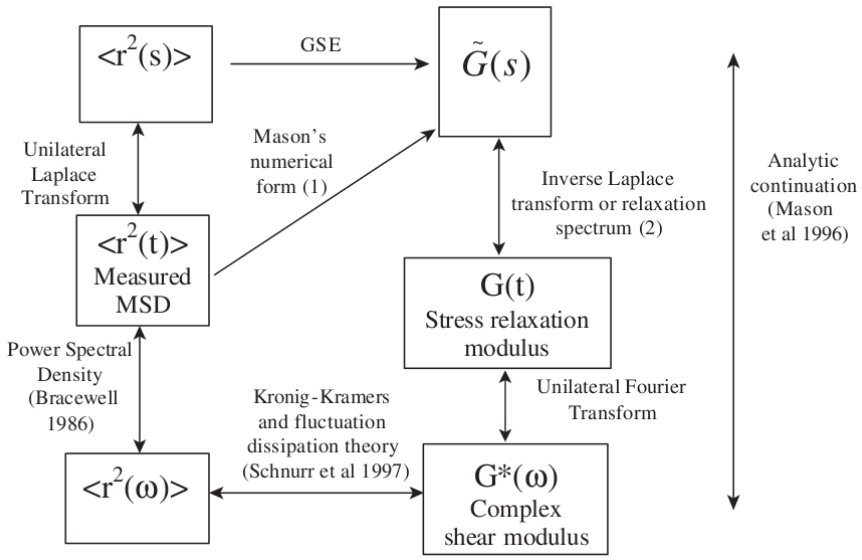

Figure 5: Possible methods of data inversion to provide the complex viscoelastic shear moduli (G', G'') from the compliance (or mean-square particle fluctuations $\langle r(t)^2 \rangle$). s is the complex Laplace frequency, and ω is the experimental frequency [38].

alized curve that resists bending. Under such assumptions bending deformations are described by the following Hamiltonian

$$H_{bend} = \frac{\kappa}{2} \int ds |\frac{\partial \vec{t}}{\partial s}|^2 \tag{1.19}$$

where κ is the bending modulus, $\vec{t}$ is a unit tangent vector along the chain and s the coordinate of the position along the backbone. In this WLC model the persistence length, the length scale at which significant bending fluctuations occur and over which the polymer "forgets" its orientation, is related to the bending modulus via $l_P = \kappa/(kT)$ (for a 3-dimensional rod with two transverse degrees of freedom). Therefore l_P provides a simple quantitative characterization of the mechanical stiffness of polymeric systems by non-intrusive optical measurements [40].
The local curvature of the WLC backbone $\frac{\partial \vec{t}}{\partial s}$ can for nearly straight filaments be expressed via the (transverse) deviation, $u(x)$, of the filament from its straight conformation $\frac{\partial \vec{t}}{\partial s} = u''$ (see Figure 6 for illustration). Filaments with a large bending stiffness or under a strong tension fulfil the required condition of nearly straight filaments, and one can express the Hamiltonian of a filament under a tensional force

Table 1.1: Persistence length and various parameters of some (bio)polymers. [42, 43, 44, 40, 45]

Polymer	Approximate diameter	Persistence length	Contour length
Polystyrene	0.5 nm	0.3 nm	$\sim$ 300 nm
Pectin	0.5 nm	10 nm	$\sim$ 450 nm
DNA	2 nm	50 nm	$\lesssim$ 1 m
F-actin	7 nm	17 μm	$\lesssim$ 50 μm
Microtubule	25 nm	1-5 mm	10s of μm

f_B in transverse coordinates

$$H = \frac{1}{2}\int_0^{l_C} dx\Big[\kappa|u''|^2 + f_B|u'|^2\Big] \tag{1.20}$$

Figure 6: A bendy filament with inextensible arc-length (contour length) l_C and one fixed end can be characterized by its transverse displacement from a straight conformation (dashed line). The transverse thermal fluctuations lead to a contraction of the end-to-end distance, which is denoted by Δl [39].

Such a single filament can respond to both, transverse and longitudinal forces by either bending or stretching/compressing. On length scales shorter than l_P, bending can be described in mechanical terms (as for elastic rods) but stretching and compression can involve, a purely elastic (mechanical) response as well as an entropic response. The latter comes from the thermal fluctuations of the filament [46]. The longitudinal single-filament response is described in terms of the force-extension (FE) relationship (Figure 7), where the force required to extend the filament is calculated in terms of the degree of extension along a line, using the Hamiltonian of Eq. 1.20. Due to the presence of thermal fluctuations at finite temperatures there prevails a resistance to extend such a filament. To derive a functional form for the FE curve, $u(x)$ is represented by a Fourier series:

$$u(x) = \sum_q u_q sin(qx) \tag{1.21}$$

with the wave vector $q = n\pi/l_C$. This series representation allows the integral in Eq. 1.20 to be rewritten as

$$H = \frac{1}{2}\int_0^{l_C} dx\Big[\kappa|u''|^2 + f_B|u'|^2\Big] = \frac{l_C}{4}\sum_q(\kappa q^4 + f_B q^2)u_q^2 \tag{1.22}$$

under a constant tension f_B. Utilizing the equipartition theorem, the equilibrium amplitudes u_q must satisfy

$$\langle|u_q|^2\rangle = \frac{2kT}{l_C(\kappa q^4 + f_B q^2)} \tag{1.23}$$

This equation points out an important property of semiflexible filaments, namely that they exhibit a strong suppression of bending fluctuations for modes of wavelength less than the persistence length $l_P = \kappa/(kT)$, as the mean-square amplitude of shorter wavelength modes are suppressed as the fourth power of the wavelength. Therefore the longest unconstrained wavelength l tends to dominate. Such scaling arguments lead to

$$\langle u^2\rangle \sim \frac{l^3}{l_P} \tag{1.24}$$

for the mean square amplitude in the absence of applied tension.

The contraction Δl (see Figure 6) can be estimated via the consideration of the constant arc-length of a filament

$$\Delta l = \int dx\Big[\sqrt{1 + |\partial u/\partial x|^2} - 1\Big] \simeq \frac{1}{2}\int dx\,|\partial u/\partial x|^2 = \frac{l_C}{4}\sum_q q^2 u_q^2 \tag{1.25}$$

and using Eq. 1.23 the average contraction $\langle\Delta l\rangle$, including a factor of 2 due to the two transverse degrees of freedom, must satisfy

$$\langle\Delta l\rangle = kT\sum_q \frac{1}{\kappa q^2 + f_B} \tag{1.26}$$

Subsequently the extension arising from the applied tension f_B can be written down as

$$\delta l = \langle\Delta l\rangle_{f=0} - \langle\Delta l\rangle_{f_B} = \frac{kTl_C^2}{\kappa\pi^2}\sum_q \frac{\Phi}{n^2(n^2+\Phi)} \tag{1.27}$$

with the dimensionless force $\Phi = f_B l_C^2/(\kappa\pi^2)$. The sum over the modes n needs to be evaluated and the FE can be obtained by a numerical inversion of the equation above. One example of providing an approximation via an analytical solution in the

high force limit was found by Marko and Siggia [47]

$$f(x) = \frac{kT}{l_P}\Big[\frac{1}{4(1-(x/l_C)^2)} - \frac{1}{4} + \frac{x}{l_C}\Big] \tag{1.28}$$

The first term in the brackets shows the analytical solution in the high force regime; the last two terms were added so that the equation is consistent with the experimentally well-observed linear elasticity in the low force regime. This only leads to a drawback in the intermediate force regime, where deviations of $\sim 10\%$ from the exact numerical solution are observed.

Force-extension curves have been measured for many biopolymers, e.g. DNA [48], titin [49, 50], polysaccharides [51], and polymers, e.g. polystyrene [42]. Modelling experimental single-molecule curves required an extension of the WLC model. The extensible wormlike chain (EWLC) successfully deals with the diverging force at extensions close to the contour length and incorporates a Hookean regime at high extensions mimicking the enthalpic stretching of bonds [52], with the only drawback of deviations in the intermediate force range similar to the Marko-Siggia model. Another enthalpic model additionally takes the force induced conformational changes of sugar rings in axial linked polysaccharides into account [53]; as macromolecules are stretched from the entropic region, through one or more ring conformational transformations, into the Hookean regime. Equilibrium between the conformational states and the difference of their Gibbs energy is exploited to calculate FE curves for such polymers, and predictions are found to deliver good fits of the experimental FE data for a variety of polysaccharides.

DNA cyclization experiments showed [54] that bending deformations with curvatures in the order of the contour length play an important role in biology, and that the high-curvature bending response is underestimated by the WLC. Models for kinkable chains [55] or the helical wormlike chain (HWLC) [56] were introduced to describe the bending of semiflexible filaments above the limit of small thermally induced bending fluctuations (WLC) with quite some success; but still with the drawback of either predicting a too soft bending response (kinks) or a breakdown of the model (HWLC) at high strains. Wiggins and Nelson [57] reviewed therefore a more general approach towards a theory of semiflexible polymers. By modelling the polymer as a chain of rigid links connected by torsional springs, stiff polymers can therefore be described by any generic model which predicts a tangent distribution function; as the statistical mechanics of the chain are completely characterized by the fundamental tangent distribution function. They show that the WLC model is the only realization, in which the bending stiffness is directly linked to the per-

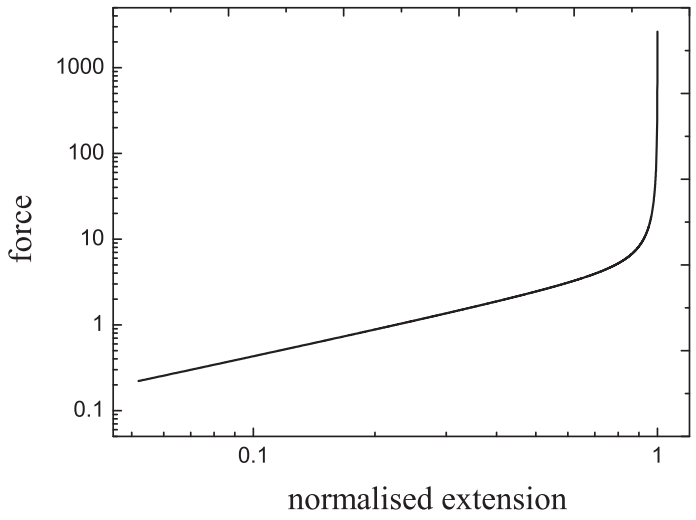

Figure 7: Force-extension relationship of a WLC; a linear region at small extensions and divergence once stretched up to the contour length is observed (excluding enthalpic deformations) [47].

sistence length; and demonstrate further that responses which are dominated by thermal fluctuations and the pulling out of entropy, such as the force-extension and the structure factor, are equally well described by the WLC and their generic SEC 'toy model'[2], but that the SEC model describes the high curvature regime more accurately.

1.2.5 Dynamics of semiflexible polymers

We have seen in Section 1.2.3, that Brownian forces cause diffusive motion in colloidal systems and induce a subdiffusive relaxation for systems of flexible chains, so it is not surprising that they also govern the dynamics of semiflexible polymers. Additional length scales start to play an important role when considering assemblies of semiflexible filaments. The typical spacing between polymers (the size of the voids in between filaments) gives rise to the mesh size l_M; the entanglement length l_e in contrast describes the length for elastically active contacts, which is in the limit of dense systems identical with the mesh size. Especially l_e influences the mechanical response of polymer solutions by restricting the thermal fluctuations of

[2] The experimentally motivated subelastic chain model (SEC), which requires that the effective bending energy density is a non-convex function of the curvature.

the single-chains [58]. This motivates the theoretical treatment of single filament dynamics to understand the high frequency shear response of semiflexible polymer solutions and networks.

For the Hamiltonian of Eq. 1.19 the equation of motion of the chain can be obtained by requiring that the variation of the action is zero, under the constraint of a fixed contour length [59]. The further influence of thermal motion is captured in this framework by a Langevin equation [60] of the transverse degree of freedom (in 2-dimensional considerations just one component u), describing the net force per unit length on the chain at position x exposed to Brownian motion in a solution

$$0 = -\zeta_\perp \frac{\partial u(x,t)}{\partial t} - \kappa \frac{\partial^4 u(x,t)}{\partial x^4} + \xi_\perp(x,t) \tag{1.29}$$

which is zero, within inertia-free (low Reynolds number) hydrodynamics. The first term in Eq. 1.29 represents the hydrodynamic drag with a constant transverse friction coefficient $\zeta_\perp$, the second term the restoring force due to bending and the last term $\xi_\perp(x,t)$ the Gaussian thermal noise. Tensional responses are neglected in this equation. Force balance of the Langevin equation [61] leads to a characteristic relaxation rate of a mode with wave vector q

$$\omega(q) = \kappa q^4/\zeta_\perp \tag{1.30}$$

Dimensional analysis of Eq. 1.29, a single time derivative along with four spatial derivatives, lets us expect the fourth-order dependence of this rate. A bending mode of wavelength λ ($\lambda \sim 1/q$ and $t \sim 1/\omega$) relaxes in a time of order $\zeta_\perp \lambda^4/\kappa$, and as the longest unconstrained wavelength (as shown above) dominates the response, one can estimate that in a time t the dominant mode that relaxes is of wavelength $l_\perp(t) \sim (\kappa t/\zeta_\perp)^{1/4}$. Together with Eq. 1.24 the time scaling of the mean-square transverse motion can be obtained

$$\langle u^2(t) \rangle \sim (l_\perp(t)^3)/l_P \sim t^{3/4} \tag{1.31}$$

and exhibits also a clear sub-diffusive exponent. Similar arguments can be followed to describe the longitudinal fluctuations of a semiflexible filament, which can explain the high-frequency visco-elastic response of biopolymer solutions and networks. This results in a power-law representation of the shear storage modulus [62, 63]

$$G'(\omega) \sim \omega^{3/4} \tag{1.32}$$

We observe that with increasing frequency the underlying dynamics of individual fil-

aments determine the macroscopic shear response, because the individual filaments are not able to fully relax on short times. This exponent of 3/4 observed for semiflexible filaments is in stark contrast to the power law of 1/2 predicted by the Rouse model. This difference points out that stiff semiflexible filaments relax quicker than their flexible counterparts.

Studies of in vitro polymerized networks agree well with the predictions made by the semiflexible polymer models introduced above, e.g. via measurements of the prominent power law of 3/4 at high frequencies [64]. Reaching intermediate, physiological more relevant time scales, small apparent power-law exponents in the frequency-dependence of the microrheological moduli are widely reported [65, 66], which is not accounted for in this theory. Furthermore microrheological studies of cells reveal a highly universal and comparatively featureless rheology in this more extended time window [67], which motivates a comparison with soft glassy systems.

1.2.6 Soft glassy rheology

Soft glassy rheology [68, 69] implements glassy dynamics to describe the non-linear rheology of complex biomaterials. The model assumes that particles are trapped in a energy landscape with many minima and the main method of stress relaxation is through the rearrangement of these densely packed bubbles (schematic sketch in Figure 8).

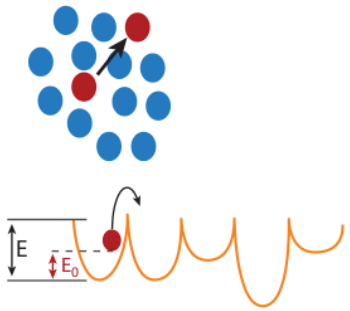

Figure 8: Stress relaxation in soft glassy materials takes place through the rearrangement of densely packed bubbles, which requires energies orders of magnitude greater than the thermal energy; a driving energy source is needed to overcome potential wells - if the energy falls below this limit the system equilibrates akin to a glass transition [68].

1.2.6.1 The glassy wormlike chain model

The implementation of sticky interactions between polymer chains, in the sense that chain damping cannot fully be attributed to the relative motion of an elastic component against a background solvent, motivated Kroy [70, 71] to modify the dynamics of a wormlike chain. The *glassy wormlike chain model* (GWLC) incorporates soft glassy rheology by a stretching of the relaxation spectrum of single chains. Therefore the linear Langevin equation in the weakly-bending rod limit for the transverse excursions $r_\perp$ of a single filament is

$$\zeta_\perp \frac{\partial u(x,t)}{\partial t} = -\kappa \frac{\partial^4 u(x,t)}{\partial x^4} + f_B \frac{\partial^2 u(x,t)}{\partial x^2} + \xi_\perp(x,t) \tag{1.33}$$

with the solvent friction per length $\zeta_\perp$, bending rigidity κ, constant backbone tension f_B and the Gaussian thermal noise $\xi_\perp$ needs to be solved. This Langevin equation implements additional to bending dynamics, as treated in Eq. 1.29, the response due to backbone tensioning. The effect of the stickiness of the wormlike chains is then implemented by an exponential stretching of the relaxation spectrum of its long-wavelength eigenmodes. This modification is just quantified by the single parameter ε, the stretching parameter, which can be thought of as a characteristic scale for the energy barriers retarding the relaxation of the chain; or in other words, biopolymers are sticky and interact with each other not just via entropic effects and cross-links, but also via weak interactions - one might speculate upon the origin of these, such as electrostatic interactions or friction via sliding branches. Such weak interactions consecutively slow down the relaxation time of the chain, as applied tension needs longer to relax completely; fully percolated networks with pinned-down cross-links can be thought of as very sticky systems with $\varepsilon \to \infty$. In contrast to the artificial choice of energy barriers in the soft glassy rheology, the trapping function is self-generated in the GWLC via the equilibrium mode spectrum (see Figure 9). Predictions for the dynamic structure factor and microrheological susceptibility exhibit the characteristics of soft glassy rheology, and compare well with experimental data of cytoskeletal networks [72].

1.2.7 Networks formed by semiflexible polymers

Compared to flexible networks, where every chain between two cross-links can be viewed as an independent entity, semiflexible networks formed by stiff filaments need to be treated as entities over longer distances than the spacing between cross-links, as the long-range correlation of the tangential backbone vectors retains information about their identity. Therefore one expects the longitudinal and the bending re-

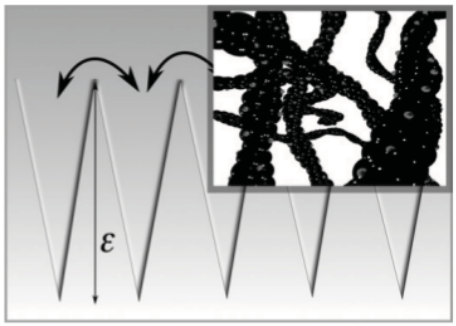

Figure 9: The GWLC is proposed as a minimalistic dynamic model for "Arrhenius gels", solutions of polymers interacting via small adhesive patches (grey spots). To break contact an energy barrier has to be overcome [71].

sponses of the constituting elements to play an important role. The high frequency behaviour of such networks can be traced back to the dynamics of single filaments, as seen in Section 1.2.5. The first elaborate theoretical studies made predictions for the rubber-like plateau modulus G_0 for associations of wormlike chains (which is in rubber elasticity only a function of the density of entanglements); these included either the features of bending and buckling [73], or assumed only affine deformations for uniform shear [46, 74]. In the absence of energetic contributions or at low frequencies a rubber like plateau modulus (as for entangled systems in Section 1.2.3) is caused by transverse entanglements [75, 76]. The modulus in this regime scales in the semiflexible limit of $l_P \sim l_e$ as $G \sim kT/(l_M^2 l_e)$, which can be confirmed by the following considerations.

The relative extension of a chain segment of entanglement length l_e under affine deformation is extended relative to the strain $\delta l \sim \gamma l_e$. Further, the extension of a semiflexible chain is described by Eq. 1.27 and leads to the following force relationship in the linear regime

$$f \sim \frac{\kappa^2}{kTl^4}\delta l \sim \frac{\kappa^2}{kTl_e^3}\gamma \tag{1.34}$$

This force gives rise to the shear stress σ, considering that there are $1/l_M^2$ chains per unit area [77]

$$\sigma \sim \frac{\kappa^2}{kTl_M^2 l_e^3}\gamma \tag{1.35}$$

and subsequently to the shear modulus $G = \sigma/\gamma$

$$G \sim \frac{\kappa^2}{kTl_M^2 l_e^3} \tag{1.36}$$

To investigate the mechanical and structural properties of semiflexible networks further two groups, Frey et al. [78, 79, 80] and Head et al. [81, 82, 83], carried out more elaborate studies. The ideas of semiflexible polymer theory, the Mikado model of Astrom et al. [84] (introduced originally to simulate two-dimensional random fibre networks (Figure 10) in a study of the stress resistance and fracture properties of

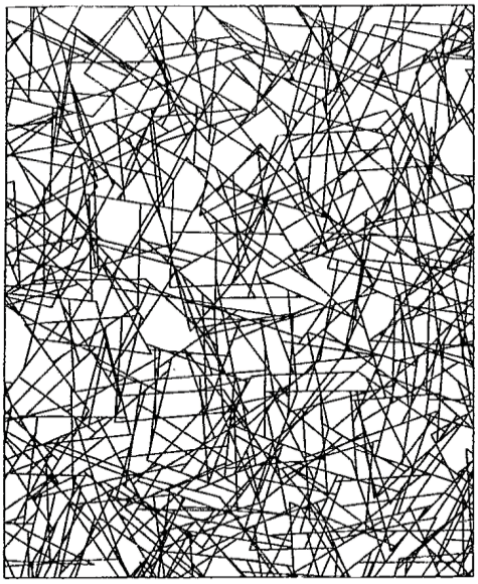

Figure 10: Random network structures generated via the Mikado model [84] - similar patterns to those in the Mikado game: 'pick-up sticks'.

paper) and percolation theory [85] form the basis for the computational and theoretical models described below.

A study of elasticity within the Mikado model and the impact of anisotropic[3] elasticity of stiff rods within a random geometry was conducted by Wilhelm and Frey [78]. Heussinger et al. [79] present a theory for the elasticity of cross-linked stiff polymer networks, where the elasticity is derived from the soft bending mode response by a self consistent effective medium approach. This approach naturally explains the

[3]The bending and the longitudinal response are highly anisotropic for semiflexible filaments.

presence of a bending dominated regime as well as its suppression with increasing filament length, and shows that the origins of the anomalous scaling properties of the linear shear modulus in random network simulations [78, 82] was due to the random geometry in the simulation set-up. Furthermore Heussinger and Frey [80] compared the elasticity of fibrous materials, composed of generalized stiff polymers, and of cellular foamlike structures under affine strain fields. The macroscopic elasticity of foamlike regular cellular structures can be explained by considering the response of a single cell, and exhibits affine deformation. In contrast, fibre networks show a hierarchical architecture and a broad distribution of pore sizes, with the macroscopic shear modulus asymptotically independent of the fibre length, but affine stretching is energetically unstable towards an energy redistribution in favour of longer segments. This leads to a correlation-induced elasticity that cannot be described within a single foam cell model.

Head et al. [81] numerically investigated the rigidity percolation transition in two-dimensional random rod networks with freely rotating cross links. These networks are dominated by bending modes near the transition. Head et al. [82] further studied the linear response of homogeneous and isotropic two-dimensional networks subject to an applied strain, and find the elastic moduli vanishing for network densities at the rigidity percolation threshold. Above the rigidity percolation threshold - for networks of higher filament concentrations or at a higher density of cross-links - three different regimes of elasticity are observed (Figure 11): a non-affine regime (NA) where the elastic modulus is determined by filament bending, an affine entropic regime (AE) with the elastic response governed by entropic longitudinal compliance, and an affine mechanical regime (AM), where the single filament compliance becomes dominated by the mechanical compliance of stretching and compression.

Predictions made within the framework of the state diagram in Figure 11 could be experimentally confirmed for actin filament networks (Figure 12) [86]. A high polymer & cross-link concentration regime where the single filament response causes strain stiffening was found, and at low concentration a soft strain response was measured, which gets explained as affine bending deformations [73]. A further increase in the actin concentration induces a transition from a regime of cross-linked filaments to a purely bundled regime [87]. Semmrich et al. [72, 88] similarly found that small variations in ambient conditions (temperature, salt) or the composition (polymer length, concentration) of F-actin solutions bring about dramatic changes in the long-time equilibrium dynamics and nonlinear rheology.

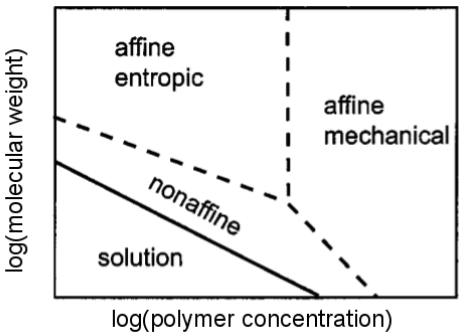

Figure 11: A sketch of the state diagram showing the various elastic regimes in terms of molecular weight (or contour length) and concentration. The solid line represents the rigidity percolation transition, where rigidity is first observed at a macroscopic level [82]. Wilhelm and Frey observed similar scaling regimes [78].

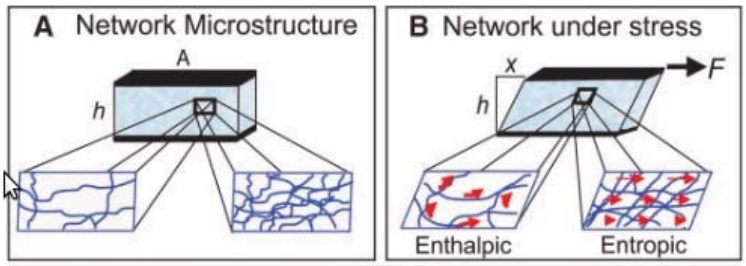

C Elastic Behavior and Models of Microscopic Deformation

Type of Elasticity	Enthalpic	Entropic
Filament Density, c_A	Low	High
Cross-link Density, R	Low	High
Filament Deformation	Bending	Stretching
Strain Distribution	Non-uniform	Uniform
Linear Elasticity	$G_0 \sim c_A^2$	$G_0 \sim c_A^{11/5}$
Elasticity at large strain, γ	Linear up to $\gamma \sim 100\%$	Stress Stiffen for $\gamma > 5\text{-}30\%$

Figure 12: Sketch of the investigations on actin networks of Gardel et al. [86], depicting the two different density regimes and its different (non)linear and (non)affine response.

1.2.7.1 Nonlinear rheology

Networks formed by semiflexible filaments undergo strain stiffening (Figure 13) and the differential shear modulus $d\sigma/d\gamma$ in dependence of the prestress σ can be described by a power-law $d\sigma/d\gamma \sim \sigma^{3/2}$ [86]; which has its origins in the nonlinear FE of the single filaments - similar to the argument of finite extensibility above, caused by non-gaussian statistics of the deformed chains. Therefore the stiffening can be tracked down to the straightening of entropic fluctuations of individual chains [89]. Assuming homogeneous, isotropic networks, which are strained uniformly, Storm et al. demonstrated that theoretical predictions based on this entropic model are able to provide good agreement to the nonlinear rheological data of a wide spectrum of biopolymers [74]. This model is in this paragraph further referred to as the affine network model (AN).

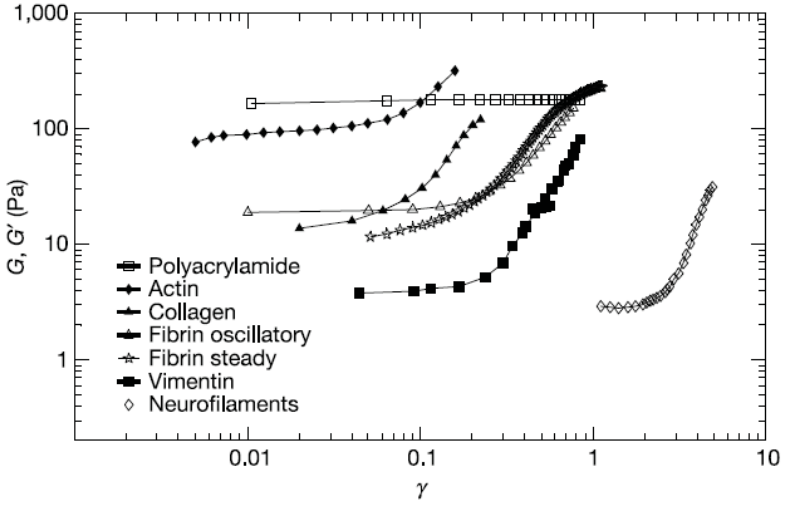

Figure 13: Shear moduli vs. strain measurements [74]; observing strain-stiffening for a series of cross-linked biopolymer networks.

Such networks typically also exhibit negative normal stresses: when sheared between two plates, they tend to pull the plate together [90]. This property is directly related to the nonlinear strain-stiffening behaviour of biopolymer gels - a natural consequence of the nonlinear force-extension of semiflexible filaments (Figure 14). This behaviour is observed inter alia for F-actin, collagen, neurofilaments, matrigel [90] and fibrin [91, 92] and is in stark contrast to a wide range of elastic solids where the torsion of a wire results in an axial elongation (Poynting effect [93]).

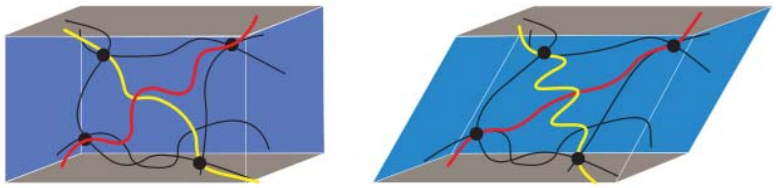

Figure 14: Schematic diagram: deformation leads to negative normal stress in an isotropic network of semiflexible filaments [90]; filaments are elongated (red) and equally many are compressed (yellow), therefore an overall negative normal force arises due to the nonlinear force-extension relation of the single filaments.

One explanation for strain stiffening, as already mentioned above, is the nonlinearity in the force extension arising from the filament's thermal fluctuations [89, 86, 74, 94]. The extension of a semiflexible chain in the high force regime is described by Eq. 1.28, where a divergence of the force $f \sim |\delta l - l_C|^{-2}$ is observed as the end-to-end distance approaches the contour length. As already argued in Section 1.2.7, the extension of a chain segment under affine deformations is proportional to the strain γ and therefore $df/d\gamma \sim f^{3/2}$ scales with a power law of 3/2. Estimating again, that this force gives rise to the shear stress $\sigma \sim f/l_M^2$, leads to

$$\frac{d\sigma}{d\gamma} \sim \frac{f^{3/2}}{l_M^2} \sim l_M \sigma^{3/2} \tag{1.37}$$

And finally, for a network of stiff chains l_M can be linked to the polymer concentration c_P via $l_M \sim c_P^{-1/2}$ [95], the differential shear modulus shows the following scaling properties

$$\frac{d\sigma}{d\gamma} \sim c_P^{-1/2} \sigma^{3/2} \tag{1.38}$$

which could be experimentally confirmed e.g. for actin [89]. Storm et al. [74] observe the strain stiffening in biomaterials such as actin, collagen, fibrin, neurofilaments and vimentin and speculate this could thereby help in living organisms to prevent large deformations that could threaten tissue integrity (Figure 13). Further experiments on the affinity of deformations in fibrin networks [91] obtain results that are consistent with the entropic model for non-linear elasticity of semiflexible polymer networks and show that strain-stiffening does not require non-affine deformations.

Intermediate filament networks are ionically cross-linked; their nonlinear elasticity has purely entropic origins for neurofilaments, and an additional enthalpic contribution due to backbone stretching for vimentin [96, 97]. The backbone stretching

causes the differential modulus to fall below the $d\sigma/d\gamma \sim \sigma^{3/2}$ behaviour at high prestresses. Strain stiffening with a similar deviation at high stresses is also found by Blundell and Terentjev [98] in their elaborations on semiflexible polymers with a mean inextensibility. Their results show three different scaling regimes: a linear entropic regime at low forces, a nonlinear entropic regime at intermediate forces (causing the slope of 3/2) and a linear mechanical regime at high forces (Figure 15).

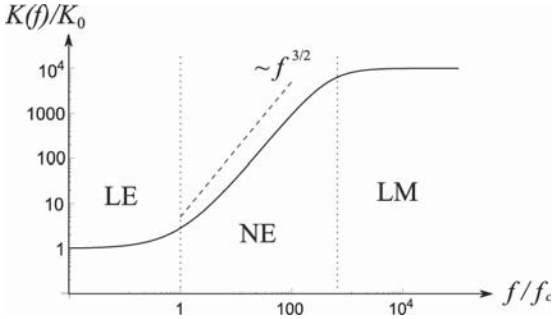

Figure 15: The normalised stiffness as a function of the applied normalised force for a semiflexible filament [98].

On the other hand a stiffening in networks formed by much thicker and stiffer fibres, where the entropic fluctuations can be neglected, can be modelled by non-affine network rearrangements, which control the transition from a bending-dominated response at small strains to a stretching-dominated response at large strains. This model is referred to as discrete network model (DN) [99]. A more elaborate three-dimensional analysis of this mechanism finds that the strain-stiffening depends additionally on the network architecture through the local topology around cross-links [100]. Another way to describe this purely geometrical effect is to address the highly non-affine response of soft transverse "floppy modes" [79]. State-of-the-art simulation studies of three-dimensional cross linked elastic fibres [101] also show stiffening without entropic contributions.

Kang et al. [92] find that fibrin gels are suitable systems to test the two different models of strain stiffening, because the fibrin monomers assemble under different conditions to form either thermally fluctuating protofibrils with persistence length on the order of the network mesh size, or thicker rigid fibres. The AN model does not allow the normal stress magnitude to exceed the shear stress, whereas the athermal[4] model does. The ratio of normal stress to shear stress, which is strain dependent,

[4] Rigid rods govern the network mechanics, not thermally fluctuating semiflexible filaments.

was found to be a parameter to experimentally determine which of the two models applies. Computational studies of van Dillen et al. [102] compare the two opposing models. At low and intermediate filament densities, the DN model deviates from the AN model as a result of non affine motions and bending deformations of the filaments in the network, resulting in a DN-stiffness that is significantly smaller than the calculated AN-stiffness. In contrast the stiffness resulting from the DN calculations does approach the affine value at high network densities. These observations suggest that, besides entropic stiffening in segments between cross-links, changes in the network architecture can play a crucial role in its mechanical response, especially at low and intermediate densities.

1.3 Further characteristics of biopolymer systems

Many biomaterials show strain stiffening [86, 74, 90], negative normal stress [90, 91, 92] and nonlinear rheology [72], which all reflect the semiflexible nature of their constituent polymers and are captured by generic semiflexible models as discussed. The sturdiness of the cross-linkers [103, 104, 105] and the activity of molecular motors [106, 107] are additional factors that can cause further prestress on single filaments [108] and stiffening or softening [101, 109] behaviour. The exhaustive studies of networks formed by semiflexible filaments also suggest that a sensitive response towards parameter changes is a special property of these "smart" biomaterials [3].

The influence of cross-links and dynamic junction zone formation needs to be considered and understood [103, 105] to shed light on observed phenomena such as strain softening. Astrom et al. [101] reported a softening in filamentous networks caused by cross-link slippages at high strains. Buckling of the filaments at high strains is an alternative explanation of softening in dendritic actin networks [109], which is interestingly found to be reversible. Erk et al. [110] designed an associating triblock copolymer to mimic the stiffening response of biopolymers and provide a model where the stiffening is accurately captured by a constitutive model with a single fitting parameter related to the midblock length of the constituting polymers. The rubbery midblock spans end-block-aggregates and dominates the stress-relaxation at small to intermediate strain values; viscoplastic chain pull-out of the end-blocks determines the stiffening at higher deformations. Torsion and compression rheological tests further reveal a similar mechanism behind the strain-hardening of alginate gels [111]. They suggest that the deformation of rod-like junction zones causes the hardening, whereas the single chains contribute in a linear fashion. Kawai et al. [112] describe a model for a class of polymer gels, which show strain hardening at

intermediate strains and softening at large deformations, as for κ-carrageenan and gellan; describing gels which are formed by long flexible chains joined by crystalline junction zones. The two regimes (flexible chains/crystalline junction zones) are in equilibrium and during deformation more and more segments are reeled out of the crystalline junction zones, this leads to entropic strain hardening due to single chain contributions at intermediate strains, and at high strains to softening due to reeling out of chain segments.

A comparison of the measurement protocols for nonlinear moduli [88, 113] suggest that the *strain ramp* and the *differential prestress* protocol agree well for entangled and cross-linked networks, while they agree only at high strain rates for more transient networks (Figure 16). Broederesz et al. [104, 114] present an effective medium approach to study composite networks of stiff polymers with flexible linkers, and find that actin cross-linked by the compliant protein filamin fits into this model, and that the observed strain stiffening is not only caused by the nonlinear force extension relation of the filaments but also due to the flexibility of the cross-links [115]. Similar ideas have been pursued in systems of cross-linked stiff filaments, where the influence of unfolding in protein cross-linkers under stress was investigated [116, 117, 118]. The unfolding sets in at higher forces than captured by the flexible linkers in the model above and consecutively causes softening at high strains. Another model system suggested that such a nonlinear response could be described by treating networks as interconnected stiff and floppy filaments [119].

Further insights into the nonequilibrium mechanics of the cell have been obtained by rheological studies on model systems with molecular motors [106, 107]. The elastic moduli increase orders of magnitudes in networks with fixed cross-links [121] and in active cross-linked biopolymer networks [122]. Mizuno et al. [106] found that stresses arising from motor activity in a three-component model system - consisting of myosin II, actin filaments and cross-linkers - can control the network mechanics and change the viscoelastic response, without changing the density, polymerization or bundling state of F-actin; the relaxed actin gels show the characteristic fingerprint of semiflexible networks, with the shear modulus $G'(\omega) \propto \omega^{3/4}$, whereas with the onset of nonequilibrium activity, the modulus exhibits a power law of $1/2$ under such introduced stress/tension [123]. Rosenblatt et al. [108] measure the rheology of prestressed semiflexible polymer chains by creep experiments and speculate that the main aspects of cell rheology are consistent with the dynamics of single polymer chains under tension; the observed power-law creep being a result of gradual stretching-induced propagation of the energy from the ends to the centre of the chain [124]. Obermayer and Frey [125] provided a theoretical framework for the

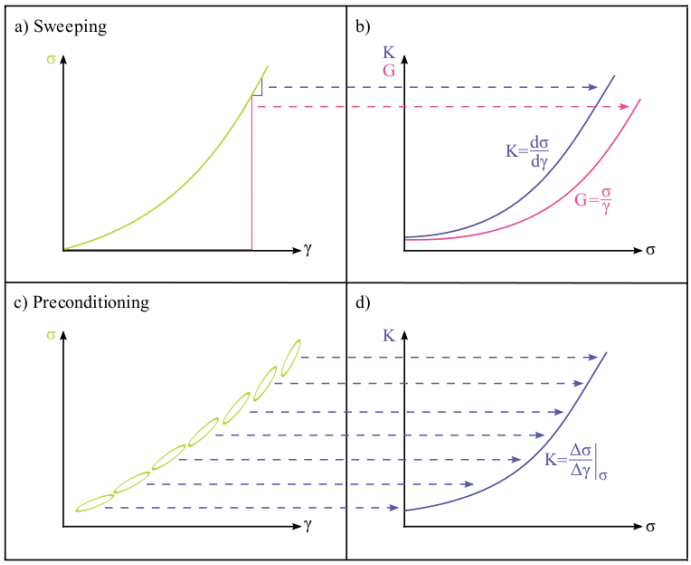

Figure 16: Stress-strain measurements, obtained either by strain sweep or preconditioning methods, lead to the same results for cross-linked networks. However a careful distinction between the two moduli, the shear modulus $G = \sigma/\gamma$ and the differential modulus $K = d\sigma/d\gamma$, needs to be made [120].

tension dynamics of stiff yet extensible WLC, where they show that prestress gives rise to distinct Rouse-like extensibility signatures in the high-frequency viscoelastic response. The opposing effects that thermal stored length density and elongational strain have on the backbone tension can be formalized: if prestress is increased, stored length is destroyed and elongational strain created, and both lead temporarily to spatial tension inhomogeneities (curvature), and vice versa for decreasing prestress. Hence, the slowed down relaxation leads to shear storage moduli following a power law of $G'(\omega) \sim \omega^{1/2}$. Internal stresses were also observed in in-vitro actin networks caused by the actin binding protein filamin through cross-linking and bundling actin filaments into a kinetically trapped network structure [126].

These research proceedings lead finally to studies of the mechanical response of living cells [66], where the entropic elasticity explains just the response at very short time scales and further on a soft glassy regime is found. A full review of the cell mechanics would go beyond the scope of this literature review and can be found elsewhere [127].

1.4 Aims of the thesis

This project aimed to apply some of the methodologies mentioned in this Chapter in order to bridge the structure-function divide in polysaccharide systems so that the rheological properties of assembled networks might be predicted from the fine structures of the constituent polymers and their mode of assembly. Most of the work in this field to date has been undertaken on proteins, motivated by the urge to understand the hierarchical responses in cytoskeletal networks, whereas polysaccharides on the other hand, whose importance in the plant cell wall is indisputable, have tended to be sidelined so far.

The polysaccharide pectin, an important constituent of the plant cell wall, can be cured into gel networks whose mechanical properties have recently come into the focus of research via extensive microrheological studies [128]. Interesting connections between the gel's mechanical response, gelation conditions and the pectin fine structure were discovered. This tunability of the mechanical response makes pectin gels therefore a promising model system for further investigations. Additionally, the molecular force-extension relation of single pectin chains is experimentally accessible. If networks can be found in which single chains are the dominating stress bearing elements - which would be in stark contrast to a multitude of biological gels, where hierarchical assembled filaments were found to be the stress bearing strands - then it could be speculated that the macroscopic mechanical response can be predicted from microscopic single molecule measurements. Supported by the utilization of small angle X-ray scattering, rheological techniques and computational simulations this thesis suggests a simple network model for enzymatically induced pectin gels that is truly bottom-up.

Firstly, information about the structures of assembled elementary network strands in different microrheologically well-characterized pectin networks is gained by small angle X-ray scattering (SAXS) experiments paired with molecular modelling techniques. This will be elaborated in Chapter 2. After finding networks in which large single chain contributions indeed play a major role, and with experimental single chain properties in hand, we propose a 2-dimensional model for such biopolymer networks. This enables questions about the possible macroscopic functionality of force induced conformational transitions to be investigated. A computational approach was then pursued to study the micro- and macroscopic network behaviour (Chapter 3). To finally test the model experimentally, rheological prestress measurements of an enzymatically induced pectin gel, a biomimetic system with dominating single-chain contributions, are made and are compared with the results from a three-

dimensional numeric simulation (Chapter 4).

References

[1] P. G. De Gennes. Soft matter. *Science*, 256(5056):495–497, 1992. doi: 10.1126/science.256.5056.495. 1

[2] A. R. Bausch and K. Kroy. A bottom-up approach to cell mechanics. *Nature Physics*, 2(4):231–238, 2006. doi: 10.1038/nphys260. 1

[3] I. Levental, P. C. Georges, and P. A. Janmey. Soft biological materials and their impact on cell function. *Soft Matter*, 3(3):299–306, 2007. doi: 10.1039/b610522j. 1, 27

[4] A. H. Clark and D. B. Farrer. Kinetics of biopolymer gelation - implications of a cascade theory description for the concentration, molecular-weight, and temperature dependences of the shear modulus and gel time. *Journal of Rheology*, 39(6):1429–1444, 1995. doi: 10.1122/1.550645. ix, 2, 7

[5] P. J. Flory. Network structure and the elastic properties of vulcanized rubber. *Chemical Reviews*, 35(1):51–75, 1944. doi: 10.1021/cr60110a002. 2

[6] Michael Rubinstein and Ralph H. Colby. *Polymer physics*. Oxford; New York: Oxford University Press, 2003. ix, 2, 8, 11

[7] Masao Doi. *Introduction to polymer physics*. New York: Oxford University Press; Oxford: Clarendon, 1995. 2

[8] H.A. Barnes, J.F. Hutton, and K. Walters. *An introduction to rheology*. Amsterdam; New York: Elsevier, 1989. 3

[9] D. T. N. Chen, Q. Wen, P. A. Janmey, J. C. Crocker, and A. G. Yodh. Rheology of soft materials. *Annual Review of Condensed Matter Physics, Vol 1*, 1:301–322, 2010. doi: 10.1146/annurev-conmatphys-070909-104120. ix, 3

[10] L. Starrs and P. Bartlett. One- and two-point micro-rheology of viscoelastic media. *Journal of Physics-condensed Matter*, 15(1):S251–S256, 2003. doi: 10.1088/0953-8984/15/1/333. ix, 3

[11] J. C. Crocker, M. T. Valentine, E. R. Weeks, T. Gisler, P. D. Kaplan, A. G. Yodh, and D. A. Weitz. Two-point microrheology of inhomogeneous soft materials. *Physical Review Letters*, 85(4):888–891, 2000. doi: 10.1103/PhysRevLett.85.888. ix, 3

[12] F. Benmouna and D. Johannsmann. Viscoelasticity of gelatin surfaces probed by afm noise analysis. *Langmuir*, 20(1):188–193, 2004. doi: 10.1021/la0355794. ix, 3

[13] I. Cohen, B. Davidovitch, A. B. Schofield, M. P. Brenner, and D. A. Weitz. Slip, yield, and bands in colloidal crystals under oscillatory shear. *Physical Review Letters*, 97(21):215502, 2006. doi: 10.1103/PhysRevLett.97.215502. ix, 3

[14] K. H. Meyer and C. Ferri. On elasticity of rubber. *Helvetica Chimica Acta*, 18:570–589, 1935. 4

[15] W. Kuhn. Relationship between molecular size, static molecular shape and elastic characteristics of high polymer materials. *Kolloid-zeitschrift*, 76(3): 258–271, 1936. 4

[16] P. J. Flory and J. Rehner. Statistical mechanics of cross-linked polymer networks i rubberlike elasticity. *Journal of Chemical Physics*, 11(11):512–520, 1943. doi: 10.1063/1.1723791. 4

[17] P. G. De Gennes. Reptation of a polymer chain in presence of fixed obstacles. *Journal of Chemical Physics*, 55(2):572–579, 1971. doi: 10.1063/1.1675789. 6

[18] T. T. Perkins, D. E. Smith, and S. Chu. Direct observation of tube-like motion of a single polymer-chain. *Science*, 264(5160):819–822, 1994. doi: 10.1126/science.8171335. 6

[19] G. Ronca and G. Allegra. Approach to rubber elasticity with internal constraints. *Journal of Chemical Physics*, 63(11):4990–4997, 1975. doi: 10.1063/1.431245. 6

[20] A. Kloczkowski, J. E. Mark, and B. Erman. A diffused-constraint theory for the elasticity of amorphous polymer networks .1. fundamentals and stress-strain isotherms in elongation. *Macromolecules*, 28(14):5089–5096, 1995. doi: 10.1021/ma00118a043. 6

[21] M. Rubinstein and S. Panyukov. Nonaffine deformation and elasticity of polymer networks. *Macromolecules*, 30(25):8036–8044, 1997. doi: 10.1021/ma970364k. 6

[22] R. S. Rivlin and D. W. Saunders. Large elastic deformations of isotropic materials .7. experiments on the deformation of rubber. *Philosophical Transactions of the Royal Society of London Series A-mathematical and Physical Sciences*, 243(865):251–288, 1951. 6

[23] M. Gordon. Goods theory of cascade processes applied to statistics of polymer distributions. *Proceedings of the Royal Society of London Series A-mathematical and Physical Sciences*, 268(1333):240–&, 1962. doi: 10.1098/rspa.1962.0136. 6

[24] M. Gordon and S. B. Rossmurphy. Structure and properties of molecular trees and networks. *Pure And Applied Chemistry*, 43(1-2):1–26, 1975. doi: 10.1351/pac197543010001. 6

[25] L. C. Case. Branching in polymers .1. network defects. *Journal Of Polymer Science*, 45(146):397–404, 1960. doi: 10.1002/pol.1960.1204514609. 6

[26] J. Scanlan. The effect of network flaws on the elastic properties of vulcanizates. *Journal Of Polymer Science*, 43(142):501–508, 1960. doi: 10.1002/pol.1960.1204314219. 6

[27] A. H. Clark. The application of network theory to food systems. In JMV Blanshard and P. Lillford, editors, *Food structure and behavior*, pages 13–34. Academic Press, London, 1987. 7

[28] A. H. Clark. Rationalization of the elastic-modulus molecular-weight relationship for kappa-carrageenan gels using cascade theory. *Carbohydrate Polymers*, 23(4):247–251, 1994. doi: 10.1016/0144-8617(94)90186-4. 7

[29] A. H. Clark, K. T. Evans, and D. B. Farrer. Shear modulus-temperature meltdown profiles of gelatin and pectin gels - a cascade theory description. *International Journal of Biological Macromolecules*, 16(3):125–130, 1994. doi: 10.1016/0141-8130(94)90038-8. 7

[30] C. Loret, V. Meunier, W. J. Frith, and P. J. Fryer. Rheological characterisation of the gelation behaviour of maltodextrin aqueous solutions. *Carbohydrate Polymers*, 57(2):153–163, 2004. doi: 10.1016/j.carbpol.2004.03.026. 7

[31] E. Frey and K. Kroy. Brownian motion: a paradigm of soft matter and biological physics. *Annalen Der Physik*, 14(1-3):20–50, 2005. doi: 10.1002/andp.200410132. 7

[32] A. Einstein. The motion of elements suspended in static liquids as claimed in the molecular kinetic theory of heat. *Annalen Der Physik*, 17(8):549–560, 1905. 7

[33] P. E. Rouse. A theory of the linear viscoelastic properties of dilute solutions of coiling polymers. *Journal Of Chemical Physics*, 21(7):1272–1280, 1953. doi: 10.1063/1.1699180. 8

[34] D. F. Hodgson and E. J. Amis. Dynamic viscoelasticity of dilute polyelectrolyte solutions. *Journal of Chemical Physics*, 94(6):4581–4586, 1991. doi: 10.1063/1.460586. 10

[35] S. C. Lin and J. M. Schurr. Dynamic light-scattering-studies of internal motions in dna .1. applicability of rouse-zimm model. *Biopolymers*, 17(2):425–461, 1978. doi: 10.1002/bip.1978.360170211. 10

[36] T. G. Mason. Estimating the viscoelastic moduli of complex fluids using the generalized stokes-einstein equation. *Rheologica Acta*, 39(4):371–378, 2000. doi: 10.1007/s003970000094. 10

[37] B. Dunweg and K. Kremer. Microscopic verification of dynamic scaling in dilute polymer-solutions - a molecular-dynamics simulation. *Physical Review Letters*, 66(23):2996–2999, 1991. doi: 10.1103/PhysRevLett.66.2996. 10

[38] T. A. Waigh. Microrheology of complex fluids. *Reports On Progress In Physics*, 68(3):685–742, 2005. doi: 10.1088/0034-4885/68/3/R04. ix, 12

[39] F. C. M. MacKintosh. Elasticity and dynamics of cytoskeletal filaments and their networks. In *Soft Condensed Matter Physics in Molecular and Cell Biology*, pages 139–155, 2006. doi: 10.1201/9781420003338.pt2. ix, 11, 13

[40] F. Gittes, B. Mickey, J. Nettleton, and J. Howard. Flexural rigidity of microtubules and actin-filaments measured from thermal fluctuations in shape. *Journal of Cell Biology*, 120(4):923–934, 1993. doi: 10.1083/jcb.120.4.923. xv, 11, 12, 13

[41] O. Kratky and G. Porod. Rontgenuntersuchung geloster fadenmolekule. *Recueil Des Travaux Chimiques Des Pays-bas-journal of the Royal Netherlands Chemical Society*, 68(12):1106–1122, 1949. doi: 10.1002/recl.19490681203. 11

[42] K. Nakajima, H. Watabe, and T. Nishi. Single polymer chain rubber elasticity investigated by atomic force microscopy. *Polymer*, 47(7):2505–2510, 2006. doi: 10.1016/j.polymer.2005.12.092. xv, 13, 15

[43] S. Cros, C. Garnier, M. A. V. Axelos, A. Imberty, and S. Perez. Solution conformations of pectin polysaccharides: Determination of chain characteristics by small angle neutron scattering, viscometry, and molecular modeling. *Biopolymers*, 39(3):339–352, 1996. doi: 10.1002/(SICI)1097-0282(199609)39:3<339::AID-BIP6>3.0.CO;2-P. xv, 13

[44] W. H. Taylor and P. J. Hagerman. Application of the method of phage-t4 dna ligase-catalyzed ring-closure to the study of dna-structure .2. nacl-dependence of dna flexibility and helical repeat. *Journal of Molecular Biology*, 212(2): 363–376, 1990. doi: 10.1016/0022-2836(90)90131-5. xv, 13

[45] F. Pampaloni, G. Lattanzi, A. Jonas, T. Surrey, E. Frey, and E. L. Florin. Thermal fluctuations of grafted microtubules provide evidence of a length-dependent persistence length. *Proceedings of the National Academy of Sciences of the United States of America*, 103(27):10248–10253, 2006. doi: 10.1073/pnas.0603931103. xv, 13

[46] F. C. MacKintosh, J. Kas, and P. A. Janmey. Elasticity of semiflexible biopolymer networks. *Physical Review Letters*, 75(24):4425–4428, 1995. doi: 10.1103/PhysRevLett.75.4425. 13, 20

[47] J. F. Marko and E. D. Siggia. Stretching dna. *Macromolecules*, 28(26):8759–8770, 1995. doi: 10.1021/ma00130a008. ix, 15, 16

[48] C. Bustamante, J. F. Marko, E. D. Siggia, and S. Smith. Entropic elasticity of lambda-phage dna. *Science*, 265(5178):1599–1600, 1994. doi: 10.1126/science.8079175. 15

[49] M. S. Z. Kellermayer, S. B. Smith, H. L. Granzier, and C. Bustamante. Folding-unfolding transitions in single titin molecules characterized with

laser tweezers. *Science*, 276(5315):1112–1116, 1997. doi: 10.1126/science.276.5315.1112. 15

[50] M. Rief, M. Gautel, F. Oesterhelt, J. M. Fernandez, and H. E. Gaub. Reversible unfolding of individual titin immunoglobulin domains by afm. *Science*, 276(5315):1109–1112, 1997. doi: 10.1126/science.276.5315.1109. 15

[51] P. E. Marszalek, Y. P. Pang, H. B. Li, J. El Yazal, A. F. Oberhauser, and J. M. Fernandez. Atomic levers control pyranose ring conformations. *Proceedings of the National Academy of Sciences of the United States of America*, 96(14): 7894–7898, 1999. doi: 10.1073/pnas.96.14.7894. 15

[52] M. D. Wang, H. Yin, R. Landick, J. Gelles, and S. M. Block. Stretching dna with optical tweezers. *Biophysical Journal*, 72(3):1335–1346, 1997. doi: 10.1016/S0006-3495(97)78780-0. 15

[53] R. G. Haverkamp, A. T. Marshall, and M. A. K. Williams. Model for stretching elastic biopolymers which exhibit conformational transformations. *Physical Review E*, 75(2):021907, 2007. doi: 10.1103/PhysRevE.75.021907. 15

[54] T. E. Cloutier and J. Widom. Spontaneous sharp bending of double-stranded dna. *Molecular Cell*, 14(3):355–362, 2004. doi: 10.1016/S1097-2765(04)00210-2. 15

[55] P. A. Wiggins, R. Phillips, and P. C. Nelson. Exact theory of kinkable elastic polymers. *Physical Review E*, 71(2):021909, 2005. doi: 10.1103/PhysRevE.71.021909. 15

[56] H. Yamakawa. *Helical wormlike chains in polymer solutions*. Berlin; New York: Springer, 1997. 15

[57] P. A. Wiggins and P. C. Nelson. Generalized theory of semiflexible polymers. *Physical Review E*, 73(3):031906, 2006. doi: 10.1103/PhysRevE.73.031906. 15

[58] H. Isambert and A. C. Maggs. Dynamics and rheology of actin solutions. *Macromolecules*, 29(3):1036–1040, 1996. doi: 10.1021/ma946418x. 17

[59] R. A. Harris and J. E. Hearst. On polymer dynamics. *Journal of Chemical Physics*, 44(7):2595–&, 1966. doi: 10.1063/1.1727098. 17

[60] S. R. Aragon and R. Pecora. Dynamics of wormlike chains. *Macromolecules*, 18(10):1868–1875, 1985. doi: 10.1021/ma00152a014. 17

[61] E. Farge and A. C. Maggs. Dynamic scattering from semiflexible polymers. *Macromolecules*, 26(19):5041–5044, 1993. doi: 10.1021/ma00071a009. 17

[62] F. Gittes and F. C. MacKintosh. Dynamic shear modulus of a semiflexible polymer network. *Physical Review E*, 58(2):R1241–R1244, 1998. doi: 10.1103/PhysRevE.58.R1241. 17

[63] D. C. Morse. Viscoelasticity of tightly entangled solutions of semiflexible polymers. *Physical Review E*, 58(2):R1237–R1240, 1998. doi: 10.1103/PhysRevE.58.R1237. 17

[64] D. C. Morse. Tube diameter in tightly entangled solutions of semiflexible polymers. *Physical Review E*, 63(3):031502, 2001. doi: 10.1103/PhysRevE.63.031502. 18

[65] B. D. Hoffman, G. Massiera, K. M. Van Citters, and J. C. Crocker. The consensus mechanics of cultured mammalian cells. *Proceedings of the National Academy of Sciences of the United States of America*, 103(27):10259–10264, 2006. doi: 10.1073/pnas.0510348103. 18

[66] L. H. Deng, X. Trepat, J. P. Butler, E. Millet, K. G. Morgan, D. A. Weitz, and J. J. Fredberg. Fast and slow dynamics of the cytoskeleton. *Nature Materials*, 5(8):636–640, 2006. doi: 10.1038/nmat1685. 18, 29

[67] B. Fabry, G. N. Maksym, J. P. Butler, M. Glogauer, D. Navajas, and J. J. Fredberg. Scaling the microrheology of living cells. *Physical Review Letters*, 87(14):148102, 2001. doi: 10.1103/PhysRevLett.87.148102. 18

[68] P. Sollich. Rheological constitutive equation for a model of soft glassy materials. *Physical Review E*, 58(1):738–759, 1998. doi: 10.1103/PhysRevE.58.738. ix, 18

[69] D. Bonn, P. Coussot, H. T. Huynh, F. Bertrand, and G. Debregeas. Rheology of soft glassy materials. *Europhysics Letters*, 59(5):786–792, 2002. doi: 10.1209/epl/i2002-00195-4. 18

[70] K. Kroy and J. Glaser. The glassy wormlike chain. *New Journal Of Physics*, 9:416, 2007. doi: 10.1088/1367-2630/9/11/416. 19

[71] K. Kroy. Dynamics of wormlike and glassy wormlike chains. *Soft Matter*, 4 (12):2323–2330, 2008. doi: 10.1039/b807018k. ix, 19, 20

[72] C. Semmrich, T. Storz, J. Glaser, R. Merkel, A. R. Bausch, and K. Kroy. Glass transition and rheological redundancy in f-actin solutions. *Proceedings Of The National Academy Of Sciences Of The United States Of America*, 104 (51):20199–20203, 2007. doi: 10.1073/pnas.0705513104. 19, 22, 27

[73] K. Kroy and E. Frey. Force-extension relation and plateau modulus for wormlike chains. *Physical Review Letters*, 77(2):306–309, 1996. doi: 10.1103/PhysRevLett.77.306. 20, 22

[74] C. Storm, J. J. Pastore, F. C. MacKintosh, T. C. Lubensky, and P. A. Janmey. Nonlinear elasticity in biological gels. *Nature*, 435(7039):191–194, 2005. doi: 10.1038/nature03521. x, 20, 24, 25, 27

[75] B. Hinner, M. Tempel, E. Sackmann, K. Kroy, and E. Frey. Entanglement, elasticity, and viscous relaxation of actin solutions. *Physical Review Letters*, 81(12):2614–2617, 1998. doi: 10.1103/PhysRevLett.81.2614. 20

[76] J. M. Adams, Y. Mao, and W. L. Vandoolaeghe. Stress relaxation in polymer networks: Equilibrium behavior and dynamics. *Journal Of Chemical Physics*, 127(11):114907, 2007. doi: 10.1063/1.2768921. 20

[77] M. Doi and S. F. Edwards. *The Theory of Polymer Dynamics*. Oxford University Press, USA, 1986. 20

[78] J. Wilhelm and E. Frey. Elasticity of stiff polymer networks. *Physical Review Letters*, 91(10):108103, 2003. doi: 10.1103/PhysRevLett.91.108103. x, 21, 22, 23

[79] C. Heussinger, B. Schaefer, and E. Frey. Nonaffine rubber elasticity for stiff polymer networks. *Physical Review E*, 76(3):031906, 2007. doi: 10.1103/PhysRevE.76.031906. 21, 26

[80] C. Heussinger and E. Frey. Stiff polymers, foams, and fiber networks. *Physical Review Letters*, 96(1):017802, 2006. doi: 10.1103/PhysRevLett.96.017802. 21, 22

[81] D. A. Head, F. C. MacKintosh, and A. J. Levine. Nonuniversality of elastic exponents in random bond-bending networks. *Physical Review E*, 68(2): 025101, 2003. doi: 10.1103/PhysRevE.68.025101. 21, 22

[82] D. A. Head, A. J. Levine, and F. C. MacKintosh. Distinct regimes of elastic response and deformation modes of cross-linked cytoskeletal and semiflexible polymer networks. *Physical Review E*, 68(6):061907, 2003. doi: 10.1103/PhysRevE.68.061907. x, 21, 22, 23

[83] D. A. Head, A. J. Levine, and F. C. MacKintosh. Deformation of cross-linked semiflexible polymer networks. *Physical Review Letters*, 91(10):108102, 2003. doi: 10.1103/PhysRevLett.91.108102. 21

[84] J. Astrom, S. Saarinen, K. Niskanen, and J. Kurkijarvi. Microscopic mechanics of fiber networks. *Journal Of Applied Physics*, 75(5):2383–2392, 1994. doi: 10.1063/1.356259. ix, 21

[85] Harry Kesten. What is... percolation? *Notices of the American Mathematical Society*, 53(5):572–573, May 2006. URL `http://www.ams.org/notices/200605/what-is-kesten.pdf`. 21

[86] M. L. Gardel, J. H. Shin, F. C. MacKintosh, L. Mahadevan, P. Matsudaira, and D. A. Weitz. Elastic behavior of cross-linked and bundled actin networks. *Science*, 304(5675):1301–1305, 2004. doi: 10.1126/science.1095087. x, 22, 23, 24, 25, 27

[87] K. M. Schmoller, O. Lieleg, and A. R. Bausch. Structural and viscoelastic properties of actin/filamin networks: Cross-linked versus bundled networks. *Biophysical Journal*, 97(1):83–89, 2009. doi: 10.1016/j.bpj.2009.04.040. 22

[88] C. Semmrich, R. J. Larsen, and A. R. Bausch. Nonlinear mechanics of entangled f-actin solutions. *Soft Matter*, 4(8):1675–1680, 2008. doi: 10.1039/b800989a. 22, 28

[89] M. L. Gardel, J. H. Shin, F. C. MacKintosh, L. Mahadevan, P. A. Matsudaira, and D. A. Weitz. Scaling of f-actin network rheology to probe single filament elasticity and dynamics. *Physical Review Letters*, 93(18):188102, 2004. doi: 10.1103/PhysRevLett.93.188102. 24, 25

[90] P. A. Janmey, M. E. Mccormick, S. Rammensee, J. L. Leight, P. C. Georges, and F. C. Mackintosh. Negative normal stress in semiflexible biopolymer gels. *Nature Materials*, 6(1):48–51, 2007. doi: 10.1038/nmat1810. x, 24, 25, 27

[91] Q. Wen, A. Basu, J. P. Winer, A. Yodh, and P. A. Janmey. Local and global deformations in a strain-stiffening fibrin gel. *New Journal of Physics*, 9:428, 2007. doi: 10.1088/1367-2630/9/11/428. 24, 25, 27

[92] H. Kang, Q. Wen, P. A. Janmey, J. X. Tang, E. Conti, and F. C. MacKintosh. Nonlinear elasticity of stiff filament networks: Strain stiffening, negative normal stress, and filament alignment in fibrin gels. *Journal of Physical Chemistry B*, 113(12):3799–3805, 2009. doi: 10.1021/jp807749f. 24, 26, 27

[93] J. H. Poynting. On pressure perpendicular to the shear planes in finite pure shears, and on the lenghtening of loaded wires when twisted. *Proceedings of the Royal Society of London Series A-containing Papers of A Mathematical and Physical Character*, 82(557):546–559, 1909. 24

[94] J. S. Palmer and M. C. Boyce. Constitutive modeling of the stress-strain behavior of f-actin filament networks. *Acta Biomaterialia*, 4(3):597–612, 2008. doi: 10.1016/j.actbio.2007.12.007. 25

[95] C. F. Schmidt, M. Barmann, G. Isenberg, and E. Sackmann. Chain dynamics, mesh size, and diffusive transport in networks of polymerized actin - a quasielastic light-scattering and microfluorescence study. *Macromolecules*, 22 (9):3638–3649, 1989. 25

[96] Y. C. Lin, N. Y. Yao, C. P. Broedersz, H. Herrmann, F. C. MacKintosh, and D. A. Weitz. Origins of elasticity in intermediate filament networks. *Physical Review Letters*, 104(5):058101, 2010. doi: 10.1103/PhysRevLett.104.058101. 25

[97] N. Y. Yao, C. P. Broedersz, Y. C. Lin, K. E. Kasza, F. C. MacKintosh, and D. A. Weitz. Elasticity in ionically cross-linked neurofilament networks. *Biophysical Journal*, 98(10):2147–2153, 2010. doi: 10.1016/j.bpj.2010.01.062. 25

[98] J. R. Blundell and E. M. Terentjev. Stretching semiflexible filaments and their networks. *Macromolecules*, 42(14):5388–5394, 2009. doi: 10.1021/ma9004633. x, 26

[99] P. R. Onck, T. Koeman, T. van Dillen, and E. van der Giessen. Alternative explanation of stiffening in cross-linked semiflexible networks. *Physical Review Letters*, 95(17):178102, 2005. doi: 10.1103/PhysRevLett.95.178102. 26

[100] E. M. Huisman, T. van Dillen, P. R. Onck, and E. Van der Giessen. Three-dimensional cross-linked f-actin networks: Relation between network architecture and mechanical behavior. *Physical Review Letters*, 99(20):208103, 2007. doi: 10.1103/PhysRevLett.99.208103. 26

[101] J. A. Astrom, P. B. S. Kumar, I. Vattulainen, and M. Karttunen. Strain hardening, avalanches, and strain softening in dense cross-linked actin networks. *Physical Review E*, 77(5):051913, 2008. doi: 10.1103/PhysRevE.77.051913. 26, 27

[102] T. van Dillen, P. R. Onck, and E. Van der Giessen. Models for stiffening in cross-linked biopolymer networks: A comparative study. *Journal of the Mechanics and Physics of Solids*, 56(6):2240–2264, 2008. doi: 10.1016/j.jmps.2008.01.007. 27

[103] O. Lieleg and A. R. Bausch. Cross-linker unbinding and self-similarity in bundled cytoskeletal networks. *Physical Review Letters*, 99(15):158105, 2007. doi: 10.1103/PhysRevLett.99.158105. 27

[104] C. P. Broedersz, C. Storm, and F. C. MacKintosh. Nonlinear elasticity of composite networks of stiff biopolymers with flexible linkers. *Physical Review Letters*, 101(11):118103, 2008. doi: 10.1103/PhysRevLett.101.118103. 27, 28

[105] O. Lieleg, M. M. A. E. Claessens, and A. R. Bausch. Structure and dynamics of cross-linked actin networks. *Soft Matter*, 6(2):218–225, 2010. doi: 10.1039/b912163n. 27

[106] D. Mizuno, C. Tardin, C. F. Schmidt, and F. C. MacKintosh. Nonequilibrium mechanics of active cytoskeletal networks. *Science*, 315(5810):370–373, 2007. doi: 10.1126/science.1134404. 27, 28

[107] G. H. Koenderink, Z. Dogic, F. Nakamura, P. M. Bendix, F. C. MacKintosh, J. H. Hartwig, T. P. Stossel, and D. A. Weitz. An active biopolymer network controlled by molecular motors. *Proceedings of the National Academy of Sciences of the United States of America*, 106(36):15192–15197, 2009. doi: 10.1073/pnas.0903974106. 27, 28

[108] N. Rosenblatt, A. M. Alencar, A. Majumdar, B. Suki, and D. Stamenovic. Dynamics of prestressed semiflexible polymer chains as a model of cell rheology. *Physical Review Letters*, 97(16):168101, 2006. doi: 10.1103/PhysRevLett.97.168101. 27, 28

[109] O. Chaudhuri, S. H. Parekh, and D. A. Fletcher. Reversible stress softening of actin networks. *Nature*, 445(7125):295–298, 2007. doi: 10.1038/nature05459. 27

[110] K. A. Erk, K. J. Henderson, and K. R. Shull. Strain stiffening in synthetic and biopolymer networks. *Biomacromolecules*, 11(5):1358–1363, 2010. doi: 10.1021/bm100136y. 27

[111] J. H. Zhang, C. R. Daubert, and E. A. Foegeding. A proposed strain-hardening mechanism for alginate gels. *Journal of Food Engineering*, 80(1):157–165, 2007. doi: 10.1016/j.jfoodeng.2006.04.057. 27

[112] S. Kawai, Y. Nitta, and K. Nishinari. Model study for large deformation of physical polymeric gels. *Journal of Chemical Physics*, 128(13):134903, 2008. doi: 10.1063/1.2894845. 27

[113] C. P. Broedersz, K. E. Kasza, L. M. Jawerth, S. Munster, D. A. Weitz, and F. C. MacKintosh. Measurement of nonlinear rheology of cross-linked biopolymer gels. *Soft Matter*, 6(17):4120–4127, 2010. doi: 10.1039/c0sm00285b. 28

[114] C. P. Broedersz, C. Storm, and F. C. MacKintosh. Effective-medium approach for stiff polymer networks with flexible cross-links. *Physical Review E*, 79(6): 061914, 2009. doi: 10.1103/PhysRevE.79.061914. 28

[115] K. E. Kasza, G. H. Koenderink, Y. C. Lin, C. P. Broedersz, W. Messner, F. Nakamura, T. P. Stossel, F. C. MacKintosh, and D. A. Weitz. Nonlinear elasticity of stiff biopolymers connected by flexible linkers. *Physical Review E*, 79(4):041928, 2009. doi: 10.1103/PhysRevE.79.041928. 28

[116] B. A. DiDonna and A. J. Levine. Filamin cross-linked semiflexible networks: Fragility under strain. *Physical Review Letters*, 97(6):068104, 2006. doi: 10.1103/PhysRevLett.97.068104. 28

[117] B. A. DiDonna and A. J. Levine. Unfolding cross-linkers as rheology regulators in f-actin networks. *Physical Review E*, 75(4):041909, 2007. doi: 10.1103/PhysRevE.75.041909. 28

[118] B. D. Hoffman, G. Massiera, and J. C. Crocker. Fragility and mechanosensing in a thermalized cytoskeleton model with forced protein unfolding. *Physical Review E*, 76(5):051906, 2007. doi: 10.1103/PhysRevE.76.051906. 28

[119] E. M. Huisman, C. Heussinger, C. Storm, and G. T. Barkema. Semiflexible filamentous composites. *Physical Review Letters*, 105(11):118101, 2010. doi: 10.1103/PhysRevLett.105.118101. 28

[120] K. Kroy and R. R Vincent. (private communication). x, 29

[121] F. C. MacKintosh and A. J. Levine. Nonequilibrium mechanics and dynamics of motor-activated gels. *Physical Review Letters*, 100(1):018104, 2008. doi: 10.1103/PhysRevLett.100.018104. 28

[122] Peng Chen and Vivek B. Shenoy. Strain stiffening induced by molecular motors in active crosslinked biopolymer networks. *Soft Matter*, 7(2):355–358, 2011. ISSN 1744-683X. URL `http://dx.doi.org/10.1039/C0SM00908C`. 28

[123] A. Caspi, M. Elbaum, R. Granek, A. Lachish, and D. Zbaida. Semiflexible polymer network: A view from inside. *Physical Review Letters*, 80(5):1106–1109, 1998. doi: 10.1103/PhysRevLett.80.1106. 28

[124] A. Majumdar, B. Suki, N. Rosenblatt, A. M. Alencar, and D. Stamenovic. Power-law creep behavior of a semiflexible chain. *Physical Review E*, 78(4): 041922, 2008. doi: 10.1103/PhysRevE.78.041922. 28

[125] B. Obermayer and E. Frey. Tension dynamics and viscoelasticity of extensible wormlike chains. *Physical Review E*, 80(4):040801, 2009. doi: 10.1103/PhysRevE.80.040801. 28

[126] K. M. Schmoller, O. Lieleg, and A. R. Bausch. Internal stress in kinetically trapped actin bundle networks. *Soft Matter*, 4(12):2365–2367, 2008. doi: 10.1039/b808582j. 29

[127] B. D. Hoffman and J. C. Crocker. Cell mechanics: Dissecting the physical responses of cells to force. *Annual Review of Biomedical Engineering*, 11: 259–288, 2009. doi: 10.1146/annurev.bioeng.10.061807.160511. 29

[128] R. R. Vincent. *Microrheological investigations of biopolymer networks*. PhD thesis, Massey University, Palmerston North, New Zealand, 2008. URL `http://hdl.handle.net/10179/764`. 30

Chapter 2

The nature & architecture of network strands in pectin gels

2.1 Introduction

In order to be able to model the mechanical properties of biomaterials, we first need to shed light on the connectivity of the network strands and the nature of the junction zones. As depicted in the previous Chapter in Figure 1 the long-range order within such gels could arise from different single chain assembly modalities. Amongst these, two extreme models contain either a pseudo rubber-like network in which short point-like junction zones are linked by long, single-chain sections, or a gel in which several molecules form fibrous structures that latterly become entangled and cross-linked. Whereas mircorheology has proven as a useful tool to conclude indirectly via the high frequency response of the shear modulus the single filament properties [1], SAXS on the other hand allows a direct structural characterization of soft matter systems and to determine the shape and size of molecular aggregations at nano-scales [2].

Pectin is a ubiquitous polysaccharide in higher terrestrial plants [3], where it is known to play a considerable role in mediating the mechanical properties of the plant cell wall and is key to many physiological processes including the regulation of the growth of a pollen tube [4] and the control of inter-cellular adhesion [5]. While unequivocally establishing the exact architecture of the pectic macromolecular complex in-muro is still a work in progress, commercial pectin samples, which are typically obtained from citrus peel or apple pomace, are found, after extraction, to consist mainly of linear chains of homogalacturonan (HG), (typically 90%), a polysaccharide consisting of one type of sugar ring, a 1,4 linked α-D-galacturonate residue that is often methyl-esterified. The degree of methylesterification (DM)

and its distribution is of primary importance to the polymer's function and is particularly closely linked to its ionic binding abilities. Specifically, the HG sections largely determine the gelling capabilities of pectin [6], with the capacity of the free (unmethyl-esterified) carboxyl groups to bind calcium ions inducing assembly of the chains and network formation. A number of consecutive unesterified sugar residues, estimated to be between 8 and 15 at ambient temperature, is required to form a stable cross-link (junction zone) between two chains in the presence of calcium ions [7, 8]. Following extraction from the cell wall the HG portions of the pectin chains are typically found to be between 60 and 85 % methylesterified and post-processing with base or demethylesterifying enzymes is typically used to control the amount and distribution of the calcium binding groups in order to produce commercial samples with desired functionality, generally with a DM < 50 (low methoxy pectins). For these low DM pectins consecutive sequences of unmethylesterifed groups are present in sufficient quantities to form ionotropic networks at around 1% polymer concentration even if the starting extract substrate has been demethylesterified simply according to random processes, as is typically carried out commercially. Alternatively, blocks of unmethylesterified galacturonic acid can be introduced by tailoring the intramolecular DM distribution with processive plant pectinmethylesterase (PME) enzymes. This can be carried out in-vitro and to some extent presents a closer biomimetic system of processes going on in the cell wall in-vivo. Indeed, using PME to gel high DM pectins in the presence of calcium has recently been of considerable interest [9, 10].

Multiple experimental approaches have been pursued in order to investigate the structure of pectin-pectin associations and attempt to decipher underlying structure-function relationships. Conformations of pectins themselves have been studied previously utilizing X-ray fibre diffraction [11], circular dichroism [12] and small angle neutron scattering (SANS) [13]; and their ionic associations in dilute solution have been further investigated by electrochemical methods [14] and isothermal calorimetry [15]. The application of transmission electron microscopy [16] and AFM imaging [17] provide real-space images of pectin chains and their assemblies and offer insights into the network architecture in calcium-induced gelled networks. Recent microrheological (MR) measurements of the high frequency mechanical response have also been interpreted with reference to the nature of the elementary building blocks of the network [18]. It was found that signatures of either semiflexible networks [19] or punctually cross-linked networks of mainly single-chain stress-bearing strands [20] could be observed, dependent on the experimental conditions of network assembly. To explain the fact that, by using different assembly conditions, gels could be

formed in which the elementary network strands were stiff to varying degrees, it was hypothesized that these different signatures reflected different network architectures, the extreme cases of which might be described as i) dimeric junction-zones of limited extent linked by considerably longer, reasonably flexible, single chain sections or ii) entangled, extensively-pre-bundled semiflexible dimeric junction zones [21, 17]. In order to test this hypothesis directly, microrheologically-distinct pectin gels have been generated using different assembly modalities (in particular by using different concentrations of polymer and cross-linking ions, or by contrasting the controlled-release of ions with the generation of ion-binding groups using a processive plant PME) and the resulting systems studied by small angle X-ray scattering (SAXS). Previous SAXS measurements of pectins undergoing the sol-gel transition [22] have indicated rod-like junction zones in the gel phase whose cross-section increased with calcium concentration, while the calcium induced gelation of another ionic polysaccharide, alginate, has been extensively investigated by SAXS [23, 24] and junction-zone bundle-size successfully estimated.

The connections between chains that facilitate network formation, the "junction-zones"; mediated by calcium ions in these ionotropic gels, have previously been described by an egg box model [7] - a cooperative pairing of chains that forms electronically negative cavities into which calcium ions are entrained. On the basis of more recent molecular modelling work, it has been proposed that, while the standard model works well for alginate gels (for which it was originally proposed), an adjusted egg-box model [25, 26], is a better description for pectin gels. This adjusted model provides slightly different dimeric conformations of minimal binding energy, and also suggests a two-stage process of calcium induced gelation, where the formation of strongly linked dimer associations is followed by the formation of weak inter-dimer associations. In the work reported here this adjusted egg-box model is used as a framework for the detailed analysis of the experimental SAXS data so that, in addition to obtaining estimates of an average cross-sectional radius of gyration by considering cross-sectional Guinier plots, estimates of the number of chains forming the network elements could be obtained.

2.2 Materials and methods

Pectin extracted from apples was purchased from Fluka Biochemika, with a DM value of (78 ± 3) % as a starting material. The sample had a quoted molecular weight of 30-100 kDa, although in-house experiments using AFM and SEC-MALLS suggest that the majority of the sample is well-described by (100 ± 10) kDa. The

galacturonic acid content of around 90% with the remaining weight made up by water, ions, and at most a few % rhamnogalacturonan I with a few % short galactose and arabinose side-chains (neutral sugar analysis puts the rhamnose content at 0.9%), so that to a very good approximation the polymers can be considered as homogalacturonan (copolymers of methylesterified or charged residues as described in the introduction). Small changes in the molecular weight or neutral sugar content of the starting material would not be expected to impact substantially on the conclusions presented herein. The sample average DM of this sample and all others produced by modification were determined using capillary electrophoresis (CE) as previously described [27, 28].

Pectinmethylesterase (PME) [EC 3.1.1.11] was purchased from Sigma Aldrich (P5400) in order to remove methyl-ester groups from the starting pectin substrate [29]. Stock solutions of the enzyme were prepared by dissolving 0.01 g of dried PME in 20 mL Milli-Q water with 0.58 g of NaCl, and were stored at 253 K in Eppendorf tubes. Aliquots were thawed prior to conducting experiments and used immediately. The enzyme was obtained from oranges and is known to largely comprise of a salt-independent isoform [30]. It has been reported that plant PMEs (pPMEs) initiate action on a methyl-esterified carboxyl group adjacent to an already de-esterified carboxyl group and then remove the neighbouring methyl ester components on the pectin chain progressively [31, 32]. This can result in areas containing long stretches of de-esterified galacturonic acid components on pectin chains, particularly if substrates are extensively de-methylesterified. pPME action is conventionally described by a multiple attack action mechanism, where the enzyme catalyses the transformation of a limited average number of residues at a time on one pectin chain [33], although this is likely to depend on the nature of the substrate and the precise mechanism of action is still a work in progress [32, 34]. It should also be noted that some evidence does exist, from the analysis of polymeric material recovered from induced gels, that if de-methylesterification is carried out in the presence of calcium, as is carried out herein for the enzyme generated gelled materials, subsequent chain association can hinder the subsequent enzyme action so that small blocks of around 10 consecutive galacturonic acid residues remain the most common motif [20].

$CaCO_3$ powder with a mean particle diameter of 1 μm was kindly provided by Provencale s.a., Avenue Frédéric Mistral, 83172 Brignoles Cedex, France.

Glucono-lactone (GDL) was purchased from Fisher Scientific, Bishop Meadow Rd, Loughbourough, LE11 5RG, UK.

Table 2.1: Pectin samples: nomenclature, polymer concentration c_P (%w/w), R_{eff} value, DM, MR exponent α (obtained from fitting data at $\tau < 10^{-4}$ s) and the gelling method; the samples are prepared as described in the text.

Sample	c_P	R_{eff}	DM	α	gelling method
SDsol	1.0	0.4	78 ± 3	–	–
PMEgel	1.0	0.4	< 60	$1/2$ (0.48 ± 0.01)	enzymatically induced
B71f	1.0	0.4	71 ± 2	$1/2$ (0.52 ± 0.02)	controlled calcium release
B63f	1.0	0.4	63 ± 2	$1/2$ (0.55 ± 0.02)	controlled calcium release
B71s	0.4	0.7	71 ± 2	$3/4$ (0.75 ± 0.01)	controlled calcium release
B63s	0.4	0.7	63 ± 2	$3/4$ (0.76 ± 0.01)	controlled calcium release

2.2.1 Sample preparation

Preparation of Calcium Sensitive Substrates. Pectin solutions of 1% w/w were made by dissolving the pectin powder in a 50 mM HEPES buffer, adjusted to pH 7.5 with NaOH. Enzyme solution (0.5 mL) was then mixed into 30 mL of the desired solution containing pectin, and the mixture left at 293 K for a chosen time, depending on the final DM decrease required and on the rate of the de-esterification processes. Assuming the enzymes followed a simple Michaelis-Menton model and were in the linear section of the product production curve (which was monitored independently using NMR to follow the liberation of methanol [35]), preliminary experiments were used to determine the rate of DM decrease as around 5.8% / h. Thus, the p-PME action could be stopped after a pre-requisite time in order to achieve a desired final DM. This quenching of the reaction was carried out by decreasing the pH and subsequently heating the solution at 353 K for 5 min to denature the enzyme. Subsequently, the modified polymers were extracted by dialysing the sample twice under acidic conditions against a 0.01 M solution of HCl, and finally twice against Milli-Q water. The dialyzed solutions were freeze dried and the engineered polymers recovered and stored dry. The recovered pectin samples had their fine structures analysed by CE. This material could then be gelled using traditional controlled release methodologies.

Controlled calcium release gels. Ionotropic pectin gels were obtained by slowly releasing calcium ions into solutions of pectin with fine structures determined by the prior enzyme processing described above [29]. The appropriate amounts of pectin were stirred, and immediately prior to loading into appropriate test cells a salt solution was added, the final mixing of which achieves the final desired concentration of the system. This aqueous salt solution was composed of $CaCO_3$ and GDL. The GDL hydrolyses with time, releasing protons that solubilise calcium ions from the $CaCO_3$. These components were introduced as powders into water, quickly mixed,

and added to the pectin solution as quickly as possible, in order to avoid significant calcium release before mixing with pectin. The quantity of $CaCO_3$ added determined the R_{eff} value, $R_{eff} = 2{\cdot}[Ca^{2+}]/[COO^-]_{eff}$ [21], and a stoichiometric ratio of $[GDL] = 2{\cdot}[Ca^{2+}]$ was used in order to maintain the pH of the solution [36]. After the addition of the salts the final prepared solution was stirred for a few minutes, and the samples were loaded into the appropriate test cell and left overnight.

Enzymatically Induced Pectin Gels. Stock pectin solutions of 1.8% w/w were prepared by dissolving the apple pectin powder in a 0.1 M HEPES buffer made with Milli-Q water, adjusting to pH 7.5 with NaOH, and stirring for 1 hour. Subsequently, desired volumes of $CaCl_2$ salt solution were added. The quantity of $CaCl_2$ and the availability of blocks of unesterified residues determines the R_{eff} value, which can, by controlling the amount and extent of interchain association, be varied to tune the elasticity of the material. Finally the sample is mixed with the desired volume of water, in order to reach a final polymer concentration of 1% w/w. As the starting pectin is of a high DM, it does not gel in the presence of the added Ca^{2+}. Before loading the solution in the test chamber, 100 μL of enzyme solution was added for 1.5 mL of pectin solution with a DM of 78, mixed and left overnight.

2.2.2 Analytical methods

Microrheological measurements. Diffusing wave spectroscopy (DWS) was used to measure the mean square displacement of probe particles in the samples. The DWS apparatus used in this study has been fully described in [37]. Briefly, the samples were contained in glass cells of width 10 mm, height 50 mm and path length of 4 mm, and were illuminated with a 35 mW He-Ne Melles-Griot laser operating at a wavelength of 633 nm. The laser beam was expanded to approximately 8 mm on the surface of the cell. The transmitted scattered light was detected using a single-mode optical fibre (P1-3224-PC-5, Thorlabs Inc., Germany). The optical fibre was connected to a Hamamatsu HC120-08 PMT photomultiplier tube module, and the intensity autocorrelation functions of the scattered light were obtained using a Malvern 7132 correlator.

SAXS. Measurements were performed at the SAXS / WAXS beamline at the Australian Synchrotron, Clayton, Australia [38] utilizing a high-intensity undulator source. An energy resolution of 10^{-4} was obtained from a cryo-cooled Si(111) double-crystal monochromator; and an X-ray beam with a wavelength of 0.83 Å (15 keV) was selected. The SAXS patterns were collected using a Pilatus 1 M detector (active area 169 x 179 mm^2 with a pixel size of 172 μm), which was located 2700 mm from the sample position, yielding a range of $q = 0.007 - 0.357$ $Å^{-1}$. Scattering

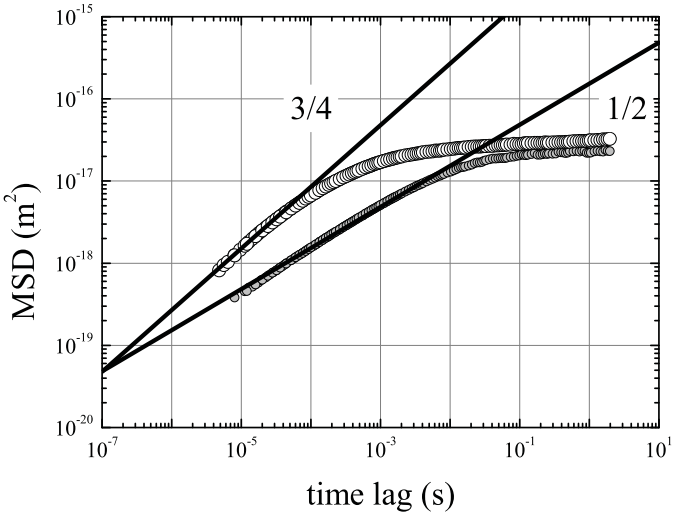

Figure 17: The resulting tracer particle MSDs obtained by DWS from gels created by the controlled release of calcium (as described in the experimental section) from B63f (small circles) and B63s (big circles).

patterns were acquired at 300 K using exposure times in the range of 1-10 s. The data processing was carried out using SAXS15ID software [39]. Acquired intensity data were normalized to equal incident count rate and equal transmission, and the contribution from reference solvents without the pectin was subtracted. Data obtained from air and water samples over exposure times of 1-60 s were utilized to obtain a calibration factor and convert the data into absolute intensities in cm^{-1}. The pectin gels were prepared as described above and cured overnight in home-made 4.2 mm thick aluminium sample cells with mica windows. The fact that in this set-up only the above mentioned detector distance is utilized, implies the limitation that angstrom-size structures cannot be resolved; but as the smallest building block of the polysaccharide gels of interest in this study is ~ 5 Å (diameter of a single sugar ring) the intricate task of resetting the detector-sample distance was elided to save beamline time.

2.3 Results and discussion

Scattering data were obtained as described from five different gelled samples, and additionally from one sample of the pre-gelled semi-dilute polymer solution (Table

2.1). In concurrent experiments another set of gelled samples was prepared in an identical manner, but additionally with the inclusion of a small phase volume of tracer particles, and their high frequency mechanical response was measured utilizing microrheological techniques as described in the materials and methods section. Typically results are shown for the gels formed with the DM 63% samples in Figure 17. The main objective of these experiments was to characterize the mechanical response of the gels and distinguish if the different networks were best described by stiffer semi-flexible entities or by more flexible single chains [21]. While this information is not contained in a simple storage modulus measurement, and difficult to access on a conventional rheometer owing to the limited frequency range accessible, it can be decided by microrheological experiments. These experiments measured the time evolution of the mean squared displacement of thermally driven probe particles embedded in the gels and allowed the exponent of the local power law t^{α} describing the data at short times to be obtained, wherein $\alpha \cong \frac{3}{4}$ is indicative of a semi-flexible regime and $\alpha \cong \frac{1}{2}$ for the more flexible regime respectively. The results are given in Table 2.1 and concur with expectations based on a previously suggested state-diagram [21].

Figure 18 shows the SAXS profiles of the studied pectin gels. Assuming that the intrinsic influence of the DM of the chains on the scattering is negligible (supported by calculations in the modelling section below) then the scattering behaviour of the initial high DM pectin solution (Figure 19 (a)) can be considered as a useful standard to compare to the behaviour exhibited by the gelled samples.

The scattering behaviour of semi-dilute polymer solutions is typically described by the Ornstein-Zernike (OZ) equation. [40]:

$$I(q) = \frac{I(0)}{1 + q^2\xi^2} \tag{2.1}$$

with ξ being the correlation length and $I(0)$ the intensity at $q = 0$. Rearranging Eq. (2.1) leads to

$$I(q)^{-1} = \frac{1}{I(0)} + \frac{\xi^2}{I(0)}q^2 \tag{2.2}$$

so that equivalently scattering profiles plotted in the Zimm representation, ($I(q)^{-1}$ vs. q^2), are predicted to be linear if the OZ equation can be successfully used to describe the behaviour (Figure 19 (b)). The data can indeed be successfully fitted by the OZ equation with a resulting correlation length (which reflects the length-scale (blob size) at which neighbouring chains start to interact [41]) of $\xi = 20.1 \pm 0.5$ Å. The deviation of the linear fit in the q range below 0.04 Å^{-1} indicates concentration

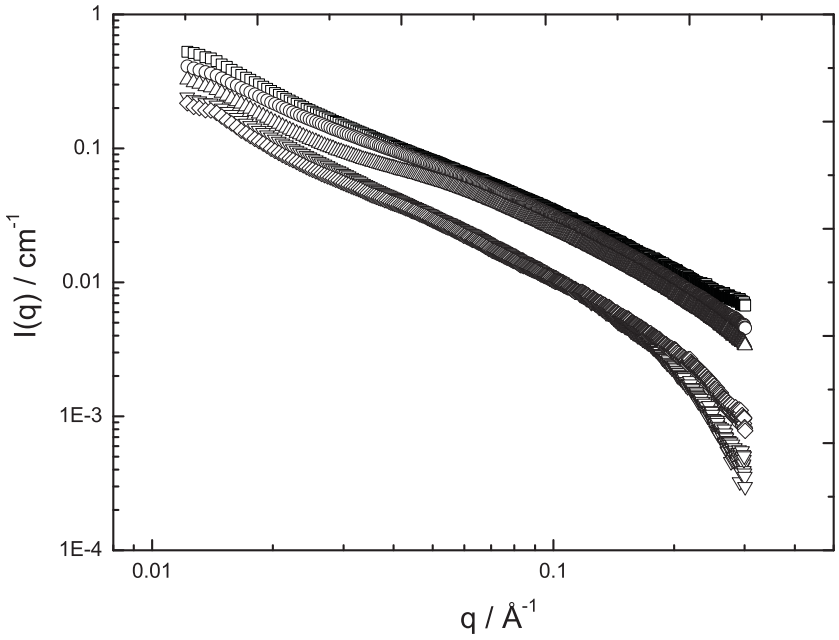

Figure 18: Small-angle x-ray scattering profiles $I(q)$ of the pectin gels PMEgel (□), B63f (◯), B71f (△), B71s (◇), B63s (▽).

fluctuations in the sample, possibly originating from a propensity for aggregation.

Moving to the gelled samples such a representation no longer captures the scattering behaviour and in order to gain insights into the dimensions of junction zones resulting from the different modes of network assembly distance distribution functions, cross-sectional Guinier plots ($ln(qI(q))$ vs. q^2), and furthermore a computer-based modelling approach have been applied.

By means of a Fourier inversion $I(q)$ can be converted into the *Distance Distribution Function* $p(r)$:

$$p(r) = \frac{1}{\pi^2} \int_0^\infty I(q) sin(qr) qr \, \mathrm{d}q \tag{2.3}$$

which contains the same information as $I(q)$, but provides in some cases a more intuitive visualization of the data [42]. Figure 20 shows $p(r)$ for all samples, gained by the application of the program GNOM [43]. The distributions are smeared out and seem to contain more complex structures which cannot easily be interpreted from visual inspection of $p(r)$. To gain insights into the dimensions of junction zones resulting from the different modes of network assembly cross-sectional Guinier plots ($ln(qI(q))$ vs. q^2), and furthermore a computer-based modelling approach have been applied.

The *cross-sectional radius of gyration* R_c of the scattering entities is accessible via fitting of the equation [42]

$$qI(q) \cong I(0) exp(-\frac{1}{2} R_c^2 q^2) \tag{2.4}$$

in the Guinier regime $q < 1/R_c$ ($0.005 < q^2 < 0.017 - 0.04$ depending on the sample) shown in Figure 21. The regions in which this approximation holds are indicated in the Figures and have been refined iteratively. This reveals information about the average bundle sizes, assuming rigid cylinders whose radius << cylinder-length. The samples exhibiting the more flexible network strands from the microrheological view, B71f and B63f, were found to give R_c values of 5.7 ± 0.1 Å and 5.6 ± 0.1 Å respectively. The uncertainties are estimated as 95% confidence intervals for fitting within the selected interval. These values are of the order of the diameter of a single sugar ring and indicate that bundles of chains larger than dimeric junction zones are, as previously postulated on mechanical grounds (Table 2.1) [20], not common in these systems. It is interesting to note that after gelling the solution through

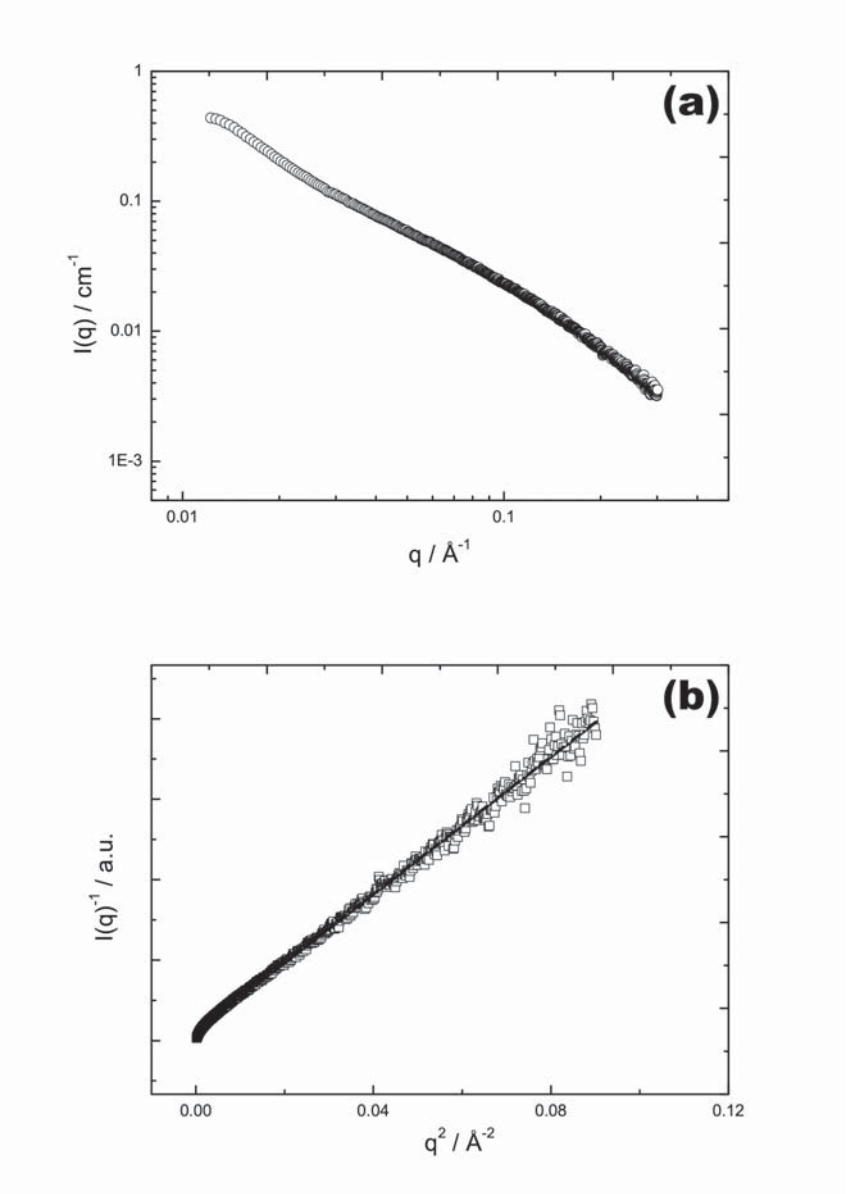

Figure 19: (a) Small-angle X-ray scattering profile $I(q)$ of the semi-dilute pectin solution. (b) Zimm-plot of the scattering profile of the starting pectin solution used to extract the correlation length ξ via Eq. (2.2).

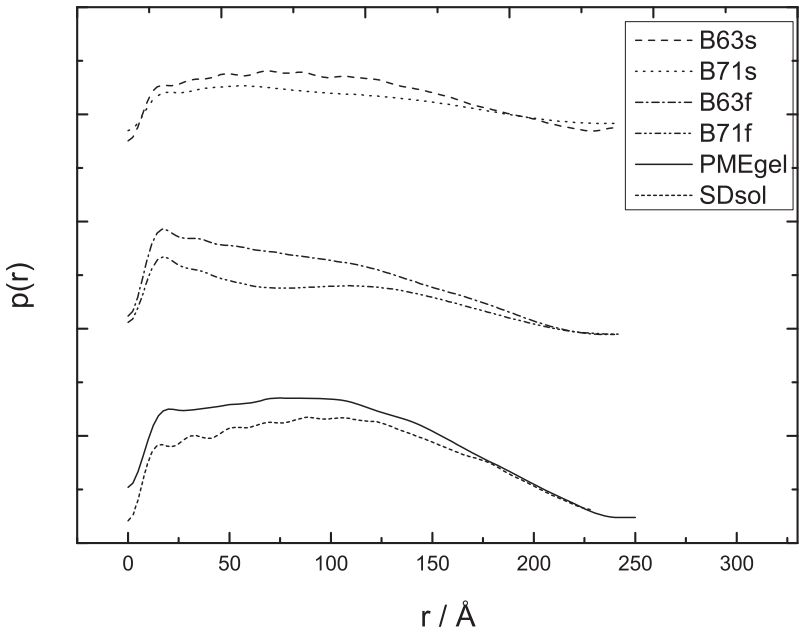

Figure 20: Distance distribution functions $p(r)$ evaluated by Fourier transform of the SAXS data from the pectin gels and the semi-dilute pectin solution.

the enzymatic mediated release of the ion-binding groups (PME action on high DM pectin in the presence of calcium) an R_c of 4.8 ± 0.1 Å is observed. In contrast, the gels inferred from their high-frequency mechanical response to contain stiffer semi-flexible strands, B71s and B63s, have estimated R_c values of 6.3 ± 0.1 Å and 8.5 ± 0.1 Å respectively. These are significantly larger than the previous values and suggest junction zones of multiple chains exist in these materials (Table 2.1) [19] with larger structures more prevalent for the polymer of lower DM. These radii are in the same range as recently observed for similarly formed ionotropic gels of alginate [23] and furthermore, the molecular modelling of junction zones of varying multiplicity (to be described in detail in due course) gives relevant dimensions of around 8 and 15 Å for tetramers and octamers respectively. While these results are suggestive, values obtained in this fashion are averages and in order to investigate the conclusions that might be drawn regarding the composition of the network strands more rigorously calculations of scattering behaviour have been undertaken with the aid of molecular modelling.

A *Molecular Model* was used to study the dependence of the scattering profile on different junction zone compositions, in analogy with previous work carried out on alginate [23]. The scattering profiles were calculated using the atomic coordinates of either 2-fold or 3-fold polygalacturonic acid helices [44, 25, 45] arranged in model junction zones based on the adjusted egg-box model [26]. The mode of packing used is shown in Figure 22. The particle scattering factor $\Theta(q)$ was calculated from the atomic coordinates of these model junction zones using the Debye Formula [46]

$$\Theta(q) = \sum_i g_i^2 \phi_i^2(q) + 2 \sum_i \sum_k g_i g_k \phi_i(q) \phi_k(q) \frac{sin(d_{ik}q)}{d_{ik}q} \tag{2.5}$$

where g_i and $\phi_i(q)$ denote the atomic scattering weight and the particle scattering factor of atom i and d_{ik} is the distance between atoms i and k. $\phi_i(q)$ is calculated by assuming the atoms are rigid spheres with corresponding van der Waals radii R_i:

$$\phi_i(q) = 3 \frac{sin(R_i q) - (R_i q) cos(R_i q)}{(R_i q)^3} \tag{2.6}$$

Scattering profiles for lateral associations of up to 32 unesterified HG chains (Figure 23) have been calculated. Primarily 2-fold helices were used as this conformation has been observed in the presence of multivalent ions and at pH values > 4.0 (appropriate for our experimental conditions) [47, 48], and has also been found to be the energetically most stable conformation for calcium chelating junction zones [26]. A comparison of the results obtained by using unesterified HG in 2-fold or 3-fold

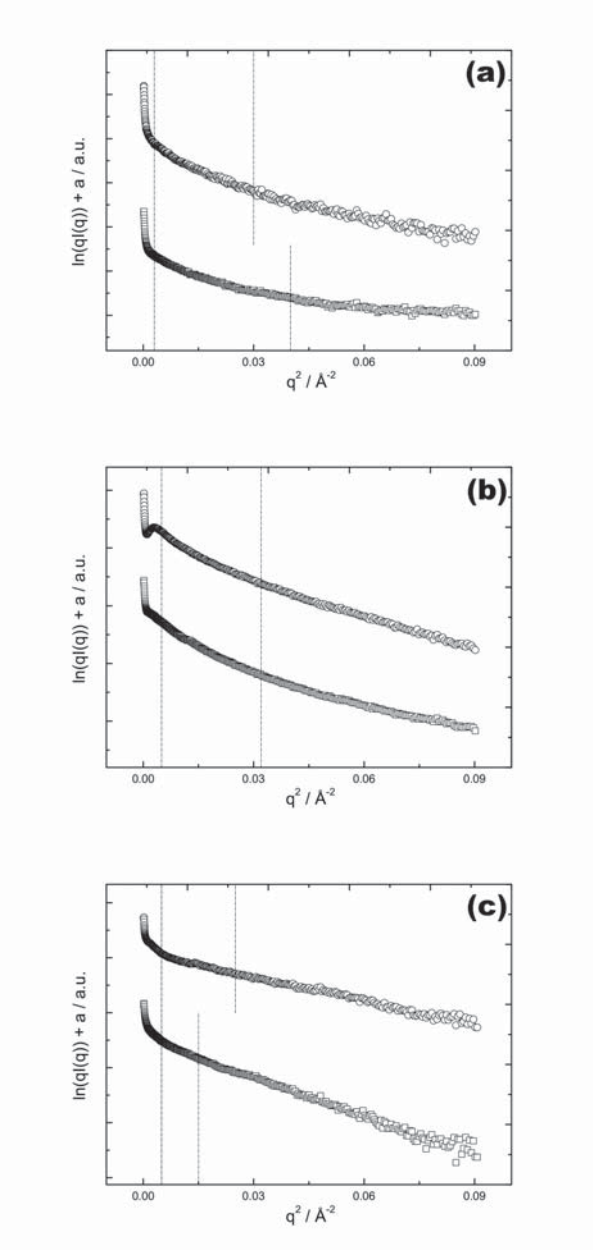

Figure 21: Cross-sectional Guinier plots of the SAXS scattering profiles of (a) SDsol (◯) and PMEgel (□), (b) B71f (◯) and B63f (□) and (c) B71s (◯) and B63s (□). The dashed lines display the Guinier regime in which R_c was evaluated via Eq. (2.4), the resulting radii are reported in Table 2.2 with the corresponding error due to the linear fit; a being an arbitrary shift to distinguish better between the plots.

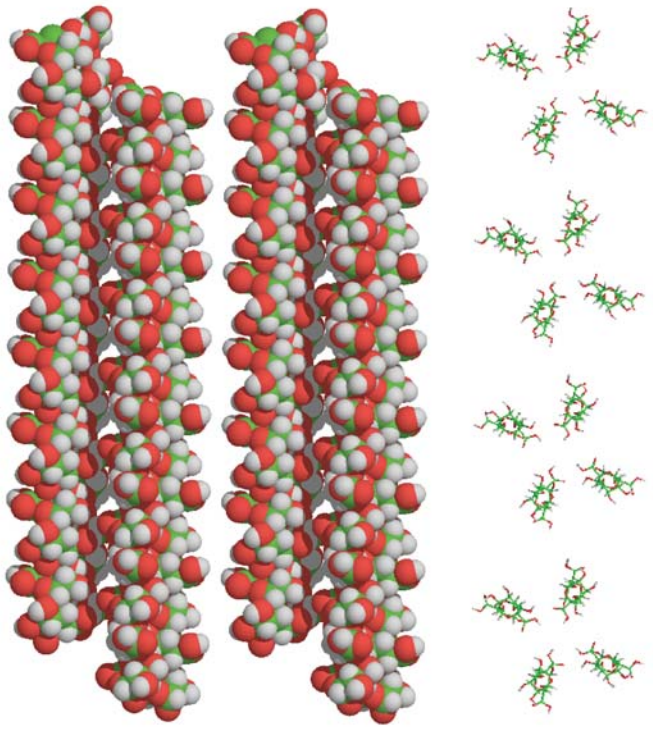

Figure 22: (left) 8-chain junction zone formed by dimers of 2-fold helices with a DP of 16 as suggested by the adjusted egg-box model [26]. (right) Projection of a 16-chain junction zone. All other calculated junction zones are arranged in the same mode of packing - either as a subset or superposition of the configurations shown here.

helices or with uncorrelated torsional angles between the sugar rings as the basic chain conformation, showed overlapping scattering profiles within a 5% standard deviation. Similarly, the effect of esterification of single chains was investigated and found not to cause a significant change of the calculated scattering profile in the experimental q-range. The calcium ions were not considered explicitly, as their main impact was considered to be mediating the formation of the junction zones, which subsequently screen their scattering contribution. Kratky plots for different degrees of polymerisation (DP) ranging between 12 - 36 were calculated; and for this DP range the normalized intensity per residue collapses onto the profiles shown in Figure 23.

After calculation of the profiles expected from junction zones of distinct multiplicities of chains, SAXS data were fitted, assuming no spatial correlation between the different components, as described previously [23] using a linear combination of

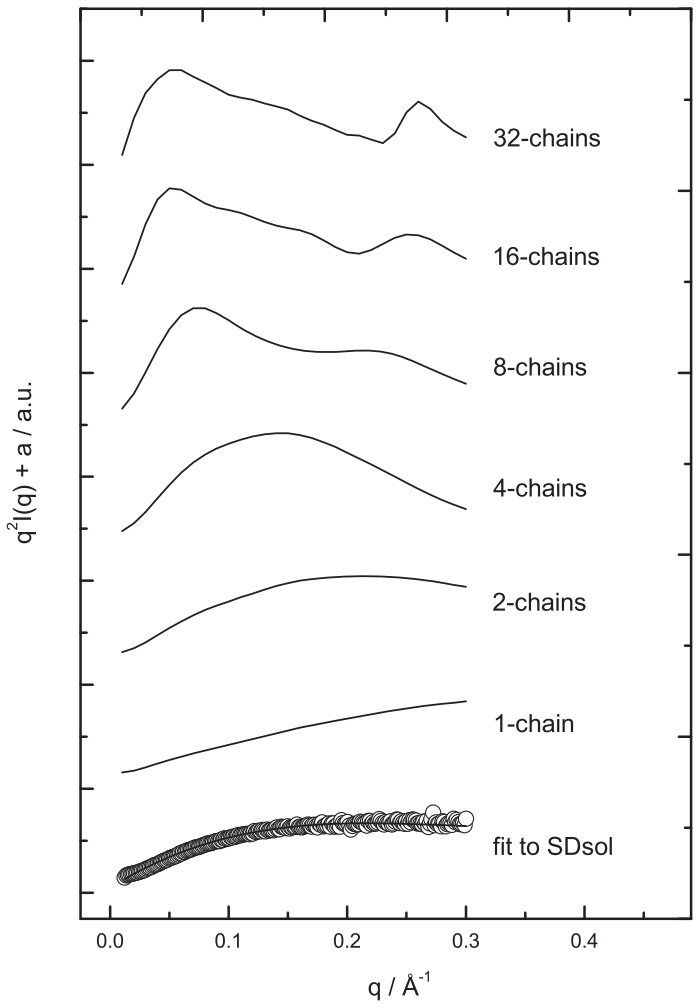

Figure 23: Scattering profiles originating from the molecular model calculation and the fit of the normalized SDsol profile; a being an arbitrary shift to distinguish better between the plots.

these basis functions:

$$I(q) = k_1\Theta_1(q) + k_2\Theta_2(q) + k_3\Theta_3(q) + k_4\Theta_4(q) \tag{2.7}$$

with the corresponding relative weights k_{1-4}. The functions given by Eq. (2.5), evaluated for the different bundle sizes as described and, in addition, an empirical polynomial fit to the data obtained from the starting polymer solution (inset Figure 23) were used as the basis functions.

It should be noted that, in fact, when the scattering data from the starting semi-dilute polymer solution is represented in this way it appears somewhat more similar to the calculated scattering from a dimeric bundle rather than a single chain, owing to the fact that the effect of the entanglements efffectivly increases a perceived cross-sectional radius when viewed in this representation. However, it should be noted that i) the fit quality of the data is affected by the alternate inclusion of the dimer or semi-dilute solution, and ii) that this issue does not affect the confident use of this methodology in assessing the contribution of bundles containing greater than 2 chains.

The Kratky plots ($q^2I(q)$ vs. q) of the data and the fits are depicted in Figure 24 with the resulting fit parameters given in Table 2.2. It should be noted that in order to gain a reasonable fit to the data that originated from the most charged of samples at lower concentration and with a large amount of ions (B63s), it was necessary to include four components as indicated, suggesting that a larger distribution of junction zone multiplicity is present in such samples. For the other samples two components were sufficient to provide a reasonable fit. While the fits to the data are not unique, they offer insight and good estimates about the size and weighting of different junction zones of varying chain multiplicity.

The fitted results can be discussed within the context of a previously postulated state diagram [21], described as a function of polymer concentration c_P and calcium concentration per available binding site (accounted for by R_{eff}), and mapped out by the different high-frequency mechanical responses of samples. This state diagram suggests:

(i) for high values of R_{eff} and low c_P the formation of more bundled networks with a semiflexible MR response.

(ii) that following an increase in c_P a regime is entered where restricted mobility of the chains hinders the formation of bigger bundles, yielding a more flexible response with a MR exponent closer to $\frac{1}{2}$.

(iii) that for low R_{eff} (independent of c_P) a regime of small dimeric junction of zones of minimal length is predicted, also with a high frequency MR exponent closer to $\frac{1}{2}$.

For the gels studied here that fall into region (i) both the model-independent analysis of the SAXS data and the detailed modelling approach (Figure 24 (c) & Table 2.2) clearly show the multiplicity of junction zones formed indeed exceeds 2, supporting the predictions of the state diagram - at least if it is assumed that, in general, larger bundles of chains have increased persistence lengths (or equivalently reduced flexibilities). In contrast the gels formed by slow calcium release that yield a more flexible microrheological signature have extracted cross-sectional radii values close to single sugar rings and can clearly be seen to have their scattering profile successfully modelled by that of the initial semi-dilute pectin solution with the addition of solely dimeric junction zones (Figure 24 (b) & Table 2.2).

Interestingly, successfully modelling the data from the gel created by enzymatic action on high DM pectin in the presence of the calcium required a large weighting of the single-chain scattering component (Figure 24 (a)). This suggests that through this assembly mechanism it is possible to build a network cross-linked by punctual dimeric junction zones largely connected by single chains. During gelation the average R_c is found to decrease slightly and the single chain nature of the scattering profile dominates over that found for the initial semi-dilute solution (Figure 24 (a) & Table 2.2). These observations can be explained by considering the enzyme's processive mode of action, and the calcium sensitivity of unesterified blocks of galacturonic acid. During enzyme action, once enough consecutive methylester groups have been removed from the polymer backbone so that the resulting unesterified block ($\approx$ 10 residues) can chelate calcium into small junction zones, these connections, which ultimately form a network, block the further enzyme activity, thereby limiting the extent of the cross-links formed and consequently maximizing their number. This enzymatically induced binding mechanism, as exploited in the plant cell wall, induces a rearrangement of the originally dense overlapping chains in the semi-dilute solution into a percolated network of mostly single chains cross-linked via minimal size junction zones; it further seems likely that such a process loads additional tension on the chains, which is also known to influence the MR response towards exponents around $\frac{1}{2}$ [49, 50]. Investigating this interesting feature in more detail forms part of ongoing work.

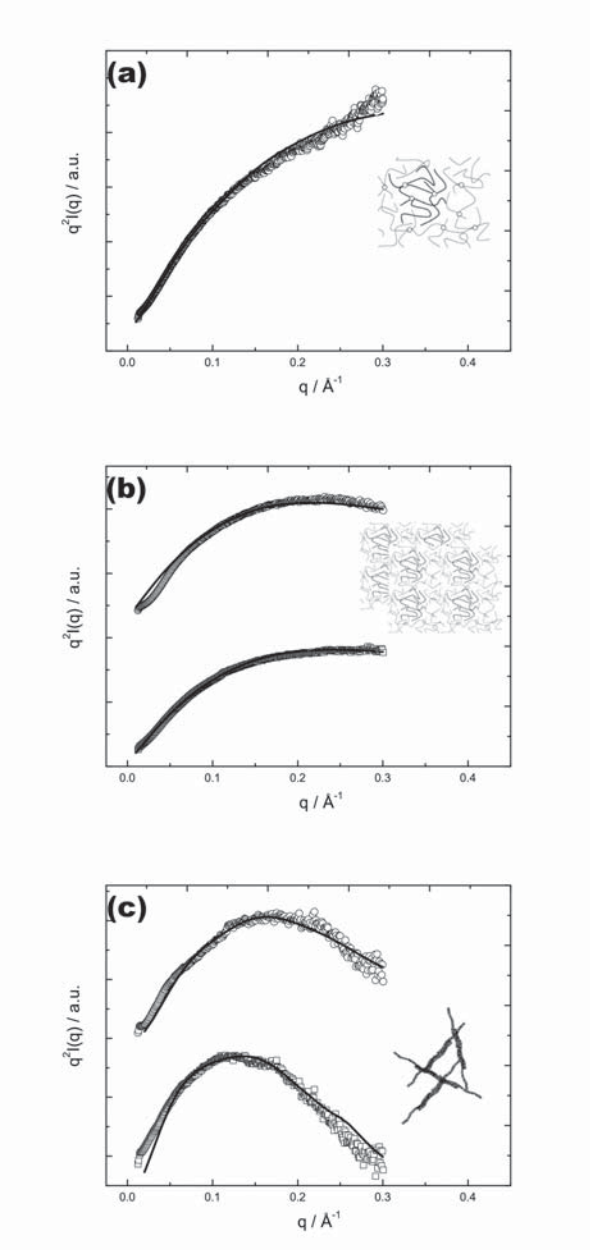

Figure 24: Kratky plot of the SAXS data and fits to the molecular model with the a sketch of the suggested network structures. (a) PMEgel network consisting of 'pinned-down' small junction zones; (b) B71f (◯) and B63f (□) showing a structure of densely confined chains cross-linked by dimeric junction zones; (c) B71s (◯) and B63s (□) containing an assembly of large rodlike bundles.

2.4 Conclusions

Microrheologically-distinct pectin gels have been generated using different assembly modalities: in particular by using different concentrations of polymer and cross-linking ions, and by contrasting the controlled-release of ions or ion-binding groups; and the resulting systems have been studied by small angle X-ray scattering. The results straightforwardly reveal that gels which are clearly more semi-flexible from a microrheological point-of-view contain larger scattering entities than those with a more flexible character. Furthermore, a more detailed interpretation of the scattering data with the aid of molecular modelling suggests that, for the gels formed here, those with a semi-flexible microrheological signature consist predominantly of network filaments consisting of at least 4 chains, while those with a more flexible signature are predominantly single chain and dimeric associations with no more than a few percent of the chains bundled to any higher extent.

These results show both that high frequency microrheological measurements are indeed useful indicators of the nature of the elementary network strands, and that stiffer filaments are generated by bundles of larger numbers of individual chains. It is also shown that biomimetic enzyme induced networks can be formed in which dimeric calcium-chelating junction-zones of limited extent are linked by considerably longer, flexible, single-chain sections. This is in contrast to existing paradigms on the hierarchical assembly of many biological gel structures, in which single-polymer properties play little direct mechanical role compared with the properties of the assembled intermediate structures.

References

[1] R. R. Vincent. *Microrheological investigations of biopolymer networks*. PhD thesis, Massey University, Palmerston North, New Zealand, 2008. URL `http://hdl.handle.net/10179/764`. 43

[2] D. I. Svergun and M. H. J. Koch. Small-angle scattering studies of biological macromolecules in solution. *Reports On Progress In Physics*, 66(10):1735–1782, 2003. doi: 10.1088/0034-4885/66/10/R05. 43

[3] W. G. T. Willats, P. Knox, and J. D. Mikkelsen. Pectin: new insights into an old polymer are starting to gel. *Trends In Food Science & Technology*, 17(3): 97–104, 2006. doi: 10.1016/j.tifs.2005.10.008. 43

[4] E. Parre and A. Geitmann. Pectin and the role of the physical properties of the cell wall in pollen tube growth of solanum chacoense. *Planta*, 220(4):582–592, 2005. doi: 10.1007/s00425-004-1368-5. 43

Table 2.2: Results of the analysis via cross-sectional Guinier plots and the parameters of the molecular model fit.

Sample name	R_c (Å)	Model composition						R^2 of the fit
SDsol	5.9 ± 0.1							
PMEgel	4.8 ± 0.1	60%	1-chain	40%	SD-polynomial			0.95
B71f	5.7 ± 0.1	10%	2-chains	90%	SD-polynomial			0.95
B63f	5.6 ± 0.1	10%	2-chains	90%	SD-polynomial			0.99
B71s	6.3 ± 0.1	60%	2-chains	40%	4-chains			0.86
B63s	8.5 ± 0.1	77.5%	4-chains	7.5%	8-chains	7.5%	16-chains 7.5% 32-chains	0.82

[5] W. G. T. Willats, C. Orfila, G. Limberg, H. C. Buchholt, G. J. W. M. van Alebeek, A. G. J. Voragen, S. E. Marcus, T. M. I. E. Christensen, J. D. Mikkelsen, B. S. Murray, and J. P. Knox. Modulation of the degree and pattern of methyl-esterification of pectic homogalacturonan in plant cell walls - implications for pectin methyl esterase action, matrix properties, and cell adhesion. *Journal of Biological Chemistry*, 276(22):19404–19413, 2001. doi: 10.1074/jbc.M011242200. 43

[6] B. M. Yapo, P. Lerouge, J. F. Thibault, and M. C. Ralet. Pectins from citrus peel cell walls contain homogalacturonans homogenous with respect to molar mass, rhamnogalacturonan i and rhamnogalacturonan ii. *Carbohydrate Polymers*, 69(3):426–435, 2007. doi: 10.1016/j.carbpol.2006.12.024. 44

[7] D. A. Powell, E. R. Morris, M. J. Gidley, and D. A. Rees. Conformations and interactions of pectins .2. influence of residue sequence on chain association in calcium pectate gels. *Journal of Molecular Biology*, 155(4):517–531, 1982. doi: 10.1016/0022-2836(82)90485-5. 44, 45

[8] F. Liners, J. F. Thibault, and P. Vancutsem. Influence of the degree of polymerization of oligogalacturonates and of esterification pattern of pectin on their recognition by monoclonal-antibodies. *Plant Physiology*, 99(3):1099–1104, 1992. doi: 10.1104/pp.99.3.1099. 44

[9] A. B. O'Brien, K. Philp, and E. R. Morris. Gelation of high-methoxy pectin by enzymic de-esterification in the presence of calcium ions: a preliminary evaluation. *Carbohydrate Research*, 344(14):1818–1823, 2009. doi: 10.1016/j.carres.2008.09.029. 44

[10] A. Slavov, C. Garnier, M. J. Crepeau, S. Durand, J. F. Thibault, and E. Bonnin. Gelation of high methoxy pectin in the presence of pectin methylesterases and calcium. *Carbohydrate Polymers*, 77(4):876–884, 2009. doi: 10.1016/j.carbpol.2009.03.014. 44

[11] M. D. Walkinshaw and S. Arnott. Conformations and interactions of pectins .2. models for junction zones in pectinic acid and calcium pectate gels. *Journal of Molecular Biology*, 153(4):1075–1085, 1981. doi: 10.1016/0022-2836(81)90468-X. 44

[12] E. R. Morris, D. A. Powell, M. J. Gidley, and D. A. Rees. Conformations and interactions of pectins .1. polymorphism between gel and solid states of calcium polygalacturonate. *Journal of Molecular Biology*, 155(4):507–516, 1982. doi: 10.1016/0022-2836(82)90484-3. 44

[13] S. Cros, C. Garnier, M. A. V. Axelos, A. Imberty, and S. Perez. Solution conformations of pectin polysaccharides: Determination of chain characteristics by small angle neutron scattering, viscometry, and molecular modeling. *Biopolymers*, 39(3):339–352, 1996. doi: 10.1002/(SICI)1097-0282(199609)39:3<339::AID-BIP6>3.0.CO;2-P. 44

[14] M. C. Ralet, M. J. Crepeau, H. C. Buchholt, and J. F. Thibault. Polyelectrolyte behaviour and calcium binding properties of sugar beet pectins differing in their degrees of methylation and acetylation. *Biochemical Engineering Journal*, 16 (2):191–201, 2003. doi: 10.1016/S1369-703X(03)00037-8. 44

[15] Y. P. Fang, S. Al-Assaf, G. O. Phillips, K. Nishinari, T. Funami, and P. A. Williams. Binding behavior of calcium to polyuronates: Comparison of pectin with alginate. *Carbohydrate Polymers*, 72(2):334–341, 2008. doi: 10.1016/j.carbpol.2007.08.021. 44

[16] C. Lofgren, S. Guillotin, and A. M. Hermansson. Microstructure and kinetic rheological behavior of amidated and nonamidated lm pectin gels. *Biomacromolecules*, 7(1):114–121, 2006. doi: 10.1021/bm050459r. 44

[17] V. J. Morris, A. Gromer, A. R. Kirby, R. J. M. Bongaerts, and A. P. Gunning. Using afm and force spectroscopy to determine pectin structure and (bio) functionality. *Food Hydrocolloids*, 25(2):230–237, 2011. doi: 10.1016/j.foodhyd.2009.11.015. 44, 45

[18] M. A. K. Williams, R. R. Vincent, D. N. Pinder, and Y. Hemar. Microrheological studies offer insights into polysaccharide gels. *Journal Of Non-Newtonian Fluid Mechanics*, 149(1-3):63–70, 2008. doi: 10.1016/j.jnnfm.2007.05.006. 44

[19] R. R. Vincent, D. N. Pinder, Y. Hemar, and M. A. K. Williams. Microrheological studies reveal semiflexible networks in gels of a ubiquitous cell wall polysaccharide. *Physical Review E*, 76:031909, 2007. doi: 10.1103/PhysRevE.76.031909. 44, 55

[20] R. Vincent, A. Cucheval, Y. Hemar, and M. Williams. Bio-inspired network optimization in soft materials - insights from the plant cell wall. *European Physical Journal E*, 28(1):79–87, 2009. doi: 10.1140/epje/i2008-10416-2. 44, 46, 52

[21] R. R. Vincent and M. A. K. Williams. Microrheological investigations give insights into the microstructure and functionality of pectin gels. *Carbohydrate Research*, 344(14):1863–1871, 2009. doi: 10.1016/j.carres.2008.11.021. 45, 48, 50, 59

[22] M. A. V. Axelos, C. Garnier, C. M. G. C. Renard, and J. F. Thibault. Interactions of pectins with multivalent cations: Phase diagrams and structural aspects. *Pectins and Pectinases*, 14:35–45, 1996. doi: 10.1016/S0921-0423(96)80244-9. 45

[23] B. T. Stokke, K. I. Draget, O. Smidsrod, Y. Yuguchi, H. Urakawa, and K. Kajiwara. Small-angle x-ray scattering and rheological characterization of alginate gels. 1. ca-alginate gels. *Macromolecules*, 33(5):1853–1863, 2000. doi: 10.1021/ma991559q. 45, 55, 57

[24] Y. Yuguchi, H. Urakawa, K. Kajiwara, K. I. Draget, and B. T. Stokke. Small-angle x-ray scattering and rheological characterization of alginate gels. 2. time-resolved studies on ionotropic gels. *Journal Of Molecular Structure*, 554(1): 21–34, 2000. doi: 10.1016/S0022-2860(00)00556-1. 45

[25] I. Braccini, R. P. Grasso, and S. Perez. Conformational and configurational features of acidic polysaccharides and their interactions with calcium ions: a molecular modeling investigation. *Carbohydrate Research*, 317(1-4):119–130, 1999. doi: 10.1016/S0008-6215(99)00062-2. 45, 55

[26] I. Braccini and S. Perez. Molecular basis of ca2+-induced gelation in alginates and pectins: The egg-box model revisited. *Biomacromolecules*, 2(4):1089–1096, 2001. doi: 10.1021/bm010008g. xi, 45, 55, 57

[27] M. A. K. Williams, T. J. Foster, and H. A. Schols. Elucidation of pectin methylester distributions by capillary electrophoresis. *Journal of Agricultural and Food Chemistry*, 51(7):1777–1781, 2003. doi: 10.1021/jf0259112. 46

[28] M. A. K. Williams, A. Cucheval, A. Strom, and M. C. Ralet. Electrophoretic behavior of copolymeric galacturonans including comments on the information content of the intermolecular charge distribution. *Biomacromolecules*, 10(6): 1523–1531, 2009. doi: 10.1021/bm900119u. 46

[29] J. A. E. Benen, H. C. M. Kester, and J. Visser. Kinetic characterization of aspergillus niger n400 endopolygalacturonases i, ii and c. *European Journal of Biochemistry*, 259(3):577–585, 1999. doi: 10.1046/j.1432-1327.1999.00080.x. 46, 47

[30] B. J. Savary, A. T. Hotchkiss, and R. G. Cameron. Characterization of a salt-independent pectin methylesterase purified from valencia orange peel. *Journal of Agricultural and Food Chemistry*, 50(12):3553–3558, 2002. doi: 10.1021/jf020060j. 46

[31] T. Sajjaanatakul and L. A. Pitifer. *The Chemistry and Technology of Pectin*, pages 135–156. Academic Press: New York, 1991. 46

[32] M. Fries, J. Ihrig, K. Brocklehurst, V. E. Shevchik, and R. W. Pickersgill. Molecular basis of the activity of the phytopathogen pectin methylesterase. *Embo Journal*, 26(17):3879–3887, 2007. doi: 10.1038/sj.emboj.7601816. 46

[33] J. M. Denes, A. Baron, C. M. G. C. Renard, C. Pean, and J. F. Drilleau. Different action patterns for apple pectin methylesterase at ph 7.0 and 4.5. *Carbohydrate Research*, 327(4):385–393, 2000. doi: 10.1016/S0008-6215(00)00070-7. 46

[34] R. G. Cameron, G. A. Luzio, K. Goodner, and M. A. K. Williams. Demethylation of a model homogalacturonan with a salt-independent pectin methylesterase from citrus: I. effect of ph on demethylated block size, block number and enzyme mode of action. *Carbohydrate Polymers*, 71(2):287–299, 2008. doi: 10.1016/.j.carbpol.2007.07.007. 46

[35] P. J. B. Edwards, M. Kakubayashi, R. Dykstra, S. M. Pascal, and M. A. K. Williams. Rheo-nmr studies of an enzymatic reaction: Evidence of a shear-stable macromolecular system. *Biophysical Journal*, 98(9):1986–1994, 2010. doi: 10.1016/j.bpj.2010.01.022. 47

[36] A. Strom and M. A. K. Williams. Controlled calcium release in the absence and presence of an ion-binding polymer. *Journal of Physical Chemistry B*, 107 (40):10995–10999, 2003. doi: 10.1021/jp034322b. 48

[37] Y. Hemar and D. N. Pinder. Dws microrheology of a linear polysaccharide. *Biomacromolecules*, 7(3):674–676, 2006. doi: 10.1021/bm0505661. 48

[38] N. Kirby, J. W. Boldeman, I. Gentle, and D. Cookson. Conceptual design of the small angle scattering beamline at the australian synchrotron. *Synchrotron Radiation Instrumentation, Pts 1 and 2*, 879:887–889, 2007. doi: doi:10.1063/1.2436203. 48

[39] David J. Cookson. Saxs15id - software for acquiring,processing and viewing saxs/waxs image data at chemmatcars, December 2007. URL `http://cars9.uchicago.edu/chemmat/`. 49

[40] P. G. de Gennes. *Scaling concepts in polymer physics*. Cornell University Press, Ithaca, N.Y. :, 1979. ISBN 080141203. 50

[41] M. Shibayama. Spatial inhomogeneity and dynamic fluctuations of polymer gels. *Macromolecular Chemistry and Physics*, 199(1):1–30, 1998. doi: 10.1002/(SICI)1521-3935(19980101)199:1<1::AID-MACP1>3.0.CO;2-M. 50

[42] O. Kratky and O. Glatter. *Small angle x-ray scattering*. Academic Press, London; New York, 1982. 52

[43] A. V. Semenyuk and D. I. Svergun. Gnom - a program package for small-angle scattering data-processing. *Journal of Applied Crystallography*, 24:537–540, 1991. doi: 10.1107/S002188989100081X. 52

[44] J. Hjortas, B. Larsen, F. Mo, and S. Thanomku. Structure of methyl alpha-d-galacturonic acid methyl-ester. *Acta Chemica Scandinavica Series B-organic Chemistry and Biochemistry*, B 28(1):133–133, 1974. 55

[45] Pubchem: 439239. URL `http://pubchem.ncbi.nlm.nih.gov/summary/summary.cgi?cid=439239`. 55

[46] O. Glatter. Computation of distance distribution-functions and scattering functions of models for small-angle scattering experiments. *Acta Physica Austriaca*, 52(3-4):243–256, 1980. 55

[47] M. J. Gidley, E. R. Morris, E. J. Murray, D. A. Powell, and D. A. Rees. Evidence for 2 mechanisms of interchain association in calcium pectate gels. *International Journal of Biological Macromolecules*, 2(5):332–334, 1980. doi: 10.1016/0141-8130(80)90060-4. 55

[48] G. Ravanat and M. Rinaudo. Investigation on oligogalacturonic and polygalacturonic acids by potentiometry and circular-dichroism. *Biopolymers*, 19(12): 2209–2222, 1980. doi: 10.1002/bip.1980.360191206. 55

[49] A. Caspi, M. Elbaum, R. Granek, A. Lachish, and D. Zbaida. Semiflexible polymer network: A view from inside. *Physical Review Letters*, 80(5):1106–1109, 1998. doi: 10.1103/PhysRevLett.80.1106. 60

[50] B. Obermayer and E. Frey. Tension dynamics and viscoelasticity of extensible wormlike chains. *Physical Review E*, 80(4):040801, 2009. doi: 10.1103/PhysRevE.80.040801. 60

Chapter 3

2D network model where connections are single chains

3.1 Introduction

It is unclear exactly which mechanisms trigger changes in the structural and mechanical properties within plants, but it is quite possible that gels, in which single chains are the mechanical response dominating network segments, exist in vivo and do play a crucial role in the cellulose-pectin matrix of the plant cell wall. Considering the results presented in Chapter 2, we have strong experimental evidence that such networks (with single chain sections playing an important role) are found in in-vitro formed pectin gels. This is in contrast to most other biological gels, where hierarchical assembled filaments form the stress bearing strands. The unique feature of the approach pursued in this study, the incorporation of an experimentally measured force-extension relation into an appropriate network model, allows us to investigate the possible function of an additional specific characteristic of polysaccharide chains, namely the existence of force induced conformational transitions.

Single molecule force spectroscopy has recently given access to an unprecedented level of information regarding the stress response of a host of biopolymers at the single chain level [1, 2, 3, 4]. Studies of polysaccharide stretching have yielded particularly interesting data, the interpretation of which requires the marriage of statistical-mechanical theories of polymer physics to the complexities afforded by possible force-induced rearrangements or even conformational transitions of the constituent sugar rings. Such monomer transitions during stretching, from classical chair forms of the pyranose ring to more elongated arrangements, function as molecular sacrificial bonds [5], increasing the polymer's contour length and thus producing characteristic deviations, or 'clicks', in the slope of the force-extension

curve. Indeed, many curves exhibiting features of this type have been measured [6, 7, 8, 9, 10, 11, 12], and while accounting for their detailed origin is still a work in progress [13, 14], the fact that they are observed in polysaccharides in which the rings are axially-linked and are completely absent in equatorially-linked analogues, gives great credence to the idea that axial bonds facilitate these transitions by acting as molecular levers. Thus, it is central to the interpretation of polysaccharide force-extension curves to understand that those polymers possessing only equatorial glycosidic linkages such as cellulose (1e-4e) do not have the possibility of undergoing stretching-driven conformational transitions, while those with one axial and one equatorial bond, such as amylose (1a-4e) or dextran (1a-6e) can undergo one conformational transformation, and those with both bonds axial, such as pectin, two (Figure 25) [15, 16, 17].

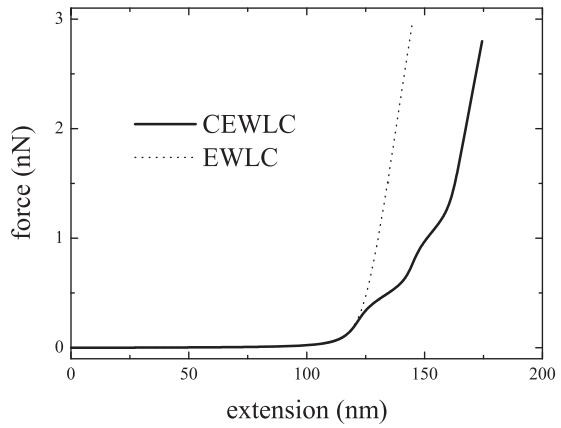

Figure 25: Force-extension curves of CEWLC and EWLC models used in the simulations described herein. The CEWLC parameters have been chosen in order to produce a curve consistent with experimentally measured data on the polysaccharide pectin. Specifically: $l_P = 1\,nm$, $l_C = 128\,nm$, $T = 298\,K$, chair length = $0.4592\,nm$, boat length = $0.5176\,nm$, inverted chair length = $0.5576\,nm$, specific stiffness = $20\,nN$, and the energy differences for the two conformational transitions $\Delta G = 12\,kJ\,mol^{-1}$ and $17\,kJ\,mol^{-1}$ respectively.

Pectin is an important structural polysaccharide, with its main characteristics already described in Chapter 2.1. Extracted directly from primary cell walls they typically have high DM of around 80%, although interestingly this structural feature is known to be modified *in-vivo* as the plant engineers its constituent polymers,

eliciting desired mechanical changes in order to facilitate varied physiological processes. The DM of pectin chains can also be modified in-vitro, using a number of chemical processes or exploiting enzymes from plants, fungi or bacteria and using such an approach the nanomechanical properties of single pectin chains have been investigated as a function of the DM of the chain [17]. These studies revealed the presence of force-induced conformational changes over the entire range of DM and detectable but small differences between the triggering forces, which were shown to be consistent with the results of density-functional theory (DFT) studies carried out on the effect of methylesterification on the energy differences between differing conformations of the ring. Recent work on bio-mimetic enzyme-induced pectin gels has shown that highly elastic networks can be formed from high DM chains where calcium-mediated junction zones of limited length are connected by significant stretches of highly methylesterifed pectin [18]. This means that the force-induced conformational transitions might still perform functions in-vivo or in bio-mimetic gels in-vitro in calcium associated networks.

In conclusion, significant lengths of single pectin chains (which are not bound to other chains via calcium owing to their high DM) might well still be active network elements in-vivo or in-vitro in enzyme-generated bio-mimetic gels. Such high DM chains have clearly been shown to exhibit force-induced conformational transitions as described, so that their possible role in such systems remains an open and interesting question. Indeed, it has been speculated that these transitions may have biological significance. This could involve acting as a sensor with a signalling role [10], or as a compliant element possessing extra elastic extensibility, directly contributing to the control and maintenance of the mechanical properties of the cell wall [7]. Whilst, since these transitions were first detected, both signalling and mechanical roles have been suggested as possible functions in-vivo, the difficulty in detecting such transitions in macroscopic chain assemblies has effectively limited experimental progress in this area. Herein, an alternative approach is pursued in order to investigate the possible macroscopic functionality of these novel nanomechanical features using numerical simulations of networks under strain.

3.2 Models

3.2.1 Simulation

Set-Up. Numerical simulations of statistically homogeneous, isotropic, randomly oriented biopolymer networks in two dimensions have been carried out in a man-

ner based on that previous described [19]. The networks were formed according to a Mikado model [20, 21, 22], by randomly placing rods of fixed length into a two dimensional cell, so that their position and orientation were equi-distributed. Each intersection point subsequently corresponds to a node, at which agents with an initial zero-length were additionally inserted. Whilst the inclusion of two network "agents" (that is: nodes connected by initially laid-down rods interacting via one potential, and those linked by the added initially zero-length "cross-linkers" interacting by another) was not required for modelling single-component networks it enabled the trivial extension to two components, described in due course. Rods were added until the average number of nodes per rod reached a pre-defined value, which parametrised the network density. In the square cell used; of length 1 in simulation units; networks of around 20 000 nodes were generated from rods of length 0.2, with an average of 30 nodes per rod. This number of nodes is comfortably in the regime where system size effects were negligible.

Single Agent Networks. Firstly, no distinction was made between the potential governing the proximity of the nodes whether they were connected by the original rods or by the added cross-linkers. In this case the agents were modelled using a single interacting potential derived from force-extension curves with a functional form given by either i) an extensible wormlike chain (EWLC) model [23] or ii) a clickable extensible wormlike chain model (CEWLC) [15, 17], generally applicable to biopolymers undergoing conformational transformations and specifically shown to successfully model the stretching of pectin. (Indeed, parameters were selected so that the chosen functional form faithfully represented an actual experimental dataset.) Simulations were carried out for differing ratios of average node-to-node distance to the contour length of the spanning chains. The range of interest for this parameter was estimated by considering experimental data on typical pectin gels, which exhibit mesh-sizes (l_M) on the order of 100 nm [24] and have contour length of around 300 nm, based on their typical molar mass [25]. Therefore network simulations with l_C/l_M of between 1 and 4 were investigated. l_M was calculated during the simulations as the average over all node distances.

Dual Agent Networks. In a second approach rod-like networks cross-linked by EWLC or CEWLC agents were modelled. In this case after the Mikado set-up process was completed, the nodes connected by initially laid-down rods were taken to interact via a simple Hookean spring potential with a fixed spring constant $\overline{k}$, while the relevant WLC potential was used to describe the interaction of nodes connected by the initially zero-length cross-linkers.

Energy Minimisation. All node-connecting chains are assumed to be freely rotating so that the system Hamiltonian depends only on the node-to-node distances. The force-extension curves of the EWLC and the CEWLC cases used to numerically derive the potentials are shown in Figure 25. The CEWLC parameters have been selected so that the model represents actual single molecule experimental data for pectin, while the specific EWLC is chosen so that at forces below the activation of any conformational transitions the curves overlap. Subsequently at higher forces two clear transitions assigned to two conformational changes in the sugar rings are evidenced in the CEWLC. The simulations are considered to be restricted to cases where the persistence length $l_P << l_C$ and with this caveat the bending of rods can be neglected [26] and in this way computational efficiency can be gained. With the potentials and the node positions in hand the equilibrium state of the network is found by minimising the energy using a conjugate gradient routine. Once the relaxed start configuration is found the network can subsequently be strained and the process repeated after each strain-step.

Straining the Network. Initially the network was deformed in an affine manner, as has been generally carried out in previous works [27]. It is worth noting however that the affinity of deformations in such networks has been the subject of relatively little experimental investigation [28]. Such an assumption, either during in-vitro experiments in rheological cells or indeed in-vivo, where internalised motors may apply strain, is unlikely to be universally justified. An advantage of numerical simulations is the ease with which other non-affine deformation fields can be applied. Herein the use of Lees-Edwards boundary conditions [29] is also briefly investigated as an example of such a case.

Affine deformation: The network was deformed by adding a constant vertical offset to the left and right boundaries, with the nodes intersecting the upper and lower boundaries adjusted in an affine manner corresponding to the magnitude of the vertical displacement; all other node positions were moved affinely at the beginning of each strain step.

Non-Affine deformation: The simulated network was sheared by adding a constant vertical offset to the nodes intersecting the left and right boundaries of the simulation box while using Lees-Edwards boundary conditions [29].

To find the initial relaxed state an annealing technique is used in order to ensure

that artefacts do not originate from the initial zero-length of the cross-link agents. Here the system is initially strained to 0.3 before being released again to strain 0. The maximum strain considered in the simulations is 1, beyond which cracks are often observed to form in experimental studies of typical polysaccharide networks [30].

3.2.2 Averaging approach to elasticity calculations for affine deformations

Storm et al. recently described a theoretical framework for the calculation of bulk elasticity in homogeneous, isotropic, random biopolymer networks under affine deformation, that describes how the manifest nonlinear network elasticity arises from the molecular force-extension behaviour [27]. The model considers a regime where the effects of bending modes and torques are minor, and stretching and compression of the constituent monodisperse filaments dominates the stress response of the network, with the molecular force-extension relation depending only on the node-to-node distance. Assuming affine deformations one can express the node positions r' under strain as a linear transformation of the unstrained positions r by just one isotropic Cauchy deformation tensor $\Lambda : r'(\gamma) = \Lambda r$ which results in the following expression for the shear strain:

$$\sigma = \frac{\rho}{det\Lambda} \left\langle f(|\Lambda r|) \frac{(\Lambda r)_x (\Lambda r)_y}{|\Lambda r|} \right\rangle_{|r|=L_R} \tag{3.1}$$

where ρ is the number of links per unit volume and $f(r)$ is the force-extension relation that governs the node-to-node potential. The average is taken over all spatial configurations with one relaxed end-to-end extension, L_R, being assumed for the whole network. To compare the predictions of the 2-dimensional simulations carried out with those of this theory, the following 2-dimensional area-conserving affine shear deformation tensor was used:

$$\Lambda = \begin{pmatrix} 1 & \gamma \\ 0 & 1 \end{pmatrix} \tag{3.2}$$

Furthermore ρ and $f(r)$ were used as in the simulation; with 20 000 nodes and the numerical force-extension data from the experimental CEWLC.

3.3 Results and discussion

3.3.1 Single agent networks

Figure 26 shows the comparison of the numerically simulated stress-strain behaviour of networks of EWLCs and CEWLCs with l_C/l_M given by (a) 1, (b) 1.8, (c) 2.5 and (d) 3.3, following the application of an affine deformation. These results are averages over ten separate simulations with identical parameters and the error bars illustrate the magnitude of the calculated standard deviations. The macroscopic mechanical response of both network types, in all cases, can be seen to be indistinguishable within the uncertainties.

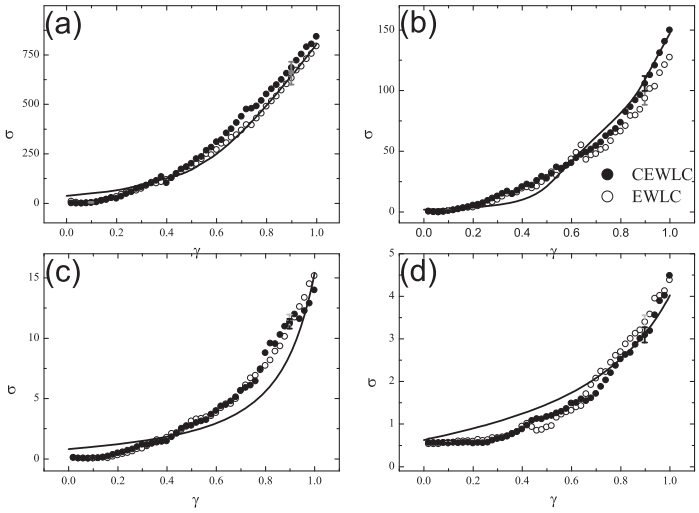

Figure 26: Plots of shear stress, σ, versus strain, γ, for networks comprising CEWLCs (solid circles) or EWLCs (open circles) at different ratios of l_C/l_M = (a) 1.0, (b) 1.8, (c) 2.5, (d) 3.3 following an affine deformation. σ is given in simulation units. The error bars show the standard deviation of an ensemble average over ten runs. Solid lines are fits described in the text.

In addition, results obtained from the averaging approach described above are also shown. These were obtained using equation 3.1 and fitting the L_R values in order to achieve the best correspondence with the results of the numerical simulation. L_R is always found to be greater than or equal to the average node-to-node distance (mesh size) but smaller than the contour length, as expected. It is clear that numeri-

cal simulations of networks under affine shear deformations, with the single-filament force-extension relation defining the Hamiltonian, show strain-stiffening in a manner as predicted by the molecular theory of nonlinear elasticity [27]. It also fortifies the view that the mechanical properties of the randomly oriented networks consisting of CEWLCs are indistinguishable from those based on EWLCs.

As no significant differences in the mechanical properties were manifest as EWLC agents had realistic polysaccharide type force-induced conformational transitions introduced, it is natural to check whether any of the network chains in the simulation actually went through transitions during network straining, as has been demonstrated at the single molecule level. The simulation technique affords just such a possibility. To illustrate the investigation of this issue Figure 27 shows the distributions of the node-to-node distances of unstrained equilibrated networks of CEWLCs and EWLCs with $l_C/l_M = 1.0$. It is clear that a number of chains in this simulation are under significant internal strains, imposed by the sparse network connectivity, such that significant populations of chains are already conformationally extended (the two additional peaks in the length distribution being reflective of the two shallower regions in the CEWLC force-extension curve). The number of CEWLCs that have undergone a) no b) one or c) two, force-induced conformational transitions in their constituent sugar rings are explicitly shown as a histogram (Inset).

Figures 28, 29 and 30 depict networks of CEWLCs at strains of (a) 0, (b) 0.3, (c) 0.5 and (d) 1.0, for the ratios l_C/l_M =1.0, 1.8, and 2.5 respectively. Corresponding node-to-node length distributions and histograms of the populations of different conformational states generated at a strain of 0.3 are also presented in Figure 31. It can be concluded, unsurprisingly perhaps, that as l_C/l_M gets smaller the chains have a greater propensity to exhibit conformational transitions. However, more interestingly, it can also be observed in the simulations that as the networks are strained the number of chains that exhibit force-induced conformational transitions increases in an approximately linear fashion (Figure 32), regardless of the fact that Figure 26 shows that, at the same time, the mechanical consequences of these populations are not significant. Furthermore this mechanism is expected to be operative at l_C/l_M ratios that are not unrealistic for pectin gels in vitro or in-vivo, as long as the architecture of the network is carefully controlled, as described above, so that it contains significant lengths of single chains. It is worth noting that additional simulations performed using a realistic polydispersity produced data with similar conclusions. While currently obtaining direct experimental evidence of force-induced conformational transitions taking place in the pectin molecule in macroscopic gels, or indeed

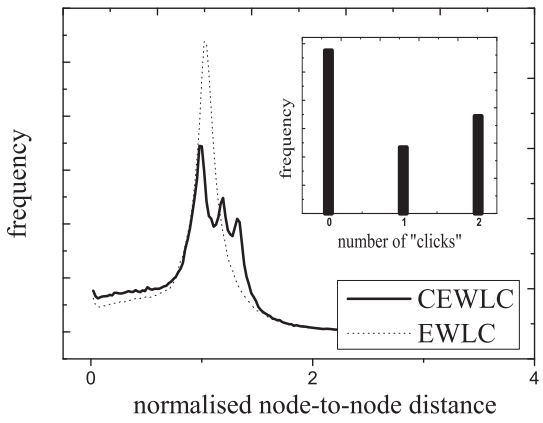

Figure 27: Distribution of the node-to-node distance of unstrained equilibrated CEWLC (thick line) and EWLC networks (thin line) with $l_C/l_M = 1.0$; normalized with respect to the length of the fully extended skew-boat conformation of the CEWLC. Inset: Histogram of the number of CEWLCs that have undergone a) no b) one or c) two force-induced conformational transitions in their constituent sugar rings.

in the plant cell wall, awaits technique developments the simulations carried out herein provide evidence for their possible role in strain-sensing and signalling as opposed to the direct manipulation of rheological properties. Such strain-sensing might involve the modification of the propensity of a ligand to bind to the biopolymer as the conformation of the sugar-ring is modified.

In detail it is unlikely that all deformations applied to biopolymer gels or indeed to the plant cell wall in-vivo during physiologically relevant processes are strictly affine [28]. Therefore further simulations were carried out examining the behaviour of networks of CEWLCs under a non-affine deformation, implemented simply using Lees-Edwards boundary conditions as described above, at gap-averaged strains of (a) 0.5 and (b) 1.0, for the ratio $l_C/l_M = 1.0$ (Figure 33). Figure 34(a) shows the corresponding node-to-node length distributions and histograms of the populations of different conformational states generated at a strain of 0.3, and finally Figure 34(b) presents the number of chains exhibiting force-induced conformational transitions as a function of strain. Once again this number increases in an approximately linear fashion as the strain increases indicating the potential of these chains to act as stress-sensors is not reliant on the affine nature of the deformation.

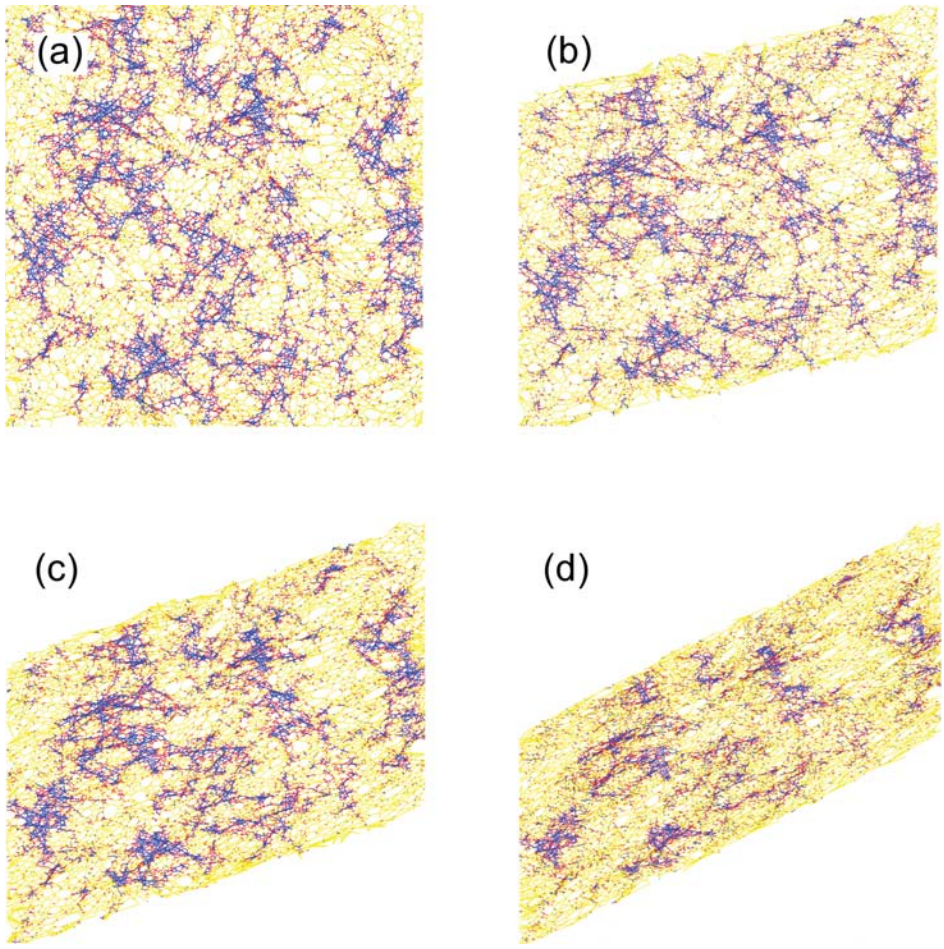

Figure 28: Snapshots of a CEWLC network with $l_C/l_M = 1.0$ at $\gamma =$ (a) 0, (b) 0.3, (c) 0.5, (d) 1. Chains are depicted in blue (no "click"), red (one "click") or yellow (two "clicks") depending on the force-induced conformational state of the sugar rings.

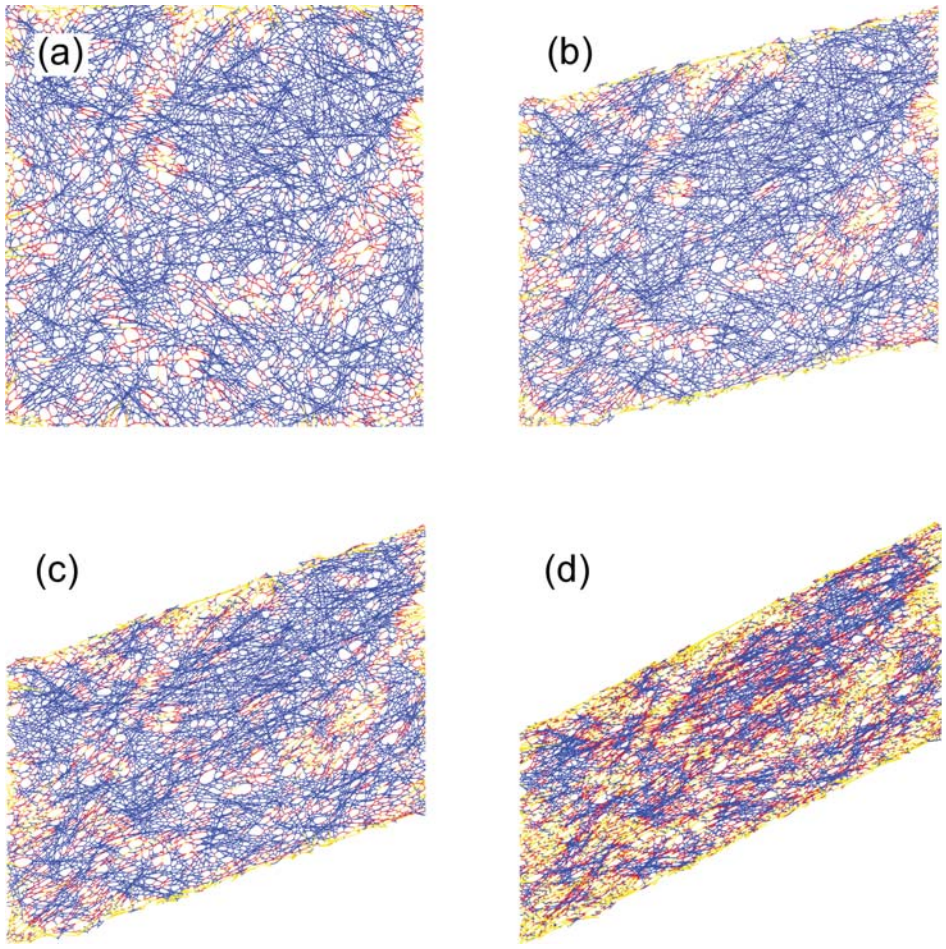

Figure 29: Snapshots of a CEWLC network with $l_C/l_M = 1.8$ at $\gamma =$ (a) 0, (b) 0.3, (c) 0.5, (d) 1. Chains are depicted in blue (no "click"), red (one "click") or yellow (two "clicks") depending on the force-induced conformational state of the sugar rings.

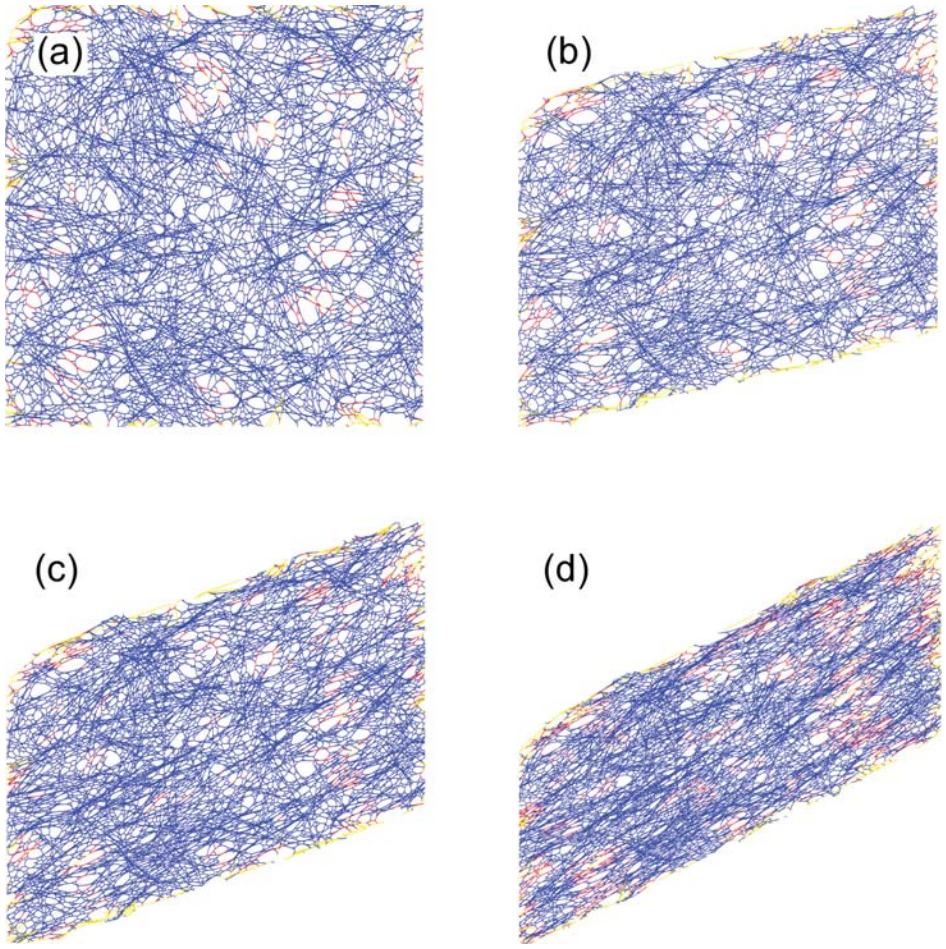

Figure 30: Snapshots of a CEWLC network with $l_C/l_M = 2.5$ at $\gamma =$ (a) 0, (b) 0.3, (c) 0.5, (d) 1. Chains are depicted in blue (no "click"), red (one "click") or yellow (two "clicks") depending on the force-induced conformational state of the sugar rings.

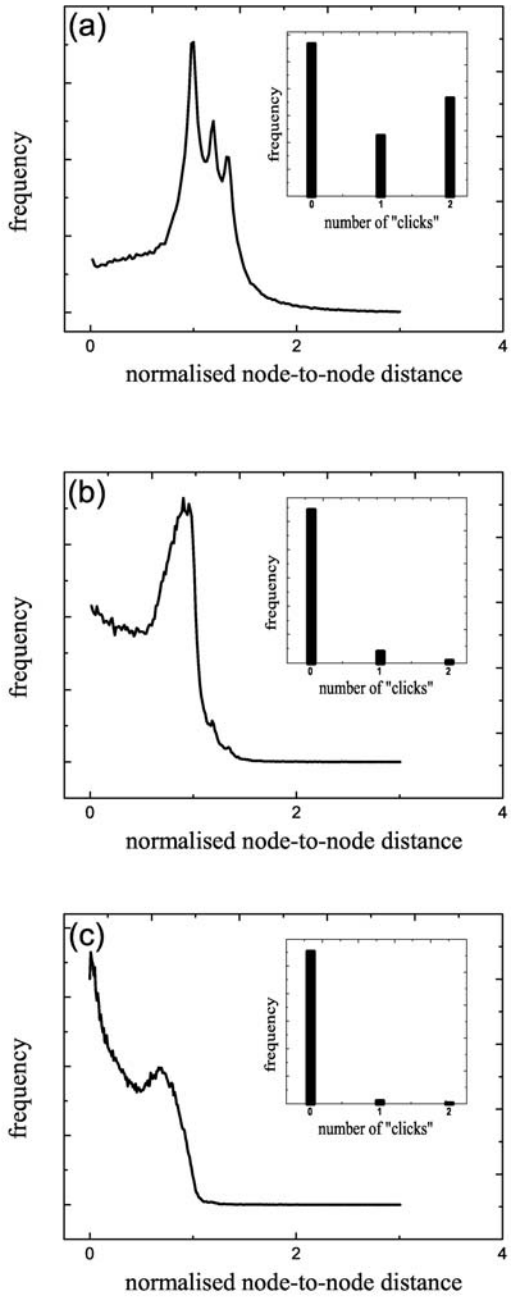

Figure 31: The node-to-node distance distribution and number of clicked chains at $\gamma = 0.3$ for $l_C/l_M =$ (a) 1.0, (b) 1.8, (c) 2.5.

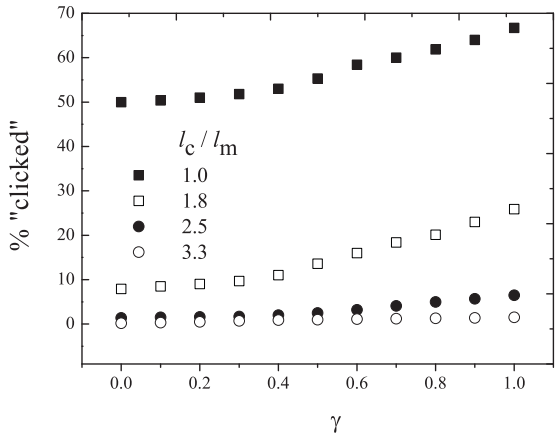

Figure 32: Percentage of chains exhibiting "clicked" states - which have undergone either one or two conformational transitions - versus strain in CEWLC networks at different l_C/l_M ratios.

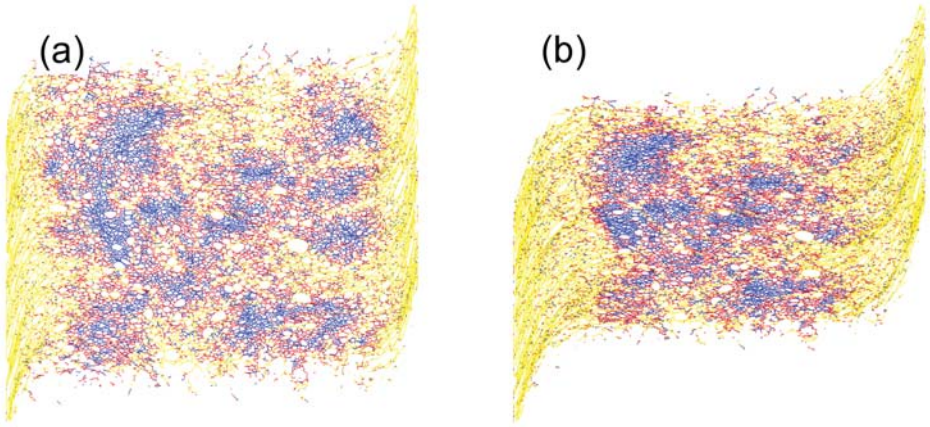

Figure 33: Snapshots of a CEWLC network with $l_C/l_M = 1.0$ at γ =(a) 0.5, and (b) 1. Chains are depicted in blue (no "click"), red (one "click") or yellow (two "clicks") depending on the force-induced conformational state of the sugar rings. Non-affine deformation using Lees-Edwards boundary conditions.

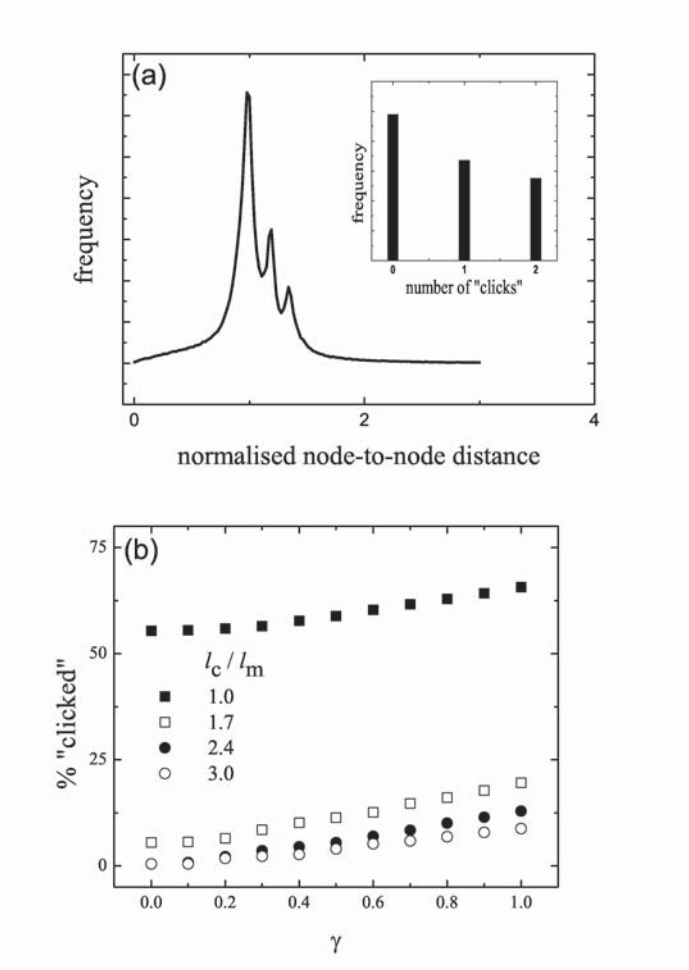

Figure 34: (a) The node-to-node distance distribution of a CEWLC network with $l_C/l_M = 1.0$ at $\gamma = 0.3$. Non-affine deformation using Lees-Edwards boundary conditions (b) Percentage of chains exhibiting "clicked" states (which have undergone either one or two conformational transitions) versus strain.

3.3.2 Dual agent - towards biological networks

While the exact architecture of the biopolymeric network in the plant cell wall is still a matter of debate to some extent, pectin networks are known to play a significant part in controlling mechanical properties, particularly in the middle lamellar or in the cellulose-sparse pollen tube. In addition, there is gathering evidence which suggests that pectin chains, rather than forming an independent gel matrix in which other components are embedded, may be coupled to cellulose fibrils [31, 32]. As such, simulations were additionally carried out with two different node-to-node potentials: CEWLCs as described above (mimicking pectin); coupled through simple Hookean springs (mimicking cellulose). The additional parameter of the Hookean spring stiffness, $\overline{k}$, influences the response of the network to strain; three different spring constants for the Hookean network element were used, the magnitudes of which are illustrated in Figure 35, compared with the CEWLC used. It is found that the shear moduli of dual-agent networks under affine deformations (independent of the spring constant and the constituting contour length of the single chains) collapse onto a master plot, displayed in Figure 36.

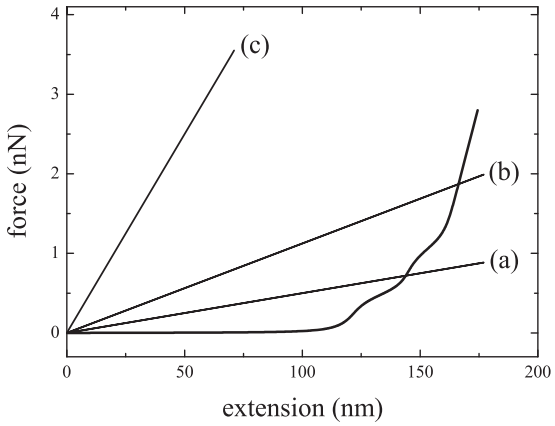

Figure 35: Force-extension curves of the implemented CEWLC (with parameters as in Figure 25) and Hookean springs as used in the dual agent network simulations described herein; with spring stiffness $\overline{k}$ = (a) 5.0 pN/nm, (b) 11.2 pN/nm, (c) 50.0 pN/nm or in simulation units $\overline{k}$ = (a) 50, (b) 112, (c) 500 respectively.

Crucially, with increasing strain the conclusion from the single CEWLC networks described above still holds and while incorporating polymers capable of force-induced conformational transitions does not grossly affect the mechanical properties of these

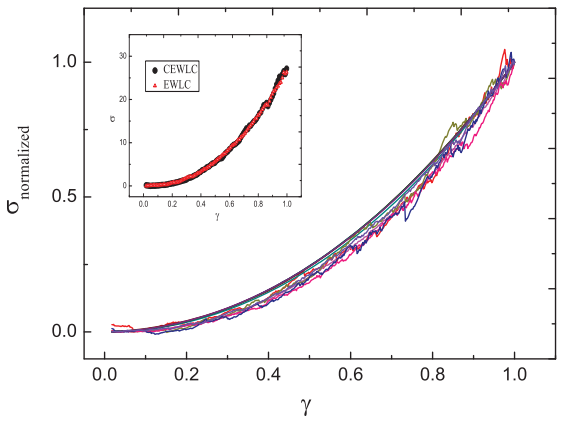

Figure 36: Plots of normalized shear stress, $\sigma_{normalized}$ (normalized by the according stress at strain 1), versus strain, γ, for dual agent networks following an affine deformation. The stress-strain curves for all parameters displayed in Figure 37 collapse on the same master-curve. Inset: Plots of shear stress, σ, versus strain, γ, for dual agent networks comprising CEWLCs or EWLCs at spring stiffness $\overline{k} = 112$ and $l_C/l_M = 4.0$.

dual-agent simulations as compared to what would result from the inclusion of standard EWLCs (inset in Figure 36), the number of chains with the sugar rings in different conformations does depend on the applied strain (Figure 37) and the number of the "clicked-states" shows the same tendency as reported already above and decreases with increasing l_C/l_M; no trivial connection between the spring stiffness of the Hookean elements and the number of clicked states is observed. A number of these dual-agent simulations at strain 0.3 are displayed in Figure 38.

It is worthwhile to ascertain which of the values used in the simulations most closely resemble the effective spring constant of cellulose microfibrils. Effective spring constants for rods of various biological materials of $10\,\mu m$ length have been cited in the literature including actin filaments (5 pN/nm); microtubules ($\sim$ 15 pN/nm); and hemicellulose ($>$ 50 pN/nm) [33, 34]. These simulations suggest that in networks, corresponding to pectin cross-linked to cellulose, a bulk of the strain is transferred to the clickable agents and large internal stresses prevail.

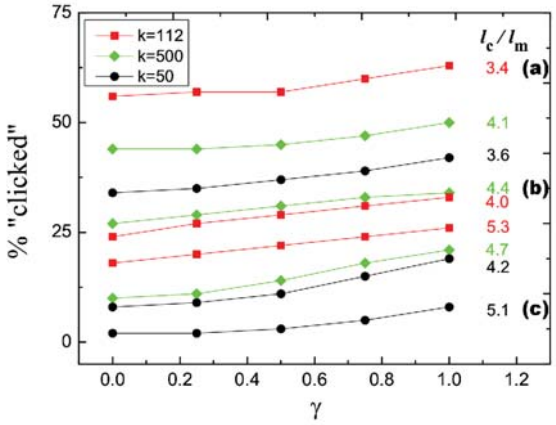

Figure 37: Percentage of chains exhibiting "clicked" states (which have undergone either one or two conformational transitions) versus strain in dual agent networks at different ratios of l_C/l_M and at different rod stiffness $\overline{k}$.

3.4 Conclusions

In this Chapter, a numerical simulation approach has been pursued in order to investigate the possible macroscopic functionality of novel nanomechanical features of polysaccharide chains; specifically force-induced conformational transitions in the sugar rings of pectin. The study in Chapter 2 showed that it is likely such networks do exist. The macroscopic mechanical properties of networks of randomly-oriented chains showed non-linear elasticity, in agreement with a recently reported averaging approach. While the bulk mechanical responses of networks consisting either of simple extensible wormlike-chains (EWLC) or CEWLC were found to be indistinguishable, the number of chains containing sugar rings in different conformational states was found to change during straining. Similar conclusions are drawn under affine or non-affine deformations and when CEWLCs are used to cross-link elastic rods in a two component system, as biomimetic model of the plant cell wall. This supports the hypothesis that in networks of randomly oriented chains such conformational transitions could have biological significance as stress-switches in signalling processes, but that they are unlikely to affect the bulk rheological properties of tissue.

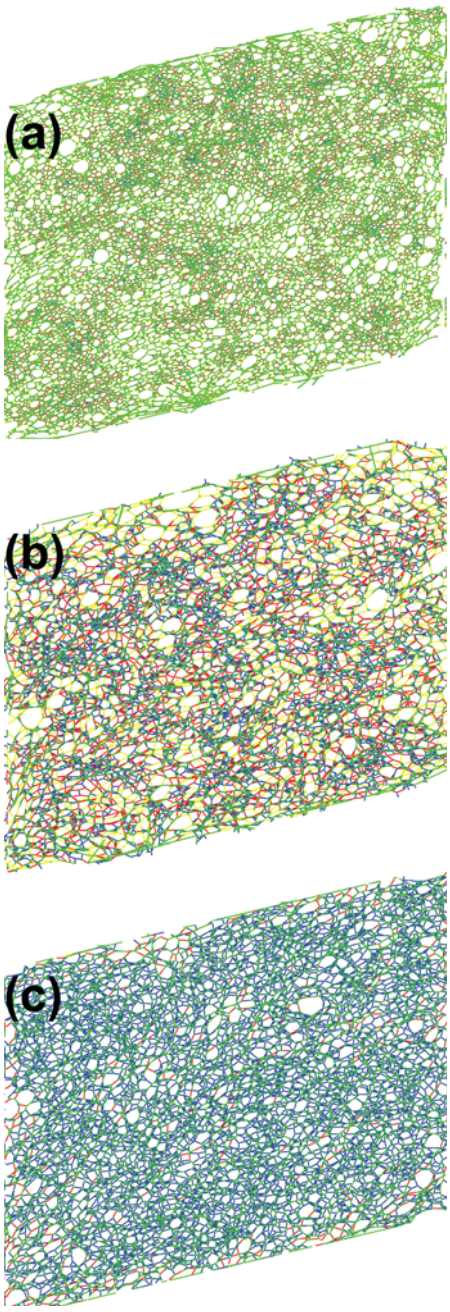

Figure 38: Snapshots of a dual agent network at $\gamma = 0.3$. CEWLCs are depicted in blue (no "click"), red (one "click") or yellow (two "click") depending on the force-induced conformational state of the sugar rings; the Hookean rods are depicted in green. The conditions of (a), (b) and (c) are marked in Figure 37.

References

[1] H. J. Butt, B. Cappella, and M. Kappl. Force measurements with the atomic force microscope: Technique, interpretation and applications. *Surface Science Reports*, 59(1-6):1–152, 2005. doi: 10.1016/j.surfrep.2005.08.003. 69

[2] T. E. Fisher, P. E. Marszalek, A. F. Oberhauser, M. Carrion-Vazquez, and J. M. Fernandez. The micro-mechanics of single molecules studied with atomic force microscopy. *Journal of Physiology*, 520(1):5–14, 1999. doi: 10.1111/j.1469-7793.1999.00005.x. 69

[3] A. Janshoff, M. Neitzert, Y. Oberdorfer, and H. Fuchs. Force spectroscopy of molecular systems - single molecule spectroscopy of polymers and biomolecules. *Angewandte Chemie-international Edition*, 39(18):3213–3237, 2000. doi: 10.1002/1521-3773(20000915)39:18<3212::AID-ANIE3212>3.0.CO;2-X. 69

[4] S. A. Harris. The physics of dna stretching. *Contemporary Physics*, 45(1): 11–30, 2004. doi: 10.1080/00107510310001624478. 69

[5] B. L. Smith, T. E. Schaffer, M. Viani, J. B. Thompson, N. A. Frederick, J. Kindt, A. Belcher, G. D. Stucky, D. E. Morse, and P. K. Hansma. Molecular mechanistic origin of the toughness of natural adhesives, fibres and composites. *Nature*, 399(6738):761–763, 1999. doi: 10.1038/21607. 69

[6] Q. M. Zhang and P. E. Marszalek. Identification of sugar isomers by single-molecule force spectroscopy. *Journal of the American Chemical Society*, 128 (17):5596–5597, 2006. doi: 10.1021/ja058828e. 70

[7] R. G. Haverkamp, M. A. K. Williams, and J. E. Scott. Stretching single molecules of connective tissue glycans to characterize their shape-maintaining elasticity. *Biomacromolecules*, 6(3):1816–1818, 2005. doi: 10.1021/bm0500392. 70, 71

[8] P. E. Marszalek, A. F. Oberhauser, H. B. Li, and J. M. Fernandez. The force-driven conformations of heparin studied with single molecule force microscopy. *Biophysical Journal*, 85(4):2696–2704, 2003. doi: 10.1016/S0006-3495(03)74692-X. 70

[9] P. E. Marszalek, H. B. Li, A. F. Oberhauser, and J. M. Fernandez. Chair-boat transitions in single polysaccharide molecules observed with force-ramp afm. *Proceedings of the National Academy of Sciences of the United States of America*, 99(7):4278–4283, 2002. doi: 10.1073/pnas.072435699. 70

[10] P. E. Marszalek, Y. P. Pang, H. B. Li, J. El Yazal, A. F. Oberhauser, and J. M. Fernandez. Atomic levers control pyranose ring conformations. *Proceedings of the National Academy of Sciences of the United States of America*, 96(14): 7894–7898, 1999. doi: 10.1073/pnas.96.14.7894. 70, 71

[11] P. E. Marszalek, A. F. Oberhauser, Y. P. Pang, and J. M. Fernandez. Polysaccharide elasticity governed by chair-boat transitions of the glucopyranose ring. *Nature*, 396(6712):661–664, 1998. doi: 10.1038/25322. 70

[12] M. Rief, F. Oesterhelt, B. Heymann, and H. E. Gaub. Single molecule force spectroscopy on polysaccharides by atomic force microscopy. *Science*, 275 (5304):1295–1297, 1997. doi: 10.1126/science.275.5304.1295. 70

[13] M. Kuttel and K. J. Naidoo. Glycosidic linkage rotations determine amylose stretching mechanism. *Journal of the American Chemical Society*, 127(1):12–13, 2005. doi: 10.1021/ja047138s. 70

[14] I. Neelov, D. Adolf, M. Ratner, O. Zhicol, and T. McLeish. Molecular dynamics simulation of dextran extension at constant pulling speed. *Macromolecular Symposia*, 237:81–89, 2006. doi: 10.1002/masy.200650510. 70

[15] R. G. Haverkamp, A. T. Marshall, and M. A. K. Williams. Model for stretching elastic biopolymers which exhibit conformational transformations. *Physical Review E*, 75(2):021907, 2007. doi: 10.1103/PhysRevE.75.021907. 70, 72

[16] P. E. Marszalek, H. B. Li, and J. M. Fernandez. Fingerprinting polysaccharides with single-molecule atomic force microscopy. *Nature Biotechnology*, 19(3):258–262, 2001. doi: 10.1038/85712. 70

[17] M. A. K. Williams, A. T. Marshall, P. Anjukandi, and R. G. Haverkamp. Investigation of the effects of fine structure on the nanomechanical properties of pectin. *Physical Review E*, 76(2):021927, 2007. doi: 10.1103/PhysRevE.76.021927. 70, 71, 72

[18] R. Vincent, A. Cucheval, Y. Hemar, and M. Williams. Bio-inspired network optimization in soft materials - insights from the plant cell wall. *European Physical Journal E*, 28(1):79–87, 2009. doi: 10.1140/epje/i2008-10416-2. 71

[19] B. A. DiDonna and A. J. Levine. Filamin cross-linked semiflexible networks: Fragility under strain. *Physical Review Letters*, 97(6):068104, 2006. doi: 10.1103/PhysRevLett.97.068104. 72

[20] J. Astrom, S. Saarinen, K. Niskanen, and J. Kurkijarvi. Microscopic mechanics of fiber networks. *Journal Of Applied Physics*, 75(5):2383–2392, 1994. doi: 10.1063/1.356259. 72

[21] B. A. DiDonna and A. J. Levine. Unfolding cross-linkers as rheology regulators in f-actin networks. *Physical Review E*, 75(4):041909, 2007. doi: 10.1103/PhysRevE.75.041909. 72

[22] D. A. Head, A. J. Levine, and F. C. MacKintosh. Deformation of cross-linked semiflexible polymer networks. *Physical Review Letters*, 91(10):108102, 2003. doi: 10.1103/PhysRevLett.91.108102. 72

[23] M. D. Wang, H. Yin, R. Landick, J. Gelles, and S. M. Block. Stretching dna with optical tweezers. *Biophysical Journal*, 72(3):1335–1346, 1997. doi: 10.1016/S0006-3495(97)78780-0. 72

[24] C. Lofgren, S. Guillotin, and A. M. Hermansson. Microstructure and kinetic rheological behavior of amidated and nonamidated lm pectin gels. *Biomacromolecules*, 7(1):114–121, 2006. doi: 10.1021/bm050459r. 72

[25] S. Cros, C. Garnier, M. A. V. Axelos, A. Imberty, and S. Perez. Solution conformations of pectin polysaccharides: Determination of chain characteristics by small angle neutron scattering, viscometry, and molecular modeling. *Biopolymers*, 39(3):339–352, 1996. doi: 10.1002/(SICI)1097-0282(199609)39:3<339::AID-BIP6>3.0.CO;2-P. 72

[26] H. Kang, Q. Wen, P. A. Janmey, J. X. Tang, E. Conti, and F. C. MacKintosh. Nonlinear elasticity of stiff filament networks: Strain stiffening, negative normal stress, and filament alignment in fibrin gels. *Journal of Physical Chemistry B*, 113(12):3799–3805, 2009. doi: 10.1021/jp807749f. 73

[27] C. Storm, J. J. Pastore, F. C. MacKintosh, T. C. Lubensky, and P. A. Janmey. Nonlinear elasticity in biological gels. *Nature*, 435(7039):191–194, 2005. doi: 10.1038/nature03521. 73, 74, 76

[28] Q. Wen, A. Basu, J. P. Winer, A. Yodh, and P. A. Janmey. Local and global deformations in a strain-stiffening fibrin gel. *New Journal of Physics*, 9:428, 2007. doi: 10.1088/1367-2630/9/11/428. 73, 77

[29] A. W. Lees and S. F. Edwards. Computer study of transport processes under extreme conditions. *Journal Of Physics Part C Solid State Physics*, 5(15):1921, 1972. doi: 10.1088/0022-3719/5/15/006. 73

[30] Anna Strom. *Characterisation of pectin fine-structure and its effect on supramolecular properties*. PhD thesis, Cork University, 2006. 74

[31] A. Zykwinska, J. F. Thibault, and M. C. Ralet. Competitive binding of pectin and xyloglucan with primary cell wall cellulose. *Carbohydrate Polymers*, 74(4): 957–961, 2008. doi: 10.1016/j.carbpol.2008.05.004. 84

[32] A. W. Zykwinska, M. C. J. Ralet, C. D. Garnier, and J. F. J. Thibault. Evidence for in vitro binding of pectin side chains to cellulose. *Plant Physiology*, 139(1): 397–407, 2005. doi: 10.1104/pp.105.065912. 84

[33] L. Salmen. Micromechanical understanding of the cell-wall structure. *Comptes Rendus Biologies*, 327(9-10):873–880, 2004. doi: 10.1016/j.crvi.2004.03.010. 85

[34] J. R. Blundell and E. M. Terentjev. Stretching semiflexible filaments and their networks. *Macromolecules*, 42(14):5388–5394, 2009. doi: 10.1021/ma9004633. 85

Chapter 4

3D network model and comparison with experiments

4.1 Introduction

In plant cells, pectin is synthesized in the Golgi apparatus with a high degree of methylesterification. This high DM prevents the formation of gels that otherwise might be induced by Ca^{2+} ions while pectin is being transported to the plant cell wall. The pectin chains are subsequently modified in-muro by PME enzymes, which de-esterifiy the polymer and subsequently allow calcium binding. This process of gelation can therefore be seen as the reverse case of the formation of traditional low DM gels in-vitro, where the release of ions into low DM substrates induces the binding – in stark contrast to the release of ion binding groups via enzymatic activity as utilized extensively herein. For pPME-induced gelation, once the processive enzyme activity has freed a sufficient number of carboxyl groups to form a stable egg-box junction zone [1], these newly induced steric constraints hinder the enzyme activity on this strand, so that the pPME moves to another chain and creates another blocky calcium binding site of minimal length. This results in a permanently cross-linked network of single pectin chains.

The SAXS studies detailed in Chapter 2 indeed support the hypotheses initially developed from high-frequency microrheological data [2] that using pPME to release ion-binding groups from high DM pectins in the presence of calcium in a biomimetic approach can form gels in which single pectin chains play an important stress bearing role. In addition, the work in Chapter 3 described the first steps toward modelling the mechanical behaviour of networks using single molecule force-extension curves as input, in a realization of a 2-dimensional random network. With these things in hand the next step has been taken in modelling a 3-dimensional network so that predictions could be tested experimentally. Specifically, the simulation of bulk net-

work rheology from experimentally measured single-chain properties constitutes a novel approach that brings a true bottom-up approach towards the directed design and understanding of biomaterials a step closer.

To be able to construct a realistic model the concentration of the starting polymer solution is first used to determine the junction-zone (node) density of the network simulation. The initial spatial distribution of these nodes is determined simply by a Mikado process as described previously. The average "contour length" of single pectin chain sections between such nodes is then estimated, and from this information and the reported functional form of the pectin single molecule force-extension curve, the stress-strain behaviour of the network was simulated. The commercial high DM pectin samples considered in our study have a molecular weight in the order of M_w= 100 kDa and as one sugar ring has a molecular weight of around 180 Da [3], this leads to the consideration of chains of 560 monomers. Further, a typical conformation in which monomers without external stress reside is the $^4C_1$ Chair, in which a monomer spacing of 0.4592 nm is found [4], which leads finally to an estimate for the contour length of a free pectin chain as: $l_C = 260$ nm. An estimate of the length of such chains that is attached between nodes is made in due course. Another length scale of interest is the persistence length l_P. Viscometry studies and SANS have estimated l_P to be between 7-10 nm [5]. This suggests, that in contrast to the intensely investigated area of F-actin networks, where the l_P and l_C are the same order of magnitude; for pectin chains, the persistence length is about one order of magnitude smaller than the contour length. This observation makes us aware that some of the elaborations on actin and protein networks (as in Chapter 1.2.7) will not be directly applicable towards polysaccharide gels. Pectin chains are thus semi-flexible, but not as stiff as actin filaments, more similar in properties to single-stranded DNA [6].

Previous work has shown that both biopolymer networks [7, 8] and synthetic polymers [9] can exhibit a non-linear strain-stiffening rheology. However, several models have been proposed as to its origins as described in Chapter 1. Most commonly it is postulated that either stiff but deformable cross-link zones and flexible chains rearrange on the application of strain and thus yield the observed behaviour, or alternatively that the non-linearities of the polymer elasticity are sufficient to account for the observed phenomenology. While a recent Nature paper [10] showed that materials made from the cross-linking of semi-flexible entities have generic rheological properties, including strain-stiffening, as long as the force response of these single filaments can be expressed by a worm-like chain Hamiltonian, exemplary networks

to date possess hierarchical filaments that are rods, tubes or fibrils, assembled by several macromolecules, whose single filament properties have not been independently probed. By utilising the understanding gleaned from recent microrheological and SAXS studies of biomimetic pectin gels, a system has been assembled where it is anticipated that single pectin chains play an important stress bearing role. Further, these polysaccharide gels do strain-stiffen and their filament properties (the single chain force-extension curve) is experimentally available. As such, this system provides the perfect bottom-up experimental test of current biopolymer network theories.

4.2 Materials and methods

Pectin. The material used had a DM of 78, and was described in Chapter 2.2.
Pectinmethylesterase (PME) [EC 3.1.1.11] was purchased from Sigma Aldrich (P5400) in order to remove methyl-ester groups from the starting pectin substrate [11]. (a) previously frozen stock solutions and (b) freshly mixed enzyme solutions were both used for the experiments: (a) Stock solutions of the enzyme were prepared by dissolving 0.01 g of dried PME in 20 mL Milli-Q water with 0.58 g of NaCl, and were stored at 253 K in Eppendorf tubes. Aliquots were thawed prior to conducting experiments and used immediately. (b) 0.01 g of dried PME were dissolved in 40 mL Milli-Q water with 1.2 g of NaCl. Aliquots were used immediately.

4.2.1 Sample preparation

Enzymatically induced pectin gels. Stock pectin solutions of 1.25% w/w were prepared by dissolving the apple pectin powder in a 50 mM HEPES buffer made with Milli-Q water, adjusting to pH 7.5 with 1 M NaOH, and stirring for 1 hour. Subsequently, desired volumes of a $CaCl_2$ salt solution were added (with a concentration as listed in Table 4.1). Finally the sample was mixed with the desired volume of 50 mM HEPES buffer, in order to reach a final polymer concentration of 1% w/w. As the starting pectin is of a high DM, it does not gel in the presence of the added Ca^{2+}. Before loading the 20 mL of the solution in the rheometer, the desired quantity of enzyme solution (as listed in Table 4.1) was added to the pectin solution with a DM of 78, mixed and the measurements started.
Plastic embedding of pectin gels. Samples for transmission electron microscopy were prepared by being embedded in a plastic resin and then thinly sliced with an ultramicrotome. The protocol for the sample preparation was as follows: Small bodies (about 2-3 mm wide) of gels were placed in a fixating solution (2 volume% glu-

Table 4.1: Pectin samples: the samples are prepared as described in the text, the specific PME and $CaCl_2$ conditions used are reported here.

Sample name	PME	$[CaCl_2]$
PMEl1	frozen. 25 μL/mL pectin solution	1.1 mM
PMEl2	frozen. 69 μL/mL pectin solution	1.1 mM
PMEh1	fresh. 25 μL/mL pectin solution	1.1 mM
PMEh2	fresh. 10 μL/mL pectin solution	3.3 mM

taraldehyde in HEPES buffer (50 mM, pH 7.5) including 1 g/dm^3 ruthenium red) for one hour to fix and stain the network structures. HEPES buffer (50 mM, pH 7.5) was used to remove any unbound glutaraldehyde and ruthenium red in two washing steps. The samples were then further fixed/stained in 2% osmium tetroxide solution for one hour. Ultrapure water was used to remove any unbound osmium tetroxide in three washing steps. The samples were dehydrated in multiple baths of ethanol - 50%, 70%, 90% and absolute alcohol and then embedding media (LR White) was added to infiltrate the samples. Finally the polymerisation of the resin was allowed to occur at 333 K overnight.

4.2.2 Methods

Rheological measurements. The viscoelastic moduli (G', G'') of pectin gels were measured using the stress-controlled Anton Paar Physcia 301 rheometer with CC27 double-gap sandblasted geometry. The elastic modulus $G'(\omega)$ measures the energy storage in which the strain is in-phase with an applied oscillatory stress $\sigma(\omega)$, while the out-of phase energy dissipation is measured by the viscous modulus $G''(\omega)$. The real part of the storage modulus reduces to the shear modulus G at zero frequency. The sample was loaded as quickly as possible onto the rheometer after the introduction of the enzyme (preset to 298 K). A thin layer of Whiterex Oil was placed on top of the sample to prevent evaporation. Firstly, the gelation profile of the sample was monitored over time using small deformations with a strain of 0.5% and a frequency of 1 Hz until a gel of desired strength was formed. Subsequently, a differential measurement [12] was utilized to quantify its nonlinear behaviour. The system is held at a constant average (pre-)stress σ, while the differential response $d\gamma$ to a small additional oscillatory stress $d\sigma$ is measured to yield the nonlinear differential modulus $K = d\sigma/d\gamma$. The first rotational stress was 1 Pa in magnitude. Subsequent stresses were, in order: 2, 3, 4, 6, 8, 12, 16, 24, 32, 48, 64, 96, 128, 192, 256, 384, 512, 868, 1024 and 1536 Pa. At each rotational stress interval, small deformation oscillations

were conducted at 1 Hz for 120 s. The magnitude of each oscillation was set at 10% of the respective rotational stress during each interval. The sample was kept at 298 K throughout the experiment.

Electron microscopy. 150 nm sections of epoxy-embedded gel, as described in the sample preparation Section, on 400 mesh hexagonal copper grids were loaded into a high-tilt cryo-tomography sample holder. A JEM-1400 transmission electron microscope (JEOL, Japan) with tungsten filament and operating at an accelerating voltage of 120 kV was used for data acquisition. The sample was cooled to the lowest stable temperature possible with this holder system (about 99 K) and then pre-irradiated at low electron flux for 10 minutes to permit occurrence of gross shrinkage and mass loss. Tomograms were recorded using a nominal magnification of 15 000, corresponding to a pixel size of 6.9 Å at the detector, a $2K \times 2K$ CCD camera (Ultrascan 1000, Gatan, Pleasanton, CA). The tilt scheme was set up without any imposed defocus and tilt series were collected with an angular increment of one degree over an angular range of at least ±70 degrees. Tomograms were aligned by feature tracking and reconstructed using iterative algorithms implemented in the TomoJ plugin [13, 14] for ImageJ [15].

Modelling methods To computationally simulate the shear deformation of a 3-dimensional biopolymer network comprised of single CEWLCs the methods described in Chapter 3.2.1 were extended. As affine deformations were previously found to describe the bulk mechanical response of biopolymer gels successfully [10, 16], especially at intermediate to high concentrations [17, 18], we focused simulations on this affine case; although the method is easily extended in this regard if required. The elaborations in Section 4.1 confirm that the bending of rods can again be neglected, as $l_P << l_C$ still holds [19] and therefore the mechanical response of the CEWLC chains captured by the experimentally measured FE curves (Figure 25) should be valid for use in networks.

The Mikado technique was used to generate random networks of desired densities, within a 3-dimensional cubic simulation box of length 1 (in simulation units). The generated nodes were linked by monodisperse CEWLC. To achieve a realisation for affine shear deformations in 3-dimensions, the methods used previously were straightforwardly extended. During the generation of the network architecture from the node positions two connectivities were preliminarily investigated: (a) if two intersecting Mikado rods were linked by an initially zero-length cross-link then a trihedral geometry could be generated, whereas (b) if the rods were pinned together at the intersection point and no additional cross links are inserted a node with four

connections is generated. From the studies in Chapter 3 it was anticipated that the influence of modifying the distribution of 3-fold and 4-fold nodes would be minimal for a randomly oriented CEWLC network structure. Simply for computational ease then further simulations were carried out in the geometry (b).

The coordinate system for the cubic simulation box was chosen, so that an affine shear deformation is applied to the bounding X-Y planes in Y-direction, nodes in the bounding X-Z planes are moved affinely and Lees-Edwards boundary conditions [20] are applied to the bounding Y-Z planes. The initial random network was relaxed first; the further straining process was carried out by the repeated step-wise displacement of the X-Y planes followed by the energy minimization routine, as described in Chapter 3.2.1. Test runs comparing simulation volumes of $(10\ \mu m)^3$ ($\sim 10^7$ nodes & several days per run), $(5\ \mu m)^3$ ($\sim 10^6$ nodes & 2 days) and 1 μm^3 ($\sim 10^5$ nodes & $<$ 12 h) showed that the 1 μm^3 set up was still able to capture the mechanical response of the network accurately if averaged over several runs. Therefore further simulations were carried out on 1 μm^3 systems, with ensemble averages being taken over 5 runs.

4.3 Results and discussion

Several enzymatically induced pectin gels were formed in the rheometer and the evolution of their viscoelastic properties measured, via dynamic shear modulus measurements as described, at a frequency of 1 Hz (Figure 39). The investigations centred around a constant polymer concentration and using differing concentrations of enzyme and calcium, as detailed in Table 4.1.

In a recent study the enzyme activity was found to be the major determinant of the speed of the gelation in these systems [21], and indeed this is supported by this study by comparing the time evolution of PMEl1 & PMEl2. However, it is further conspicuous that the activity of the enzyme after being thawed from a previously frozen aliquot that had been stored in a freezer was significantly lower than that found using a sample freshly made from the powdered enzyme, with the former exhibiting an additional delay of around 6 hours before a significant gelling behaviour could be measured. The reason for this was not pursued in detail but may be indicative of a renaturing of the enzyme.

It is also clear that, as expected, the strength of the fully cured gel has a plateau modulus, G_0, that is sensitive to calcium concentration, the source of cross-link forming ions. The calcium concentration was found to be a limiting factor in the gelation of PMEh1; which plateaued after only 2 h, whereas a $CaCl_2$ increase (together with a slight reduction of the enzyme concentration) resulted in moduli one

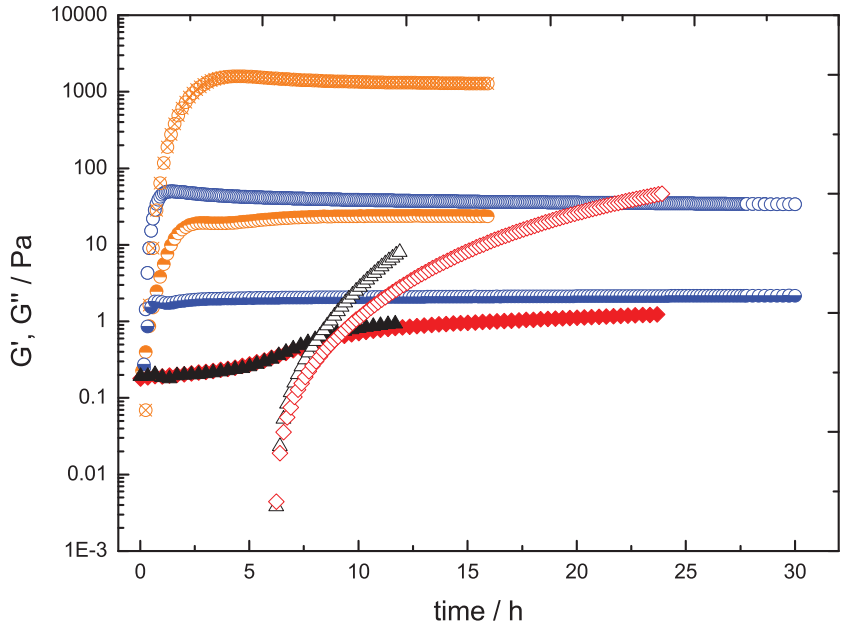

Figure 39: Gel evolution as a function of time during in situ de-esterification of the samples reacting with different activities of each enzyme and at different concentrations of $CaCl_2$, as in Table 4.1. Empty markers, G'; full markers, G''; diamond, PMEl1; triangle upwards, PMEl2; circle, PMEh1; crossed circle, PMEh2.

order of magnitude stronger than observed before.

After the gel formation had been investigated for some 10 hours, the nonlinear elasticity of the networks formed was tested by performing measurements of the differential modulus K (Figure 40 (a)) as a function of prestress. These measurements took around 2 minutes per prestress value, so that even in the cases where the modulus was still slowly evolving the experimental results were not influenced by the ongoing kinetics, and they were performed up to prestresses at which the additional oscillatory stress caused a breakdown, or a dramatic rearrangement of the network. Typically this occurred once the superposed strains reached around $\sim 3\%$. The resultant plots from all four samples exhibit scaling behaviour and collapse onto a master plot (Figure 40 (b)) indicating that the same single-chain physics is governing the observed responses irrespective of the different initial conditions. Despite the fact that the sample with the highest modulus only provides a limited number of data points, it still maps agreeable onto the other data in the master plot.

4.3.1 Comparison with previous work on protein networks

Raw results from the two samples PMEl1 & PMEh2 (the extreme cases studied of a soft and a strong gel) can be compared with previous measurements made on a variety of proteinaceous biomaterials in which the single filaments are not themselves single chains but assembled intermediate structures (Figure 41). The general agreement between the behaviour of the previous ecclectic selection of protein gel samples with the biomimetic polysaccharide network investigated here can be seen to be remarkable.

To illuminate the comparison and permit further a facile comparison with theory, the strain and stress dependence of the differential moduli was evaluated (Figure 41 (a) & (b)). If the origin of this behaviour is the nonlinearity of the single filament Hamiltonian then it is expected that the differential modulus would follow a power law with an exponent of $3/2$ when plotted against the stress (as discussed in in Chapter 1.2.7.1). Such a mapping of prestress measurements onto a strain dependent differential modulus K is valid for permanently cross-linked systems; as a comparison of the measurement protocols for nonlinear moduli [22, 23] suggest that the strain ramp and the differential prestress protocol agree well for such cases, while they agree only at high strain rates for more transient networks. Pinned network structures have been suggested for pectin networks [18] and have also been supported by the previous SAXS study in Chapter 2. The mapping is performed via a numeric integration, with the strain measured at the lowest prestress of 1 Pa

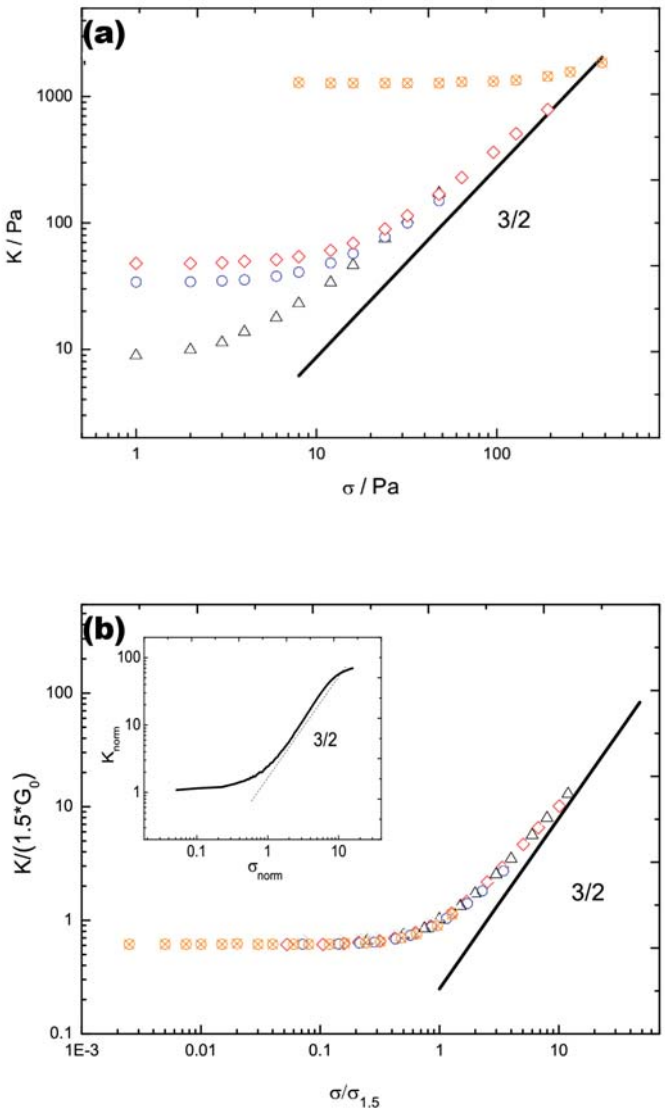

Figure 40: (a) The differential elastic modulus, K, as a function of applied prestress σ for the samples: diamond, PMEl1; triangle upwards, PMEl2; circle, PMEh1; crossed circle, PMEh2. (b) the moduli are scaled by the corresponding modulus at a stress of $1.5{*}G_0$ of the plateau modulus; the inset shows the prediction of the spatial averaging approach (described in Section 4.3.2) in the K vs. σ representation.

used as the initial value, and the results are shown in (Figure 41). In this respect it can be seen that these pectin networks trend towards the 3/2 prediction, and again match the behaviour of the previously measured biopolymer networks remarkably well.

The data recorded for the two samples PMEl1 & PMEh2, exhibiting the extreme cases of a soft and a strong gel, are further compared with the quantitative predictions obtained from the numerical simulation.

4.3.2 Comparison with simulations

From preliminary studies and the calcium and enzyme concentrations used in generating the strongest gel a simulation was first devised in which all the pectin chains in the simulation box are connected to the network. First, the effective length of the pectin chain sections between nodes (cross-links) in the fully-cured network was estimated using basic statistical considerations. Assuming the basic single polymers (of a contour length of around 260 nm as described previously) get pinned together by a *random* enzyme activity, this allows estimates to be made of (a) the average chain length between two randomly chosen cross-link points along the polymer backbone, and (b) the functionality of the nodes generated by the attachment, i.e. how many of the connections are to nodes with additional connections, and how many chains are just elongated by a connection which only pins together two chains.
Assuming process (a) can be modelled by an equidistributed random process, in which two points within an interval of length L are chosen; and assuming therefore a classical Bernoullian process where each event occurs independently with the probability of $1/L$, then the probability density ρ of two selected points being separated by the distance d along the polymer backbone is proportional to

$$\rho \propto (1/L)^2(1-1/L)^d \tag{4.1}$$

as depicted in Figure 42. After normalisation of the probability distribution the average distance $< x >$ between two randomly chosen points can be calculated as:

$$< x >= \frac{p^L(Lln(p)-1)+1}{(p^L-1)ln(p)} \tag{4.2}$$

with $p = (1-1/L)$, and this leads directly to an estimate of an average distance between nodes of around 110 nm.
Point (b) can be captured by considering the likelihood for the occurrence of more than 2 connections per node. Assuming again that the node formation follows a simple Bernoulli process, the probability for a node with c connections to be formed

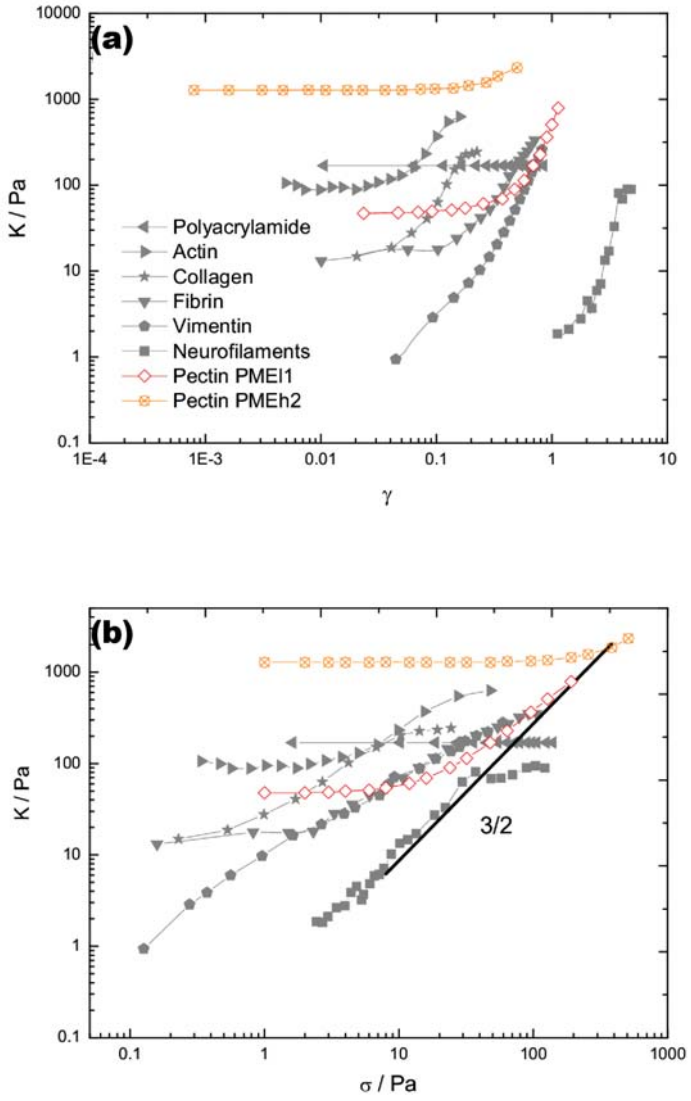

Figure 41: Differential shear moduli K plotted as a function of the dimensionless strain γ, for the two samples PMEl1 & PMEh2; the pectin gels are compared with the measurements on cross-linked biopolymer networks, the data taken from [10].

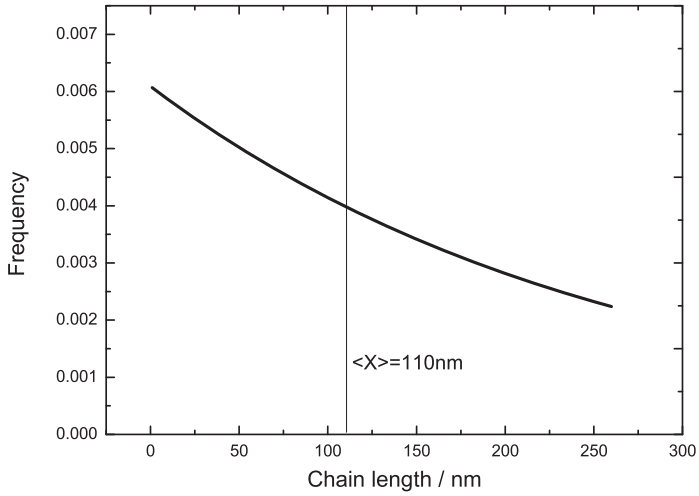

Figure 42: Probability distribution of the distance between two randomly placed points, see Eq. 4.1, applied to a chain of 260 nm contour length; resulting in an average distance of $< x > = 110$ nm.

follows a power-law p_1^c, with the probability p_1 for the existence of a single connection at the point of interest. Considering this power-law decay of the probability for nodes of high connectivities, (and spurred on by attempting to limit the computational expense of the modelling approach), it is argued that the node forming physics is captured within functionalities of up to 4, with the occurrence of nodes with higher connectivities assumed negligible. Considering the dense reasonably homogeneous semi-dilute starting state, every functionality would have the same weighting factor, and therefore (with the cut-off described above) it can be assumed that:

$$p_1^2 + p_1^3 + p_1^4 = 1 \tag{4.3}$$

This results in $p_1 = 0.68$ and therefore in a probability of 47% for the creation of a "2-node", following p_1^2.

These statistical estimates can subsequently be used in the set-up of a 3-dimensional CEWLC numerical simulation of the gel structure, with the aim of predicting the mechanical response of the 1%w/w pectin gel PMEh2. The realization of the system simulated used a network of 130 000 chains (corresponding to the 1%w/w pectin

gel in a 1 μm^3 simulation box). In this framework the above mentioned 47% of "2-nodes" are taken into account via doubling the average effective contour length between nodes, whereas the other effective chain sections between junctions are represented by an average chain length of 110 nm, as described above. PMEh2 resembles a reasonably stiff gel so that although it does not "break down" or dramatically reorganize until prestresses of kPa are reached this only corresponds to a strain of 40% and limits the amount of data available to compare with the prediction. Nevertheless in Figure 43 it is shown that the modelling is remarkably successful in predicting network properties from those of the constituent polymers. A snapshot of the simulated network at zero strain is displayed in Figure 44.

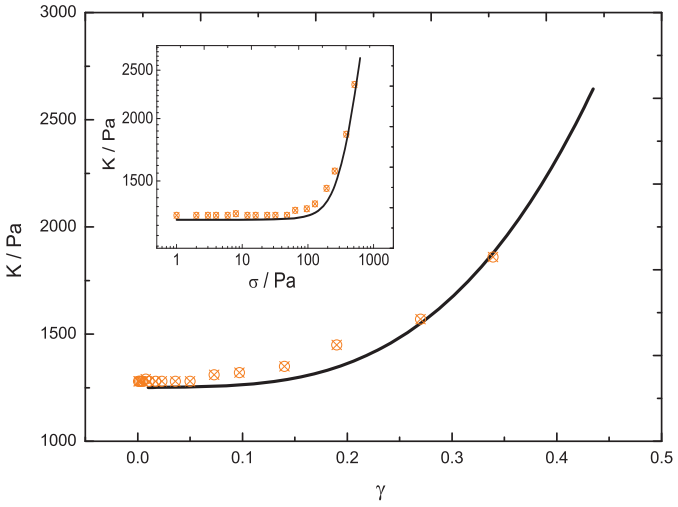

Figure 43: Differential shear moduli K plotted as a function of the dimensionless strain γ, for the sample PMEh2 and the results of the simulation; inset: K versus σ of the simulation results.

Similarly, the stress-strain response for the PMEl1 system (Figure 45) has been investigated within the CEWLC model and the statistics elaborated above. It is clear that the plateau modulus G_0 at zero strain differs by almost two orders of magnitude from the gel investigated above that was hypothesised to have all the chains connected to the network. A further insight into the network structure of the weaker gel can be found in an electron micrograph, obtained as described in the experimental Section above, Figure 46 & 47. It seems clear that while the network

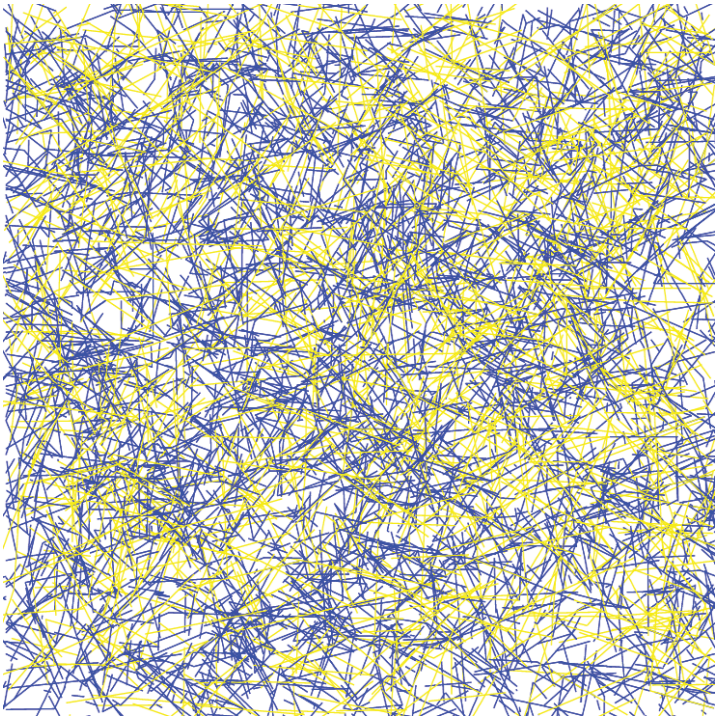

Figure 44: Snapshot of the CEWLC network in a 1 μm^3 simulation box, a slice parallel to the shear plane of 10% sample thickness, at 0 strain. The longer chain section of "2-nodes" are depicted in yellow, the remaining chain segments in blue.

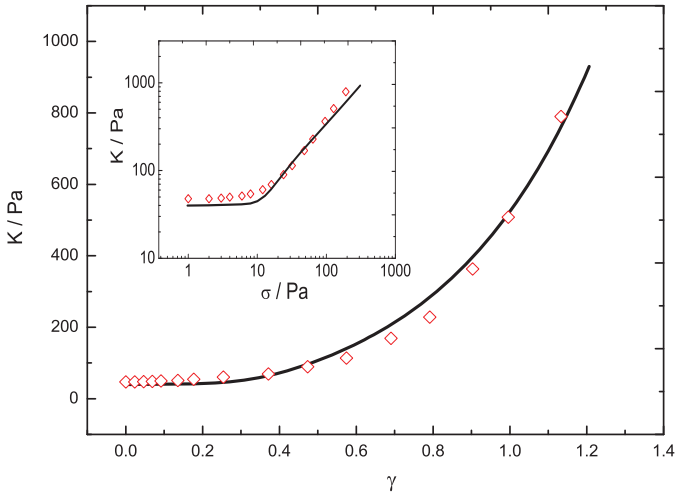

Figure 45: Differential shear moduli K plotted as a function of the dimensionless strain γ, for the sample PMEl1 and the results of the simulation; inset: K versus σ of the simulation results.

is a percolated structure of mainly single chain sections, there do exist obvious gaps in the network, suggesting that not all the chains were attached to the network and that these were perhaps lost in sample preparation for the microscopy. As such, in an attempt to capture the behaviour of this weaker network, the numerical network forming process mentioned above was adapted, in which an initially connected network has nodes removed; motivated by the gaps observed in the TEM micrograph "chunks" of 5 000 neighbouring nodes were treated as one cluster, and each cluster was exposed to random removal. A reduction of nodes was found to reduce the number of the chain segments contributing to the mechanical modulus and yields a lower modulus value in the spirit of classical rubber elasticity or cascade theory. The number of nodes was reduced in such a random fashion until the experimentally measured modulus G_0 (in the order of 100 Pa) was reached in the simulation. This procedure revealed that only around one third of the available chains effectively contribute to the mechanical response in this weak gel, with the other two thirds of the available chains just forming smaller clusters. Interestingly, assuming that chains are not retained for the EM visualization process, resulting in Figure 46, unless they are connected to the percolated network suggests that only around one third of the chains should be visualised, which appears very reasonable. The resulting simulated

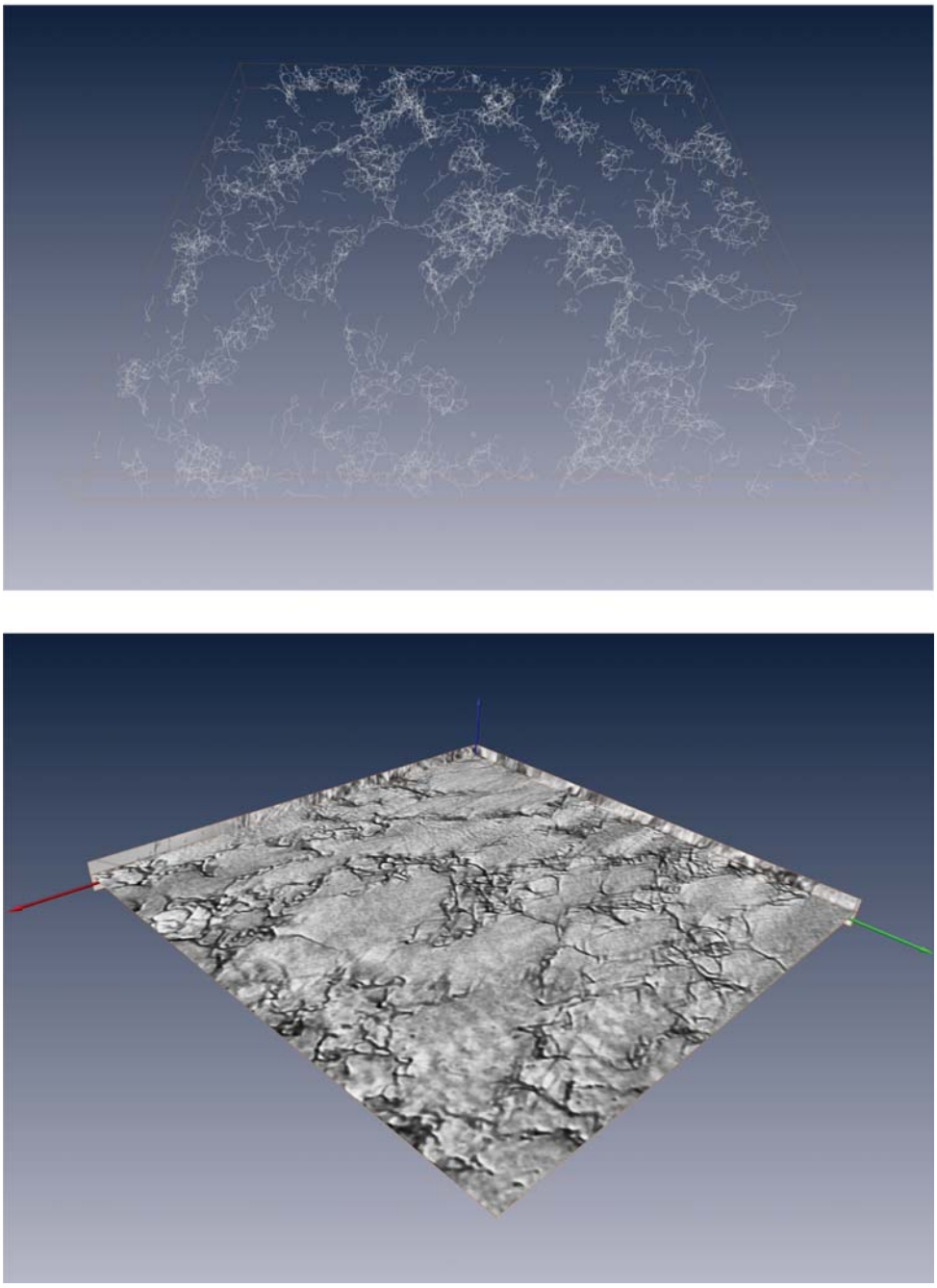

Figure 46: Preliminary perspective images of the network structure of the gel PMEh1; top: TEM micrograph of a slice of 150 nm thickness; bottom: tomography image of a slice of 150 nm thickness.

strain dependence of the differential modulus is depicted in Figure 45; using 44 000 chains in an identical simulation to that performed above, simply with one third of the physiologically available number of chains (consistent with the modulus and the imaging). Once again it is seen that there is remarkably good quantitative agreement between the predicted and the measured mechanical behaviour. A snapshot of such a sparse network at zero strain, via modelling PMEl1, and a comparison with the TEM micrograph is depicted in Figure 47. It should be remembered that such a visualisation essentially shows the node linkages and not the trajectories of actual polymer walks.

The results can further be compared with a 3-dimensional averaging approach to calculate the shear modulus of affine deformations, as introduced in Chapter 3.2.2 for 2-dimensions, using the affine shear deformation tensor as:

$$\Lambda = \begin{pmatrix} 1 & \gamma & 0 \\ 0 & 1 & 0 \\ 0 & 0 & 1 \end{pmatrix} \tag{4.4}$$

The evaluation of Eq. 3.1 results in a shear stress σ for each strain step γ. The differential modulus K was further obtained by a numerical differentiation of this stress-stain curve.
It was seen previously that the experimental results reported here for all the biomimetic pectin gels, in the form of the differential moduli vs. strain plot collapsed also onto a master plot (Figure 48). A comparison with the calculations of the averaging approach reveals that using the experimentally measured force-extension relation is sufficient to fit the master plot (drawn line in Figure 48). The averaging approach evaluates the CEWLC (as in Figure 25) at one average extension, and averages the result over all orientations. The calculation of this normalized stress-strain behaviour depends on the value of this relaxed end-to-end extension L_R, the extension at which the force extension relation is evaluated at 0 strain. While this approach is efficient the value of L_R (depicted in the inset of Figure 48) is extracted by fitting and difficult to estimate otherwise. The result, that L_R equals 53% of the chain's apparent contour length between nodes fits the experimental data within this theoretical framework and indicates that the chains are extended towards the end of the linear entropic regime. Further applied strain extends the chains into the nonlinear regime and causes the stiffening response, as explained in detail in Chapter 1.2.7.1.

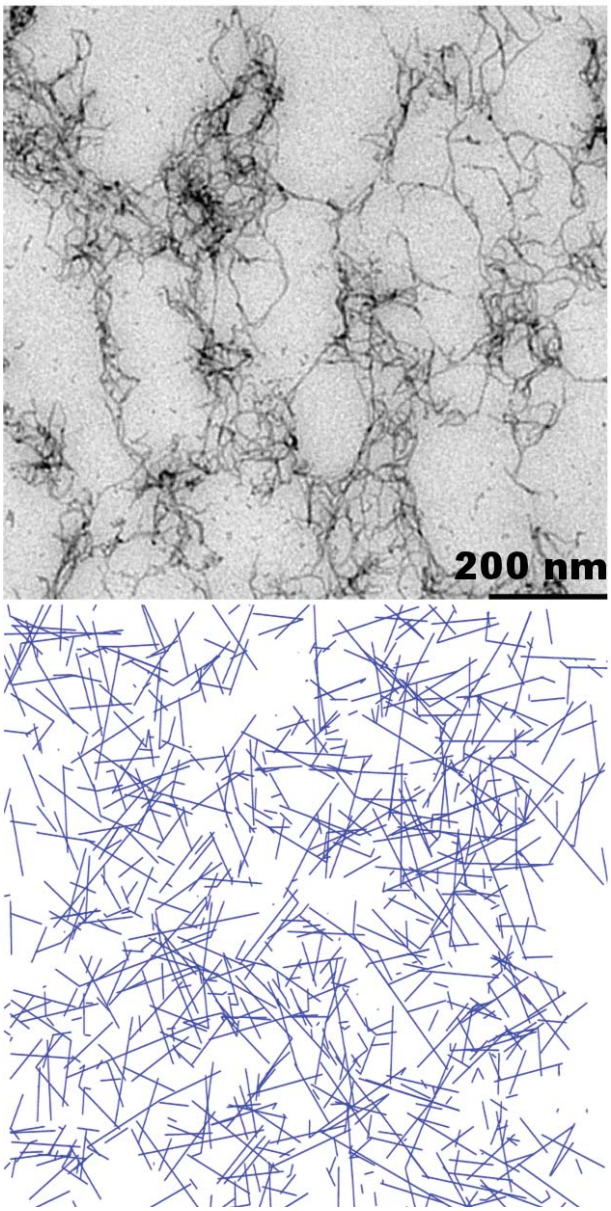

Figure 47: Visualisation of the unstrained network structure of the gel PMEh1, with a cross-section of 1 μm^2; top: TEM micrograph; bottom: snapshot of the CEWLC network, 2/3 of the nodes of the set-up in Figure 44 were randomly removed in "chunks" as described.

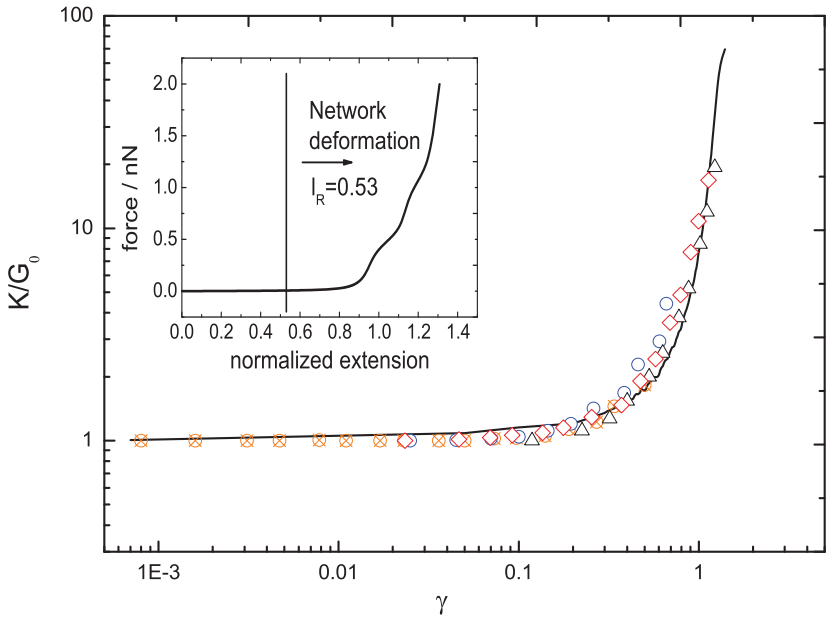

Figure 48: Normalized differential shear moduli K/G_0 plotted as a function of the dimensionless strain γ, for the samples: diamond, PMEl1; triangle upwards, PMEl2; circle, PMEh1; crossed circle, PMEh2. Eq. 3.1 was utilized to fit this master plot, with a normalized relaxed end-to-end extension of $L_R = 0.53$, as depicted in the inset.

4.3.3 Conformational transitions

Lastly, the numerical simulation allows the monitoring of the node-to-node distances and the investigation of whether force-induced conformational transitions of the sugar-ring might be triggered in single pectin chains during network straining. This question has been addressed in two dimensions (Chapter 3), but in this case the 3D model is a more realistic model for considering the likelihood of such events in gels or even in-vivo. To illustrate the investigation of this issue Figure 49 shows the distribution of the node-to-node distances of the fully percolated network, mimicking PMEh2, and its evolution during the shear deformation. It is observed that it is very unlikely for chains to be extended into a "clicked" state (around the extension of 1). For PMEh2, out of the 130 000 available chains, 60 chains are in a "clicked" state at strain $\gamma = 0$, and 430 chains are found to be clicked at strain $\gamma = 0.5$. Hence, throughout the straining process less than $<<$ 1% of the chains undergo a conformational transition. The same conclusions can be drawn for the case of PMEl1.

Similar to the previous results in Chapter 3, the overall node-to-node distribution is shifted towards higher extensions and the number of clicked states increases under applied shear stress. This redistribution causes the observed strain stiffening, but in contrast to the 2D studies, a smaller proportion of the chains are found to be extended sufficiently to yield "clicks" in the 3-D enzymatically induced pectin gels investigated here.

4.4 Conclusions

In this work, enzymatically-induced biomimetic pectin gels were formed in a rheometer, and their viscoelastic moduli measured during gelation. Subsequently the dependence of the differential shear modulus of the gels on prestresses was investigated. It was found that the moduli increase nonlinearly with increasing prestress, converging towards the characteristic power-law behaviour with an exponent of 3/2 [24, 17]. This indicates that the elastic response in these networks originates from the nonlinear entropic response of the single chains.

The results compared favourably with previous work carried out on protein systems, and clearly shows that polysaccharide gel behaviour exhibits similar phenomenology. However, in contrast to previous systems investigated, where the fundamental filaments of the network were predominantly intermediate protein bundles such as rods, tubes and fibrils, the polysaccharide gels described herein can be manipulated so as to form networks in which lengths of single chains dominate the

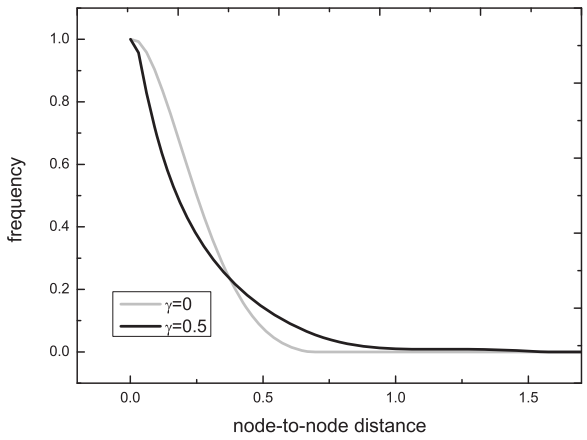

Figure 49: Distribution of the of the node-to-node distance of a fully percolated network, mimicking PMEh2; unstrained equilibrated (grey line) and strained $\gamma = 0.5$ (black line). The extensions are normalized with respect to the length of the fully extended skew-boat conformation of the CEWLC.

stress-bearing elements. As the molecular force extension curve for pectin is well known (in contrast to the difficulty of independently measuring the mechanical properties of hierarchical structures in the archetypal protein networks) the system offers a unique test of bottom-up modelling of the mechanical properties of gels made from pectin.

The numerical simulation reported here shows good quantitative agreement between the calculated and measured rheological properties, for the first time providing a true bottom-up example to the properties of soft materials. Such an approach can be used to investigate how macroscopic network properties might be affected by changes in the single molecule properties of the polymers from which the network is constructed.

References

[1] D. A. Powell, E. R. Morris, M. J. Gidley, and D. A. Rees. Conformations and interactions of pectins .2. influence of residue sequence on chain association in calcium pectate gels. *Journal of Molecular Biology*, 155(4):517–531, 1982. doi: 10.1016/0022-2836(82)90485-5. 91

[2] R. Vincent, A. Cucheval, Y. Hemar, and M. Williams. Bio-inspired network

optimization in soft materials - insights from the plant cell wall. *European Physical Journal E*, 28(1):79–87, 2009. doi: 10.1140/epje/i2008-10416-2. 91

[3] Pubchem: 439239. URL http://pubchem.ncbi.nlm.nih.gov/summary/summary.cgi?cid=439239. 92

[4] M. A. K. Williams, A. T. Marshall, P. Anjukandi, and R. G. Haverkamp. Investigation of the effects of fine structure on the nanomechanical properties of pectin. *Physical Review E*, 76(2):021927, 2007. doi: 10.1103/PhysRevE.76.021927. 92

[5] S. Cros, C. Garnier, M. A. V. Axelos, A. Imberty, and S. Perez. Solution conformations of pectin polysaccharides: Determination of chain characteristics by small angle neutron scattering, viscometry, and molecular modeling. *Biopolymers*, 39(3):339–352, 1996. doi: 10.1002/(SICI)1097-0282(199609)39:3<339::AID-BIP6>3.0.CO;2-P. 92

[6] B. Tinland, A. Pluen, J. Sturm, and G. Weill. Persistence length of single-stranded dna. *Macromolecules*, 30(19):5763–5765, 1997. doi: 10.1021/ma970381+. 92

[7] J. H. Zhang, C. R. Daubert, and E. A. Foegeding. A proposed strain-hardening mechanism for alginate gels. *Journal of Food Engineering*, 80(1):157–165, 2007. doi: 10.1016/j.jfoodeng.2006.04.057. 92

[8] S. Kawai, Y. Nitta, and K. Nishinari. Model study for large deformation of physical polymeric gels. *Journal of Chemical Physics*, 128(13):134903, 2008. doi: 10.1063/1.2894845. 92

[9] K. A. Erk, K. J. Henderson, and K. R. Shull. Strain stiffening in synthetic and biopolymer networks. *Biomacromolecules*, 11(5):1358–1363, 2010. doi: 10.1021/bm100136y. 92

[10] C. Storm, J. J. Pastore, F. C. MacKintosh, T. C. Lubensky, and P. A. Janmey. Nonlinear elasticity in biological gels. *Nature*, 435(7039):191–194, 2005. doi: 10.1038/nature03521. xiii, 92, 95, 101

[11] J. A. E. Benen, H. C. M. Kester, and J. Visser. Kinetic characterization of aspergillus niger n400 endopolygalacturonases i, ii and c. *European Journal of Biochemistry*, 259(3):577–585, 1999. doi: 10.1046/j.1432-1327.1999.00080.x. 93

[12] N. Y. Yao, R. J. Larsen, and D. A. Weitz. Probing nonlinear rheology with inertio-elastic oscillations. *Journal of Rheology*, 52(4):1013–1025, 2008. doi: 10.1122/1.2933171. 94

[13] C. Messaoudil, T. Boudier, C. O. S. Sorzano, and S. Marco. Tomoj: tomography software for three-dimensional reconstruction in transmission electron microscopy. *Bmc Bioinformatics*, 8:288, 2007. doi: 10.1186/1471-2105-8-288. 95

[14] C. O. S. Sorzano, C. Messaoudi, M. Eibauer, J. R. Bilbao-Castro, R. Hegerl, S. Nickell, S. Marco, and J. M. Carazo. Marker-free image registration of electron tomography tilt-series. *Bmc Bioinformatics*, 10:124, 2009. doi: 10.1186/1471-2105-10-124. 95

[15] M. D. Abramoff, P. J. Magelhaes, and S. J. Ram. Image processing with imagej. *Biophotonics Int*, 11(7):36–42, 2004. 95

[16] Q. Wen, A. Basu, J. P. Winer, A. Yodh, and P. A. Janmey. Local and global deformations in a strain-stiffening fibrin gel. *New Journal of Physics*, 9:428, 2007. doi: 10.1088/1367-2630/9/11/428. 95

[17] M. L. Gardel, J. H. Shin, F. C. MacKintosh, L. Mahadevan, P. Matsudaira, and D. A. Weitz. Elastic behavior of cross-linked and bundled actin networks. *Science*, 304(5675):1301–1305, 2004. doi: 10.1126/science.1095087. 95, 110

[18] R. R. Vincent and M. A. K. Williams. Microrheological investigations give insights into the microstructure and functionality of pectin gels. *Carbohydrate Research*, 344(14):1863–1871, 2009. doi: 10.1016/j.carres.2008.11.021. 95, 98

[19] H. Kang, Q. Wen, P. A. Janmey, J. X. Tang, E. Conti, and F. C. MacKintosh. Nonlinear elasticity of stiff filament networks: Strain stiffening, negative normal stress, and filament alignment in fibrin gels. *Journal of Physical Chemistry B*, 113(12):3799–3805, 2009. doi: 10.1021/jp807749f. 95

[20] A. W. Lees and S. F. Edwards. Computer study of transport processes under extreme conditions. *Journal Of Physics Part C Solid State Physics*, 5(15):1921, 1972. doi: 10.1088/0022-3719/5/15/006. 96

[21] A. Slavov, C. Garnier, M. J. Crepeau, S. Durand, J. F. Thibault, and E. Bonnin. Gelation of high methoxy pectin in the presence of pectin methylesterases and calcium. *Carbohydrate Polymers*, 77(4):876–884, 2009. doi: 10.1016/j.carbpol.2009.03.014. 96

[22] C. Semmrich, R. J. Larsen, and A. R. Bausch. Nonlinear mechanics of entangled f-actin solutions. *Soft Matter*, 4(8):1675–1680, 2008. doi: 10.1039/b800989a. 98

[23] C. P. Broedersz, K. E. Kasza, L. M. Jawerth, S. Munster, D. A. Weitz, and F. C. MacKintosh. Measurement of nonlinear rheology of cross-linked biopolymer gels. *Soft Matter*, 6(17):4120–4127, 2010. doi: 10.1039/c0sm00285b. 98

[24] F. C. MacKintosh, J. Kas, and P. A. Janmey. Elasticity of semiflexible biopolymer networks. *Physical Review Letters*, 75(24):4425–4428, 1995. doi: 10.1103/PhysRevLett.75.4425. 110

Chapter 5

Conclusion and future work

5.1 Scope of the thesis

How does nature assemble structures which are dynamic and responsive and how can we learn from this when designing man-made structures with different functionality? The aim of this thesis was to bridge the structure-function divide in polysaccharide networks so that the rheological properties of assembled biopolymers might be predicted from the fine structures of the constituent polymers and their mode of assembly. Most of the work in this field to date has been undertaken on proteins, motivated by the urge to understand the hierarchical responses in cytoskeletal networks, whereas polysaccharides on the other hand, whose importance in the plant cell wall is indisputable, have tended to be sidelined so far.

The polysaccharide pectin is an important constituent of the plant cell wall and the mechanical properties of its assembled networks have recently come into the focus of research via extensive microrheological studies that revealed interesting connections between the gel's mechanical response, gelation conditions and the pectin fine structure. Additionally, the molecular force-extension relation of single pectin chains is experimentally accessible. Networks were constructed in which single chains were the dominating stress bearing elements - in stark contrast to a multitude of biological gels, where hierarchical assembled filaments were found to be the stress bearing strands - and it was speculated that the macroscopic mechanical response could be predicted from microscopic single molecule measurements. This tunability of the mechanical response makes pectin gels therefore a promising model system for further investigations. In this thesis small angle X-ray scattering, rheological measurements, and computer aided modelling techniques have been exploited in the investigation of these systems (see the schematic Figure 50).

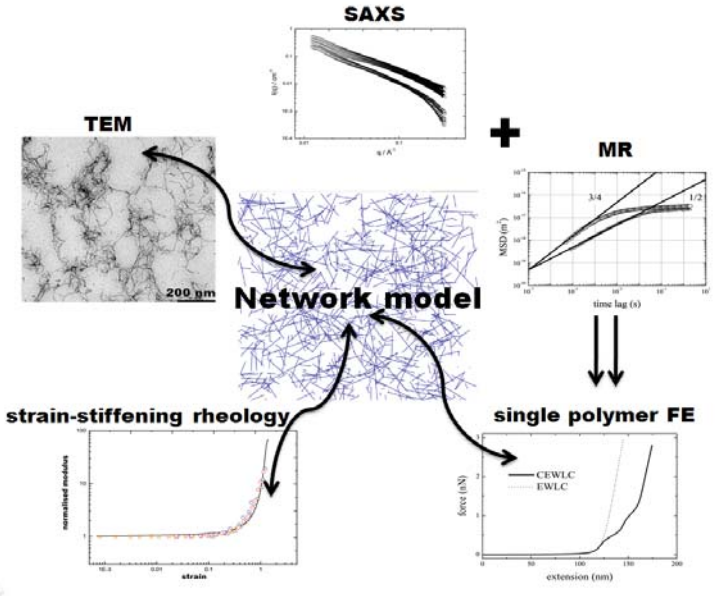

Figure 50: A schematic of experiments and methods utilized in this thesis; and how such a structure-function approach motivated a network model (in this case for biomimetic pectin gels).

5.2 Summary

Firstly, a small angle X-ray scattering (SAXS) study of different microrheologically (MR) well-characterized ionotropic pectin gels was undertaken in order to gain insights into the structures of the assembled elementary network strands. It had previously been hypothesized, based on the microrheological measurements, that such networks can be described either by architectures of dimeric junction-zones of limited extent, linked by considerably longer, flexible, single-chain sections or by semiflexible bundles of aggregated dimeric junction zones that latterly become entangled and cross-linked. The results of the SAXS experiments straightforwardly revealed that gels which are clearly more semiflexible from a MR point-of-view contained larger scattering entities than those with a more flexible character. Furthermore, a more detailed interpretation of the scattering data with the aid of molecular modelling suggested that, for the gels formed here, those with a semi-flexible MR signature consisted predominantly of network filaments of at least 4 chains, while those with a more flexible signature were predominantly single chain and dimeric associations with no more than a few percent of the chains bundled to any higher extent. It was also shown that biomimetic - enzyme induced - networks resemble the

latter, single-chain-dominated, case. This is in contrast to existing paradigms on the hierarchical assembly of many biological gel structures, in which single-polymer properties play little direct mechanical role compared with the properties of the assembled intermediate structures.

Secondly, after finding networks in which large single chain contributions indeed play a major role, and with experimental single chain properties in hand, a 2D model for such biopolymer networks was proposed. A numerical simulation approach was pursued in order to investigate the behaviour of biopolymer networks comprised of single polysaccharide chains using the experimentally measured force extension relation for pectin. This allowed the interesting force-induced conformational transitions exhibited by such polymers to be investigated. The macroscopic mechanical properties of networks of randomly-oriented chains showed nonlinear elasticity, in agreement with a recently reported averaging approach. While the bulk mechanical responses of networks consisting either of simple extensible wormlike chains or the experimentally measured clicked-extensible wormlike chains (CEWLC) were found to be indistinguishable, the number of chains containing sugar rings in different conformational states was found to change during straining. Similar conclusions are drawn under affine or non-affine deformations and when CEWLCs are used to cross-link elastic rods in a two component system, as a biomimetic model of the plant cell wall. This supports the hypothesis that in networks of randomly oriented chains such conformational transitions could have biological significance as stress-switches in signalling processes, but that they are unlikely to affect the bulk rheological properties of tissue.

Finally, the CEWLC network model developed herein, whose novelty lies in the incorporation of experimentally measured single-chain force extension relations, was further expanded into 3-dimensions to test quantitatively its predictions of shear moduli. To this end a comparison with rheological prestress experiments on enzymatically induced pectin gels was undertaken. The differential modulus was found to exhibit similar strain-stiffening behaviour as observed for a plethora of biological materials (to-date only proteins) and to increase nonlinearly with increasing prestress and to converge slowly towards the characteristic power-law of 3/2. This indicates that the elastic response in these networks originates from the nonlinear entropic response of the single chains. The results compared favourably with previous work carried out on protein systems, and clearly show that the polysaccharide gel behaviour exhibits similar phenomenology. The numerical simulation reported here shows good quantitative agreement between the calculated and measured rheological properties, for the first time providing a true bottom-up example of understanding the properties of soft materials. Such an approach can be used to investigate how

macroscopic network properties might be affected by changes in the single molecule properties of the polymers from which the network is constructed.

5.3 Conclusions

- SAXS and microrheology of pectin gels confirmed that by controlling the gelling conditions networks of different architectures and bundle-sizes can be tailored.
- Biomimetic, enzymatically induced, pectin gels exhibit structures where the stress-bearing network-elements are predominantly single chains.
- The single-molecule force extension curve is experimentally known and could be incorporated in a network model.
- 2-D numerical simulations suggested that force induced conformational transitions of the network-constituting single polymer chains do not influence the bulk rheology in random network structures but might act as strain-sensors.
- The bulk rheology of biomimetic networks could be modelled successfully in a bottom-up approach using 3-D numerical simulations.
- Preliminary electron micrographs were found to be consistent with the model, in the sense that the observed structures clearly showed that not all the chains were connected to the network, and the successful modelling of the rheological properties required the removal of nodes to a similar degree.

5.4 Future Work

In this thesis the structure and assembly of network strands in ionotropic, calcium induced, pectin gels was studied via the utilization of SAXS paired with molecular modelling. Acidic pectin gels were recently found to exhibit a semiflexible MR response and a strain-stiffening behaviour as well [1]. It has been speculated that hydrogen bonds are the main cross-linking mechanism in such systems, but the detailed mechanism behind the junction zone formation is not yet well-established. A SAXS study hand-in-hand with a molecular modelling technique would offer a next step to investigate the nature of the junction zones in such acidic gels and the resultant network structure.

Another interesting path for future work would be an extended model for the biomimetic, enzymatically induced, pectin gels, based on node structures gained by

TEM micrographs. Polydispersity of the bundle sizes, as observed in the SAXS study and indicated by preliminary TEM images, and an inclusion of the bending stiffness (as it cannot be neglected for thicker bundles) would represent the most accurate model based on the recent experimental results. Such a model could then be extended towards a two-component network, a structure where stiff rods are interconnected by flexible single pectin chains, in an attempt to describe the cellulose-pectin mediated network and shed more light on the structural mechanisms in the plant cell wall. In other words, a general structure-function approach could be applied to more heterogeneous and polydisperse biopolymer networks.

References

[1] R. Vincent and M. A. K. Williams. (private communication). 118

Appendix A

Small angle X-ray scattering

A.1 Basic principle

Small angle X-ray scattering [1, 2] is a powerful technique for the structural characterization of condensed matter systems and to determine the shape and size of molecular aggregations at nano-scales, e.g. (bio)polymer solutions or gels. The origins of this scattering technique date back to the 1930s, to Guinier's studies on metal alloys [3], leading to the first textbook on SAXS by Guinier and Fournet [4], where it is already demonstrated that not just information on size and shape of particles can be gained by this method, but also conclusions on the internal structure of disordered systems can be drawn. The 1970s brought a breakthrough for SAXS experiments with the availability of synchrotron radiation. Such radiation offers the advantages of a higher flux than usually achieved in laboratory small angle devices, better collimated beams and in third generation synchrotron radiation sources the availability of tunable energy (wave length) via undulators (as e.g in the Australian Synchrotron, a third generation advanced light source, with a typical design of such machines displayed in Figure 51).

The principle behind SAXS experiments is simple: the sample gets irradiated by incident X-rays, the scattered X-rays are detected by a detector and their angular dependence measured; the analysis of the obtained scattering profiles allows therein the determination of size and shape of the scattering body. The higher flux in modern synchrotron radiation sources allows subsequently higher accuracies so that studies of solutions, whose scattering intensity and contrast is very weak, can be followed in real time. This technique is therefore applicable to a broad range of conditions: structures of dilute to semi-dilute solutions (from ~ 1 to ~ 100 mg/mL) and wide molecular-mass ranges (kDa to hundreds of MDa) are applicable, kinetics and interactions in nearly native conditions without initial processing can be analysed,

as well as mixtures and non-equilibrium systems, on which biology often relies (e.g. at large-scale conformational changes). The analysis is sometimes difficult, owing to the fact that the only observable is a one-dimensional scattering curve (scattering intensity $I(q)$ versus the scattering vector q) which is not a real image as found in microscopy; the random orientation of particles in solution leads to spherical averaging of the single particle scattering and yields a one-dimensional scattering pattern. The main challenge lies in the extraction of the three-dimensional structural information from these experimental data. That is where computer aided modelling can determine *ab initio* shape and domain structures or utilize rigid body refinements to understand the scattering profiles of macromolecular complexes better. Due to its low resolution ($\sim$ nm, as SAXS is mostly dealing with scattering data in the absence of crystalline order) additional external information is required to resolve the ambiguity in model building.

For such structural studies hard X-ray photons with an energy ~ 10 keV and wave length ~ 10 nm ($\lambda = 1.256/E$ with λ in nm, E in keV) are generally utilized. Once an object gets illuminated by a monochromatic plane wave with wave vector $k = 2\pi/\lambda$, atoms within the object interact with the incident radiation and become sources of spherical waves. In a first approximation only elastic scattering is considered. The scattering-length f_x, the amplitude of the wave scattered by each atom, is for hard X-rays interacting with electrons described by $f_x = N_e r_0$ (with N_e the number of electrons and $r_0 = 2.82 \times 10^{-13}$ cm the Thomson radius of an electron). The atomic scattering-length does in general not depend on the wavelength. Further, the scattering process can be described in the first Born approximation by a Fourier transformation from the real space of laboratory coordinates to the reciprocal space of scattering vectors. The X-ray scattering amplitudes, representing the Fourier transform of the electron density distribution in the (spherical) atom, are functions $f(s)$ of the momentum transfer $q = 4\pi sin(\theta)/\lambda$ (where 2θ is the scattering angle and $f(0) = f_x$). To characterize the scattering from assemblies of atoms, it is convenient to describe the scattering amplitude from a single particle relative to that of the equivalent solvent volume, which is defined by the Fourier transform of the excess scattering-length density distribution $\Delta\rho(r) = \rho(r) - \rho_s$

$$A(q) = \int_V \Delta\rho(r) exp(iqr) dr$$

with $\rho(r)$ as the total scattering-length of the atoms per unit volume, and assuming that the solvent is a featureless matrix with a constant scattering density ρ_s. The integration is performed over the particle volume. Scattering experiments cannot

measure the amplitude directly but only the scattering intensity $I(q) = A(q)A^*(q)$, which is proportional to the number of photons scattered in the given direction q.

In a single crystal all particles have defined correlated orientations and are regularly distributed in space, therefore the amplitudes of individual particles have to be summed up accounting for inter particle interferences. The total scattered intensity is an anisotropic discrete three-dimensional scattering function $I(s_{hkl})$ - corresponding to the density distribution in a single unit cell of the crystal. If particles are randomly distributed and positions and orientations are uncorrelated - as is the case for macromolecules in solution - their scattering intensities rather then their amplitudes are summed (no interference!). It follows that the scattered intensity from the ensemble is a continuous isotropic function proportional to the scattering from a single particle averaged over all orientations. Dilute solutions of monodisperse non-interacting molecules correspond to this limiting case. In cases with interaction, local correlations between neighbouring particles need to be taken into account and in these cases the intensity can be described as a product $I(q) = P(q)S(q)$ of the form factor $P(q)$ and the structure factor $S(q)$, which describes the particle interactions.

A detailed and structured introduction into small angle scattering techniques and a sound presentation of the theory, instrumentation and data processing involved can be found in [5, 6].

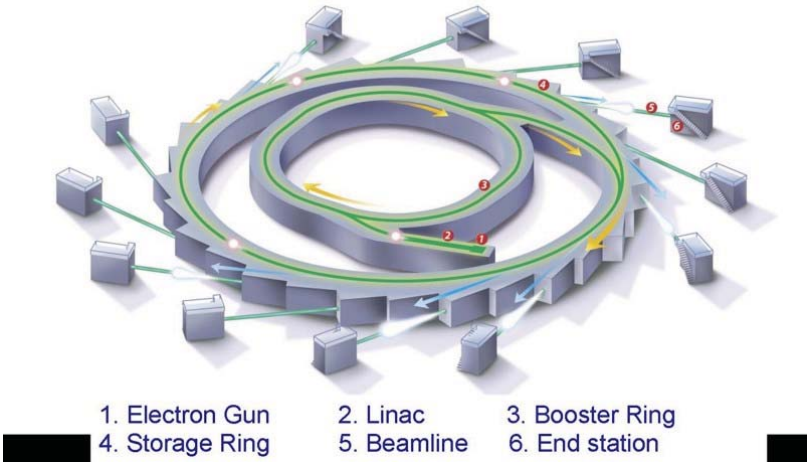

Figure 51: Illustration of the Australian Synchrotron, Melbourne [7].

References

[1] D. I. Svergun and M. H. J. Koch. Small-angle scattering studies of biological macromolecules in solution. *Reports On Progress In Physics*, 66(10):1735–1782, 2003. doi: 10.1088/0034-4885/66/10/R05. 121

[2] Y. Yuguchi. Nano-structure analysis of sugar chains by small angle x-ray scattering. *Trends In Glycoscience and Glycotechnology*, 21(117):1–12, 2009. doi: 10.4052/tigg.21.1. 121

[3] A. Guinier. La diffraction des rayons x aux tres petits angles; application a l'etude de phenomenes ultramicroscopiques. *Annales de Physique*, 12:161–237, 1939. 121

[4] A. Guinier and G. Fournet. *Small-angle scattering of x-rays*. New York: Wiley, 1955. 121

[5] O. Kratky and O. Glatter. *Small angle x-ray scattering*. Academic Press, London; New York, 1982. 123

[6] L. A. Feigin and D. I. Svergun. *Structure analysis by small-angle x-ray and neutron scattering*. New York: Plenum Press, 1987. 123

[7] Australian synchrotron. URL `http://www.synchrotron.org.au/images/SynchrotronScience/machine-fact-sheet_23oct08_final.pdf`. xiv, 123

Appendix B

Modelling methods and the conjugate gradient scheme

This appendix is intended to explain the technical details of the numeric simulation and to give insights into the basic function of the applied conjugate gradient (CG) algorithm. To simulate the network's mechanical response during the straining process, as exploited in Chapters 3 & 4, the total energy of the system needs to be minimized with respect to the node-to-node distances Δx_i; which means that a set of new node-coordinates x needs to be found to relax the network structure maximal.

For the considerations in this thesis, the bending response of the single network strands could be ignored (as argued in Section 4.2.2) and the numeric simulations could be restricted to the search for the optimum node positions with respect to radial node-to-node interaction potentials only. Hence the following energy needs to be minimized

$$E = \sum_{\texttt{neighboring nodes}\, i} \frac{1}{2} k \Delta x_i^2 + E_{FE}(\Delta x_i) = \mathbf{A} \cdot x \tag{B.1}$$

where k is the spring constant for rod-like network segments (in the case of 2-component networks), and E_{FE} is the energy at a certain extension Δx_i, determined by the experimentally measured FE relation (Figure 25); this FE relation is taken into account numerically. The sum over the neighbouring nodes can be captured by a matrix multiplication, where for 3-dimensional networks the matrix $\mathbf{A}$ is of size $N \times 3 \cdot \#\texttt{nodes}$ and x is the vector of all node coordinates, hence in 3-dimensions a vector of the size: $3 \cdot \#\texttt{nodes} \times 1$. Further, $\mathbf{A}$ is a very sparse matrix consisting of only 2 entries per row, which assign the type of the interaction potential (rod or numerical FE) and allocate two interacting neighbouring nodes. The number of rows N corresponds to the number of all pair interactions in the network.

The optimization of systems determined by such sparse matrices is performed very effectively within the conjugate-gradient scheme, an iterative method for the numerical solution of systems of linear equations. The algorithm is applied in such areas as e.g. engineering design, neural net training and nonlinear regression.

We choose as well the CG scheme to solve Eq. B.1 numerically, more precisely by the utilization of the well-engineered algorithm provided in the numerical recipes collection [1]. A general and more elaborate description of the CG method can be found in [2]. In the following section the function of the CG algorithm is demonstrated on the descriptive example of the minimization of a quadratic function [3].

The task of solving the equation $\mathbf{A} \cdot x = b$ may be interpreted as a minimization problem of the scalar function

$$f(x) \equiv \frac{1}{2}|\mathbf{A} \cdot x - b|^2 \tag{B.2}$$

with the matrix $\mathbf{A}$ and the constant vector b. We only need to find the vector x that minimizes $f(x)$. The conjugate gradient method needs no inversion at all and is particularly efficient for quadratic functions as in Eq. B.2. However the matrix multiplication $\mathbf{A} \cdot x$ must be performed more often, and is therefore computationally just economical for sparse matrices $\mathbf{A}$.
The *steepest decent method*, an easy to visualize but less efficient method, motivates the CG method. Cauchy introduced this method considering the lines of equal elevation (e.g displayed for a quadratic function in Figure 52). Starting from some point P_0 the strategy is to follow the local gradient

$$g_0 = -\nabla f(P_0) \tag{B.3}$$

which is the steepest descent in this functional landscape, until it "is going uphill again" (at point P_1); that is the starting point for an iteration, in which subsequently the local gradient of $f(x)$ at P_1 is followed and so on, until the extremal point is finally reached.

The question is therefore: Can we chose the direction h_1, starting form point P_1, to reach the minimum directly, instead of zig-zagging towards the goal and wasting computational time? This can be achieved by choosing a direction where the *change of the gradient* of $f(x)$ should have no component parallel to g_0, thus the vector h_1 can be obtained.

A recipe for the usage of the CG technique is presented according to [3]:

(i) Let P_0 (with the position vector x_0) be the starting point of the search; the local gradient at P_0 is

$$g_0 \equiv -\nabla f(x_0) = -\mathbf{A}^T \cdot [\mathbf{A} \cdot x_0 - b] \tag{B.4}$$

The next low point P_1 is then situated at

$$x_1 = x_0 + \lambda_1 g_0 \tag{B.5}$$

with

$$\lambda_1 = \frac{|g_0|^2}{|\mathbf{A} \cdot g_0|^2} \tag{B.6}$$

(ii) From P_1 we proceed **not** along the local gradient

$$g_1 = -\mathbf{A}^T \cdot [\mathbf{A} \cdot x_1 - b] \tag{B.7}$$

but along the gradient conjugate to g_0, i.e.

$$h_1 = g_1 - \frac{g_1 \cdot \mathbf{A} \cdot g_0}{g_0 \cdot \mathbf{A} \cdot g_0} g_0 \tag{B.8}$$

The low point along this path is at

$$x_2 = x_1 + \lambda_2 h_1 \tag{B.9}$$

with

$$\lambda_2 = \frac{|g_1 \cdot h_1|}{|\mathbf{A} \cdot h_1|^2} \tag{B.10}$$

(iii) For systems of more than two-dimensions, one has to go on from x_2 in the direction

$$h_2 = g_2 - \frac{g_2 \cdot \mathbf{A} \cdot h_1}{h_1 \cdot A \cdot h_1} h_1 \tag{B.11}$$

until the next low point is reached at

$$x_3 = x_2 + \lambda_3 h_2 \tag{B.12}$$

with

$$\lambda_3 = \frac{|g_2 \cdot h_2|}{|\mathbf{A} \cdot h_2|^2} \tag{B.13}$$

And so on for further dimensions; a system of N equations requires a total of N steps to gain the solution x.

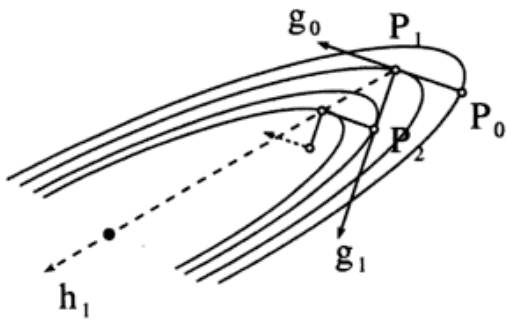

Figure 52: Conjugate gradients: g_0 denotes the direction of steepest descent at point P_0; h_1 points out the direction of the gradient conjugate to g_0. To reach the minimum of this quadratic function: the steepest descent method follows the zig-zag course, whereas the conjugate gradient h_1 gets to the goal in just two steps [3].

References

[1] W. H. Press, S. A. Teukolsky, W. T. Vetterling, and B. P. Flannery. *Numerical Recipes 3rd Edition: The Art of Scientific Computing*. Cambridge, UK; New York: Cambridge University Press, 2007. 126

[2] J. R. Shewchuk. An introduction to the conjugate gradient method without the agonizing pain. Technical report, School of Computer Science, Carnegie Mellon University, Pittsburgh, PA, USA, 1994. URL `www.cs.cmu.edu/~quake-papers/painless-conjugate-gradient.pdf`. 126

[3] F. J. Vesely. *Computational physics : an introduction 2nd Edition*. New York: Kluwer Academic/Plenum Publishers, 2001. xiv, 126, 127, 128